TABLE DES MATIÈRES

Page

INTRODUCTION 1

CHAPITRE 1 REVUE DE LITTÉRATURE 11
1.1 L'imagerie par ultrasons 11
1.2 Les transducteurs micromachinés 13
1.3 Les transducteurs ultrasoniques piézoélectriques micromachinés (PMUT) 17
1.3.1 Formation de faisceaux 17
1.3.2 Matériaux piézoélectriques utilisés dans la fabrication des PMUT 19
1.3.3 Technique de fabrication des membranes suspendues 20
1.3.4 Circuit intégré pour la formation de faisceaux 21

CHAPITRE 2 FREQUENCY TUNING TECHNIQUE OF PIEZOELECTRIC ULTRASONIC TRANSDUCERS FOR RANGING APPLICATIONS 23
2.1 Introduction 23
2.2 Theory and Modeling 26
2.3 Design and Fabrication 29
2.4 Simulations 31
2.5 Electrical Characterisation Results 33
2.5.1 Effect of Parylene-C on eigenfrequency 33
2.5.2 1.4.2 Chip-to-chip transmission 35
2.5.3 Ranging 38
2.6 Conclusion 41

CHAPITRE 3 A NOVEL TOPOLOGY FOR PROCESS VARIATION-TOLERANT PIEZOELECTRIC MICROMACHINED ULTRASONIC TRANSDUCERS 43
3.1 Introduction 43
3.2 Theoretical Background 45
3.3 Design 49
3.3.1 Fabrication Process 49
3.3.2 Finite-element Simulations 51
3.4 Measurement Results 53
3.5 Conclusion 56

CHAPITRE 4 ELECTROMECHANICAL DAMPING FOR LONG-RANGE AND HIGH-PRECISION PIEZOELECTRIC ULTRASONIC TRANSDUCERS 59
4.1 Introduction 59
4.2 Theoretical Background 62

4.2.1 Operating principle 62
4.2.2 Influence of the mechanical damper on the resonant frequency 63
4.2.3 Key parameters for stiffnesses k_1 & k_2 and masses m_1 & m_2 65
4.2.4 Influence of the mechanical damper on the displacement amplitude at resonance 66
4.3 Design 66
4.3.1 Fabrication process 66
4.3.2 Finite-element simulations 68
4.4 Measurement Results 72
4.4.1 Time domain 73
4.4.2 Frequency domain 75
4.5 Conclusion 78

CHAPITRE 5 PIEZOELECTRIC MICROMACHINED ULTRASOUND TRANSDUCER BASED SYSTEM IN PACKAGE FOR ULTRASOUND APPLICATIONS 81
5.1 Introduction 81
5.2 System Overview 82
5.3 Design, Fabrication and Characterization of the PMUT Matrix 84
5.3.1 PMUT Equivalent Circuit 84
5.3.2 Fabrication Process 84
5.3.3 Finite-element Simulations 85
5.3.4 Characterization 85
5.4 Design of the CMOS Chip 87
5.4.1 Design of the High-voltage Pulser 88
5.4.2 Design of the Transimpedance Amplifier 88
5.5 Measurement Results 89
5.6 Conclusion 90

CONCLUSION ET RECOMMANDATIONS 93

LISTE DE RÉFÉRENCES 96

LISTE DES TABLEAUX

Page

Tableau 2.1 Value of λ_{ij} for selected modes. 28

Tableau 2.2 List of the different physical parameters used to perform eigenfrequency simulation 34

Tableau 3.1 List of the different physical parameters used to perform eigenfrequency simulation 52

Tableau 4.1 PMUT dimensions used for fabrication..... 70

Tableau 4.2 Comparison of state-of-the-art PMUTs resolutions..... 78

LISTE DES FIGURES

Page

Figure 0.1 Prévisions du marché des transducteurs ultrasoniques pour la période 2017-2023 2

Figure 0.2 Micrographie d'un PMUT effectuée avec un microscope électronique à balayage 3

Figure 1.1 Émission (a) et réception (b) d'un pulse 11

Figure 1.2 Formation de faisceaux : (a) Génération d'un front d'onde à angle par rapport à l'émetteur et formation et (b) focalisation de la pression en un point. 12

Figure 1.3 Schématique d'un transducteur conventionnel 13

Figure 1.4 Schématique d'un CMUT 16

Figure 1.5 Schématique d'un PMUT 16

Figure 1.6 Schéma de fabrication d'une gaufre cavity SOI 21

Figure 2.1 Representation of the multi-layer PMUT for the calculation of the neutral plane 27

Figure 2.2 PiezoMUMPS process flow for the fabrication of a PMUT and post-processing. a) SOI wafer, b) growth of thermal oxide, c) patterning of thermal oxide by wet etching, d) deposition of aluminum nitride by reactive sputtering, e) AlN patterning by wet etching f) resist deposition, g) resist patterning, h) aluminum pad deposition, i) resist removal, j) DRIE etching of silicon, k) membrane release, and l) post processing with Parylene-c coating 30

Figure 2.3 SEM micrographs of the fabricated PMUTs. a)-b) close-up of a device, and c) matrix of PMUTs, each column with 4 PMUTs connected in parallel 31

Figure 2.4 Harmonic simulation at the center of the membrane and eigenvalue simulation for the first (a) and second (b) modes of resonance of the PMUT without Parylene-C 32

Figure 2.5 Comparison between theoretical, simulated and measured resonant frequencies as a function of Parylene-C thickness for the (a) first mode and (b) second mode of resonance 33

Figure 2.6 Measurement of the resonance frequency for different Parylene thicknesses for the (a) first mode and (b) the second mode of resonance 34

Figure 2.7 Scattering parameter measurements for chip to chip transmission with a Parylene-c thickness of (a) 0 nm, (b) 180 nm, (c) 280 nm, (d) 620 nm and (e) 1079 nm for the 1st mode of resonance 36

Figure 2.8 Scattering parameter measurements for chip to chip transmission with a Parylene-c thickness of (a) 0nm, (b) 180 nm, (c) 280 nm, (d) 620 nm and (e) 1079 nm for the 2nd mode of resonance 37

Figure 2.9 Chip to chip transmission measurements in time domain with a Parylene-c thickness of (a) 0nm, (b) 180 nm, (c) 280 nm, (d) 620 nm and (e) 1079 nm for the 1st mode of resonance 39

Figure 2.10 Chip to chip transmission measurements in time domain with a Parylene-c thickness of (a) 0nm, (b) 180 nm, (c) 280 nm, (d) 620 nm and (e) 1079 nm for the 2nd mode of resonance 40

Figure 2.11 Measurement setup : a) time domain ranging measurements, b) close-up of the PCB for time domain measurements, c) close-up of the chip under frequency domain measurements, and d) close-up of the chip and package for time domain measurements 41

Figure 2.12 Measurements of the received pulse for six different reflection distances : 2 mm, 6 mm, 8 mm, 12 mm, 16 mm and 20 mm 41

Figure 3.1 Schematic of a PMUT with toroid anchor; (a) Cross view of the PMUT with toroid anchor with the designation of the trench and its variation as a result of process variations. (b) Top view of the PMUT with toroid anchor with the designation of the section illustrated in (d). (c) Top view of the PMUT without toroid anchor with the designation of the section illustrated in (e). (d) Anchor section of the PMUT with toroid and identification of the spring constant, length and width and their variations. (e) Anchor section of the PMUT without toroid and identification of the spring constant, length and width and their variations 47

Figure 3.2 PiezoMUMPS process flow for the fabrication of a PMUT and post-processing. a) SOI wafer, b) growth of thermal oxide, c) patterning of thermal oxide by wet etching, d) deposition of aluminum nitride by reactive sputtering, e) AlN patterning by wet etching f) resist deposition, g) resist patterning, h) aluminum pad deposition, i) resist removal, j) DRIE etching of silicon and k) membrane release 50

Figure 3.3 SEM micrographs of the fabricated PMUTs. a) Top view of the device and, b) close-up of a device 50

Figure 3.4 Simulation of frequency variation for PMUT devices with and without a toroidal anchor. (a) Schematic of the PMUT devices illustrating the used fixed constraints and variable dimensions, (b) frequency variation as a function of trench diameter, and (c) resonant frequency variation ratio, ζ, as a function of the support dimension of interest (width or length) for a PMUT with toroidal anchor 51

Figure 3.5 Impedance of PMUT devices from 16 different dies (a) for PMUT devices without toroid and (b) for PMUT devices with toroid anchor. Impedance of 12 PMUT devices on same die (c) for PMUT devices without toroid anchor and (d) for PMUT devices with toroid anchor 55

Figure 3.6 Photograph of the measurement setup and (b) ranging measurement results in air for distances from 1 mm to 6 mm 56

Figure 4.1 Schematic of the PMUT and its actuator (a) when no voltage is applied and (b) when voltage is applied 62

Figure 4.2 Schematic representation of the influence of the actuator on the acoustic pulse (a), and (b) conceptual impact of the actuator on the PMUT resonant frequency 63

Figure 4.3 PiezoMUMPS process flow for the fabrication of a PMUT. a) SOI wafer, b) growth of thermal oxide, c) patterning of thermal oxide by wet etching, d) deposition of aluminum nitride by reactive sputtering, e) AlN patterning by wet etching f) resist deposition, g) resist patterning, h) aluminum pad deposition, i) resist removal, j) DRIE etching of silicon and k) membrane release 67

Figure 4.4 Micrograph of the PMUT and its actuators and masses 68

Figure 4.5 Schematic of the simulated structures : (a) PMUT with actuators and masses as a single structure with its design dimensions, and (b) PMUT without actuators or masses 69

Figure 4.6 Simulation of the displacement of the PMUT device. The displacement is plotted as a function of the frequency with and without the actuator enabled for $L_{m,1}$ equal to 70 μm. Drawings of the mode shapes are included at the corresponding frequencies 69

Figure 4.7 For the enabled actuator, the maximum displacement is plotted as a function of $L_{m,1}$ varying between 50 μm and 90 μm. Three

frequencies are considered : the working frequency, the frequency of the first mode and the frequency of the second mode 71

Figure 4.8 For the enabled actuator, the maximum displacement is plotted as a function of the length of k_1 varying between 10 μm and 30 μm. Three frequencies are considered : the working frequency, the frequency of the first mode and the frequency of the second mode 72

Figure 4.9 For the enabled actuator, the maximum displacement is plotted as a function of the beamwidth of k_2 varying between 2 μm and 4 μm. Three frequencies are considered : the working frequency, the frequency of the first mode and the frequency of the second mode 73

Figure 4.10 Measurement of the PMUT velocity (a) when the actuator is disabled but the excitation signal is turned off, (b) when the actuator is enabled, (c) measurement of the resonant frequency of the PMUT as a function of time during the damper activation, and (d) measurement of the transmission characteristic (S_{12} scattering parameter) with and without the actuator enabled 74

Figure 4.11 Mode shape at 8 different phases of the vibration cycle a) without actuator enabled and b) with actuator enabled 76

Figure 5.1 Block diagram of the proposed PMUT SiP 82

Figure 5.3 Micrograph of the fabricated PMUT matrix 83

Figure 5.2 Equivalent circuit of a PMUT 84

Figure 5.4 COMSOL simulation. a) model used for simulation and b) simulation results of acoustic pressure level in dBV 86

Figure 5.5 Measurement of the conductance of a PMUT as a function of frequency 87

Figure 5.6 Schematic of (a) the RGC TIA and (b) the high-voltage pulser 87

Figure 5.7 Time domain measurements of the high-voltage pulser 88

Figure 5.8 Frequency domain measurements of the RGC TIA 90

Figure 5.9 (a) Schematic and (b) photograph of the measurement setup 91

Figure 5.10 Ranging measurement results in air for distances of a) 2 mm, b) 4 mm, c) 6 mm, d) 8 mm, e) 10 mm, and f) 12 mm 91

LISTE DES ABRÉVIATIONS, SIGLES ET ACRONYMES

AlN	Aluminium nitride
AMS	Austria Mikro Systeme
CG	Common gate
CMOS	Complementary metal-oxide-semiconductor
CMUT	Capacitive micromachined ultrasonic transducers
CS	Common source
FPGA	Field-programmable gate array
GSG	Ground signal ground
IC	Integrated circuit
MEMS	Microelectromechanical systems
MUT	micromachined ultrasonic transducers
NFC	near field communication
NSERC	Natural Sciences and Engineering Research Council of Canada
PCB	Printed circuit board
PMUT	piezoelectric micromachined ultrasonic transducers
PZT	Titano-Zirconate de Plomb
PVDF	Polyvinylidene Fluoride
Q	Facteur de qualité
ReSMiQ	Regroupement stratégique en microsystèmes du Québec
RFID	radio-frequency identification
RGC	Regulated cascode
SEM	Scanning Electron Microscope
SiP	System in package
SOI	Silicon on Insulator
TIA	transimpedance amplifier

INTRODUCTION

Les premières applications des ultrasons remontent à la Première Guerre mondiale lorsqu'ils ont été utilisés pour la détection de sous-marins. Depuis, cette technologie est utilisée dans une vaste gamme de domaines. Notamment, en médecine, cette technologie qui a vu ses premières applications apparaître dans les années 1950 et est aujourd'hui utilisée dans un très grand nombre de spécialités comme en cardiologie, en orthopédie ainsi que pour le dépistage du cancer et pour les tests prénataux pour ne citer que quelques exemples (Burrascano, Callegari, Montisci, Ricci & Versaci, 2014). Son utilisation est aussi très répandue dans plusieurs domaines de l'industrie comme dans celle de la métallurgique pour le contrôle de qualité et l'identification de défauts à l'intérieur des matériaux (Schmerr & Song, 2007). Finalement, les capteurs ultrasoniques sont utilisés pour effectuer des mesures de distance. Or, bien que cette technologie soit très répandue, les transducteurs ultrasoniques conventionnels posent des défis en termes d'efficacité, de complexité de fabrication et de coûts de mise en oeuvre. De plus, ils sont généralement volumineux et difficiles à intégrer.

Toutefois, un nouveau type de senseurs ultrasoniques fait présentement l'objet d'un intérêt croissant. Il s'agit des transducteurs ultrasoniques micromachinés (MUT). Ces dispositifs sont fabriqués à l'aide de procédés et de techniques de microfabrication issue des technologies MEMS et des semiconducteurs, et peuvent donc être produits en masse à très faible coût et peuvent également être fabriqués de façon monolithique avec leur circuit intégré de contrôle (Gurun, Tekes, Zahorian, Xu, Satir, Karaman, Hasler & Degertekin, 2014 ; Lemmerhirt, Cheng, White, Rich, Zhang, Fowlkes & Kripfgans, 2012).

Ainsi, les MUT ont le potentiel de rendre beaucoup plus accessibles et moins coûteuses les applications déjà existantes énumérées plus haut et de permettre l'émergence de nouvelles applications dans le domaine de la biométrie, de la détection de mouvement, du biomédical et dans une multitude d'autres domaines. Par exemple, des senseurs d'empreinte digitale et

des détecteurs de mouvement utilisant la technologie des MUT (Yole Développement) sont en développement. De ce fait, le marché de la détection par ultrasons connaît présentement un essor considérable. Ainsi, il est prévu que ce marché qui était de 2 milliards de dollars américains en 2017 atteigne environ 6 milliards de dollars américains en 2023 (Yole Développement) comme le montre la figure 0.1.

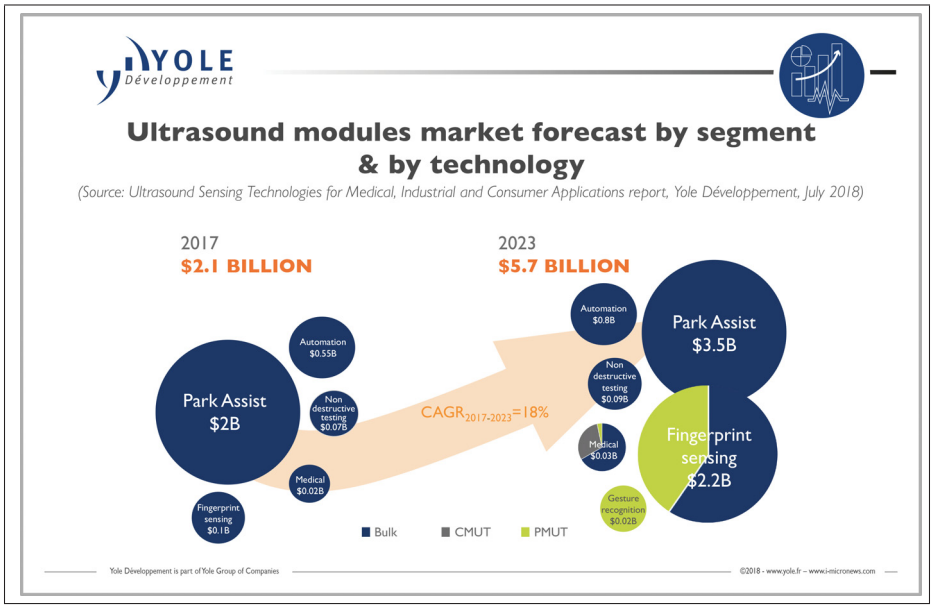

Figure 0.1 Prévisions du marché des transducteurs ultrasoniques pour la période 2017-2023
Tirée de Yole (2018)

Il existe principalement deux types de MUT, le MUT capacitif (CMUT) et le MUT piézoélectrique (PMUT). Le PMUT est principalement constitué d'une couche de matériau piézoélectrique disposé entre deux électrodes. Lorsqu'une différence de potentiel est appliquée entre celles-ci, le piézoélectrique subit une déformation latérale. Le PMUT est ancré de façon à ce que cette déformation soit orientée vers l'extérieur du plan. Cette déformation permet de générer des ondes ultrasoniques. Aussi, lorsqu'une onde ultrasonique entre en contact avec le PMUT, une différence de potentiel est mesurée à ces bornes. Ainsi, il peut jouer le rôle d'émetteur-récepteur

ultrasonique. La figure 0.2 montre une micrographie effectuée au moyen d'un microscope électronique à balayage.

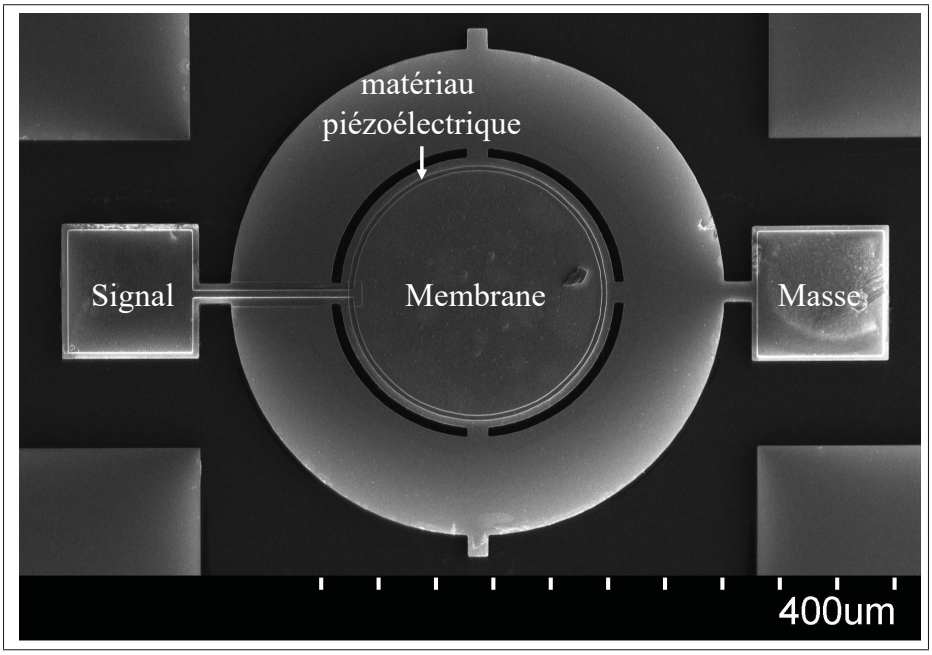

Figure 0.2 Micrographie d'un PMUT effectuée avec un microscope électronique à balayage

La recherche sur les PMUT constitue un domaine en pleine effervescence et le PMUT, qui fait l'objet de cette thèse, est un excellent candidat pour révolutionner les technologies conventionnelles des ultrasons. Ainsi, les efforts de recherche sur les PMUT permettront de démocratiser cette technologie et de rendre possible l'émergence de nombreuses nouvelles applications.

Objectifs

L'objectif de cette thèse est d'investiguer la possibilité de développer une micropuce pour les applications ultrasoniques comme la mesure de distances et l'imagerie qui soit faible coût e facile à intégrer. La puce sera composée d'une matrice de transducteurs ultrasoniques piézoélectriques micromachinés (PMUTs) et d'un circuit intégré pour le contrôle des transducteurs. Tous les composants du dispositif seront intégrés dans un même boîtier et le dispositif pourra ensuite être

directement intégré dans les téléphones intelligents et d'autres appareils portatifs, permettant de démocratiser cette technologie de l'avenir et de rendre plus accessible une multitude d'applications dans les domaines du biomédical et de la biométrie et d'ouvrir la voie à de nouvelles applications encore inexplorées.

Principales contributions

Les principales contributions de cette thèse par articles sont les suivantes :

1. **Technique de réglage de fréquence des PMUT pour les applications de mesure de distances**

Une technique de calibration de la fréquence de résonance des PMUT pour les applications de mesures de distances a été développée. Le dispositif est optimisé pour maximiser la puissance acoustique de sortie à la fréquence cible et de ce fait, son facteur de qualité est relativement élevé. Par conséquent, il est essentiel que le périphérique ait sa fréquence de résonance correspondant à la fréquence d'application pour maximiser le transfert de puissance. En conséquence, une nouvelle technique peu coûteuse pour régler la fréquence de résonance des PMUT après fabrication est présentée. La technique ne nécessite qu'une seule étape de post-traitement qui consiste en un dépôt conforme d'une couche mince de Parylene-C sur le PMUT. Cette contribution a été publiée dans une revue scientifique : *A. Robichaud, P. Cicek, D. Deslandes and F. Nabki, "Frequency Tuning Technique of Piezoelectric Ultrasonic Transducers for Ranging Applications," in IEEE Journal of Microelectromechanical Systems, vol. 27, no. 3, pp. 570-579, June 2018.*

2. **Nouvelle architecture de PMUT tolérante aux variations de procédés**

Une nouvelle topologie d'ancrage pour les PMUT qui permet de réduire drastiquement l'influence de variations de procédés sur la fréquence de résonance des PMUT a été développée. Les PMUT ont été fabriqués avec l'aide de la technologie commerciale PiezoMUMPS. Pour libérer les

membranes, cette technologie utilise le procédé DRIE qui est soumis à des variations de procédé relativement élevées. Cela a pour effet de faire varier les dimensions des PMUT et de ce fait, la fréquence de résonance. L'article présente une explication théorique du phénomène ainsi que des résultats de simulation et des mesures qui confirment la théorie. Les résultats de mesure montrent que la variation de fréquence de résonance peut être réduite d'un facteur d'environ 4 lorsque la topologie proposée est utilisée. Cette contribution a été publiée dans une revue scientifique : *A. Robichaud, D. Deslandes, P. Cicek and F. Nabki, "A Novel Topology for Process Variation-Tolerant Piezoelectric Micromachined Ultrasonic Transducers," in IEEE Journal of Microelectromechanical Systems, vol. 27, no. 6, pp. 1204-1212, Dec. 2018.*

3. Actuateur électrostatique permettant d'amortir l'oscillation d'un PMUT

Afin d'obtenir une résolution axiale raisonnable, les systèmes d'imagerie conventionnels n'ont d'autre choix que de recourir à des transducteurs à faible facteur de qualité (Q), de manière à minimiser les oscillations qui autrement augmenteraient considérablement la durée de l'impulsion acoustique produite. Toutefois, la puissance acoustique des transducteurs ayant une valeur de Q faible est distribuée sur une large bande passante. Ainsi, la distance sur laquelle l'imagerie peut être effectuée est réduite ce qui limite les applications possibles. Ce travail consiste à combiner le meilleur des deux mondes, en démontrant une méthode d'utilisation de transducteurs ayant une valeur de Q élevée pour permettre l'imagerie à haute résolution axiale. Ceci est accompli en introduisant un actuateur électrostatique permettant d'amortir rapidement l'oscillation d'un PMUT ayant une valeur de Q élevée afin de réduire la durée d'impulsion dans le domaine temporel et ainsi améliorer la résolution axiale sans sacrifier la transmission de puissance acoustique. Cette contribution a été publiée dans une revue scientifique : *A. Robichaud, D. Deslandes, P. Cicek and F. Nabki, "Electromechanical Damping for Long-Range and High Precision Piezoelectric Ultrasonic Transducers", IEEE Journal of Microelectromechanical Systems*

4. Système dans un boîtier (SiP) pour les applications ultrasoniques composé d'une matrice de PMUT et d'un circuit de contrôle

Pour permettre de réduire la taille, le coût, d'augmenter les performances et de réduire la consommation d'énergie, un système dans un boitier (SiP) a été conçu. Le système est composé d'une matrice de 4x8 PMUT et d'un circuit intégré de commande tous deux combinés dans un seul boitier. La matrice de PMUT est fabriquée à l'aide du processus PiezoMUMPS et le circuit intégré est implémenté dans avec la technologie AMS 0,35 . Le circuit de commande est composé de pulseurs haute tension pour piloter les PMUT et d'amplificateurs transimpédances pour amplifier l'écho. La fréquence de fonctionnement du système est de 1,5 MHz. Le système est finalement utilisé pour effectuer des mesures de distance. Cette contribution a été soumise pour publication dans une revue scientifique : *A. Robichaud, D. Deslandes, P. Cicek and F. Nabki, "A System in Package Based on a Piezoelectric Micromachined Ultrasonic Transducer Matrix for Ranging Applications", IEEE Transactions on Circuits and Systems II*

Publications, Brevets et droits de propriété intellectuelle

Finalement, voici la la liste complète des publications et brevets qui ont été le fruit de cette thèse.

Brevets

[1] A. Robichaud, D. Deslandes, P. Cicek and F. Nabki, PMUT architecture and post processing techniques for reducing the influence of process variations on resonant frequency and for enabling increased bandwidth, Régulier US no. 16/867,080 ; 2020-05-05.

[2] Amirkhan, F., Robichaud, A., Ropagnol, X., Gratuze, M., Ozaki, T., Nabki, F., Blanchard, F., Terahertz modulation system and method of modulating a terahertz signal, Provisoire US no. 62/993,113 ; 2020-03-23.

Publications

[1] A. Robichaud, D. Deslandes, P. Cicek and F. Nabki, "Electromechanical Tuning of Piecewise Stiffness and Damping for Long-Range and High-Precision Piezoelectric Ultrasonic Transducers," in Journal of Microelectromechanical Systems, doi : 10.1109/JMEMS.2020.3005917, 2020.

[2] A. Robichaud, D. Deslandes, P. Cicek and F. Nabki, "A System in Package Based on a Piezoelectric Micromachined Ultrasonic Transducer Matrix for Ranging Applications" (soumis)

[3] A. Robichaud, P. Cicek, D. Deslandes and F. Nabki, "Frequency Tuning Technique of Piezoelectric Ultrasonic Transducers for Ranging Applications," in IEEE Journal of Microelectromechanical Systems, vol. 27, no. 3, pp. 570-579, June 2018.

[4] A. Robichaud, D. Deslandes, P. Cicek and F. Nabki, "A Novel Topology for Process Variation-Tolerant Piezoelectric Micromachined Ultrasonic Transducers," in IEEE Journal of Microelectromechanical Systems, vol. 27, no. 6, pp. 1204-1212, Dec. 2018.

[5] Amirkhan, F., Robichaud, A., Ropagnol, X., Gratuze, M., Ozaki, T., Nabki, F., Blanchard, F. (2020). Active terahertz time differentiator using piezoelectric micromachined ultrasonic transducer array. Optics Letters, 45(13), 3589-3592.

Structure de la thèse

Le présent travail constitue une thèse par articles et son organisation est la suivante.

Tout d'abord, le chapitre 1 présente une revue de littérature. Notamment, une revue de l'état de l'art des transducteurs micromachinée est exposée.

Puis, afin d'étudier la possibilité de créer la puce qui fait l'objet de cette thèse, une première architecture de PMUT a été développée. Il s'agit de PMUT ayant un facteur de qualité relativement élevé et de ce fait, il est capital que la fréquence de résonance soit précise. Ainsi, une technique pour calibrer la fréquence de résonance des PMUT a été développée et les résultats sont présentés au chapitre 2. Le chapitre traite de la théorie sur les PMUT, de leur modélisation et de leur fabrication. Il présente la première puce de PMUT fonctionnelle de cette thèse. Elle sera réutilisée et améliorée dans les chapitres suivants.

Ensuite, l'idée d'améliorer la précision en fréquence est approfondie. Le réglage de la fréquence de résonance a été réalisé à l'aide d'une technique de post-traitement présentée au chapitre 2. Afin d'augmenter davantage la précision de la fréquence, en se basant sur les résultats obtenus au chapitre 2, l'étude d'une topologie étant moins sensible aux variations de procédé a été faite et les résultats sont présentés au chapitre 3. Le chapitre présente donc une puce de PMUT qui constitue une amélioration en termes de précision de la fréquence de résonance par rapport à celle présentée au chapitre 2.

Les puces jusqu'ici fabriquées présentent des performances intéressantes et ont été utilisées avec succès pour effectuer des mesures de distance. Leur facteur de qualité relativement élevé a pour avantage de permettre de maximiser la puissance acoustique de sortie à la fréquence cible. Toutefois, cela a aussi pour conséquence une longueur de pulse assez longue et donc une résolution axiale amoindrie. En se basant sur les résultats obtenus au chapitre 2 et 3 et sur les puces qui y sont présentés, une technique pour amortir rapidement l'oscillation a été

développée. La technique et les résultats sont présentés au chapitre 4. Ce travail constitue donc l'aboutissement d'une série d'améliorations convergent vers l'atteinte de l'objectif de cette thèse.

Finalement, un circuit intégré de contrôle a été développé. Celui-ci ainsi que la puce de PMUT ont été intégrés dans un même boitier pour obtenir un dispositif compact pouvant permettre de faire de l'imagerie par ultrasons. La fonctionnalité du dispositif a été mise à l'épreuve en effectuant des mesures de distance. Les résultats sont présentés au chapitre 5. Ce chapitre présente donc le dispositif ultrasonique complet qui a fait l'objet de cette thèse.

CHAPITRE 1

REVUE DE LITTÉRATURE

1.1 L'imagerie par ultrasons

Le principe de base de l'imagerie par ultrasons est le suivant. Tout d'abord, un transducteur ultrasonique convertit une impulsion de tension en impulsion acoustique. Celui-ci voyage dans le milieu en observation et sera éventuellement réfléchi par un objet / particule pour ensuite retourner vers l'émetteur où il sera transformé à nouveau en impulsion de tension. Ceci est illustré à la figure 1.1.

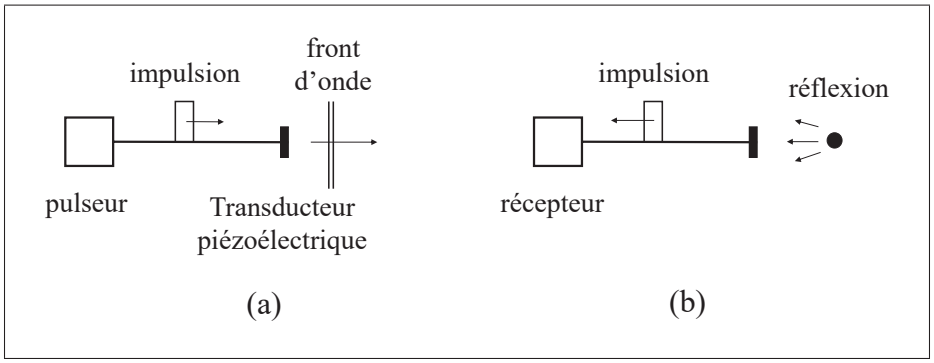

Figure 1.1 Émission (a) et réception (b) d'un pulse
Adaptée de Schmeer Jr. (2008)

Connaissant la vitesse du son dans le milieu observé, il est possible de calculer la position de la particule détectée. Toutefois, avec un seul émetteur statique, très peu d'information sur la particule est obtenue. En effet, seule la position est connue. La taille, la géométrie et d'autres informations restent inconnues. Pour obtenir plus d'information, il faudrait déplacer l'émetteur pour obtenir plus de mesures. Cela peut être fait de façon mécanique ou électronique en utilisant la technique de formation de faisceaux (beamforming).

Pour faire de la formation de faisceaux, cela prend une matrice de transducteur (1D ou 2D). En excitant les transducteurs de la matrice à différent moment dans le temps, il est possible

d'obtenir un front d'onde ayant une géométrie et une direction désirée. Par exemple, lorsque les transducteurs sont excités un après l'autre dans l'ordre avec un délai entre les éléments toujours de même valeur, on peut générer un front d'onde à angle par rapport à l'émetteur comme illustré à la figure suivante. De façon similaire, en utilisant un agencement de délai plus complexe, il est possible de focaliser la pression acoustique sur un point bien précis. Ainsi, il est possible de balayer une région à l'aide de la formation de faisceaux afin d'obtenir une image. La figure 1.2 illustre ces deux cas.

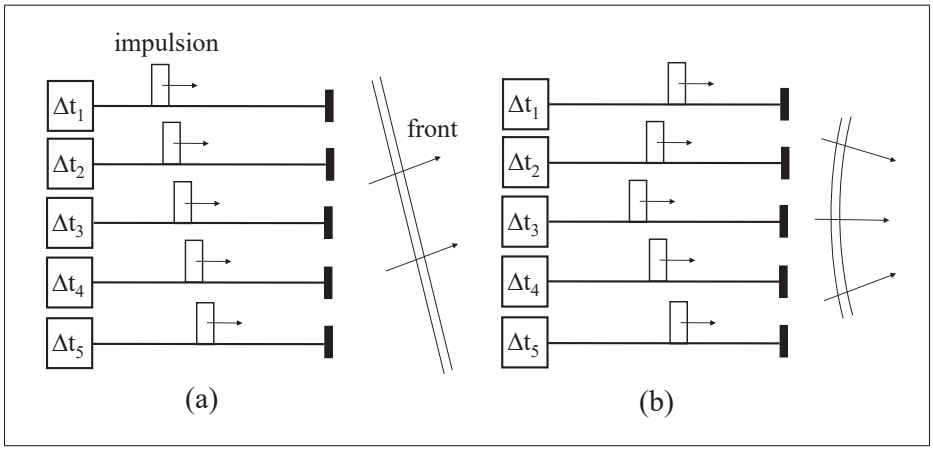

Figure 1.2 Formation de faisceaux : (a) Génération d'un front d'onde à angle par rapport à l'émetteur et formation et (b) focalisation de la pression en un point
Adaptée de Schmeer Jr. (2008)

Puisqu'à l'émission, les pulses sont délayés dans le temps, ils devront l'être aussi à la réception. Généralement, à la réception, les délais sont appliqués de façon à ce que les pulses soient tous reçus en même temps. On fait ensuite la somme des pulses reçus sur tous les éléments afin d'obtenir un seul pulse d'amplitude supérieure.

Puisque les éléments de la matrice sont adressés individuellement, il est aussi possible de varier l'amplitude de chaque élément indépendamment. Par exemple, pour réduire des lobes latéraux (side lobes) il est généralement pertinent d'émettre des pulses de plus grande amplitude avec les éléments du centre de la matrice et d'émettre des pulses d'amplitude inférieure sur les éléments

des côtés. Cette technique où les éléments sont excités avec l'amplitude variable est appelée apodization (Schmmer Jr, 2008).

1.2 Les transducteurs micromachinés

Les transducteurs piézoélectriques ultrasoniques conventionnels sont composés d'une couche de matériau piézoélectrique disposée entre deux électrodes. Il s'agit de la technologie qui domine actuellement le monde de l'imagerie par ultrasons (Chen, 2010). La figure 1.3 présente le schématique d'un transducteur conventionnel.

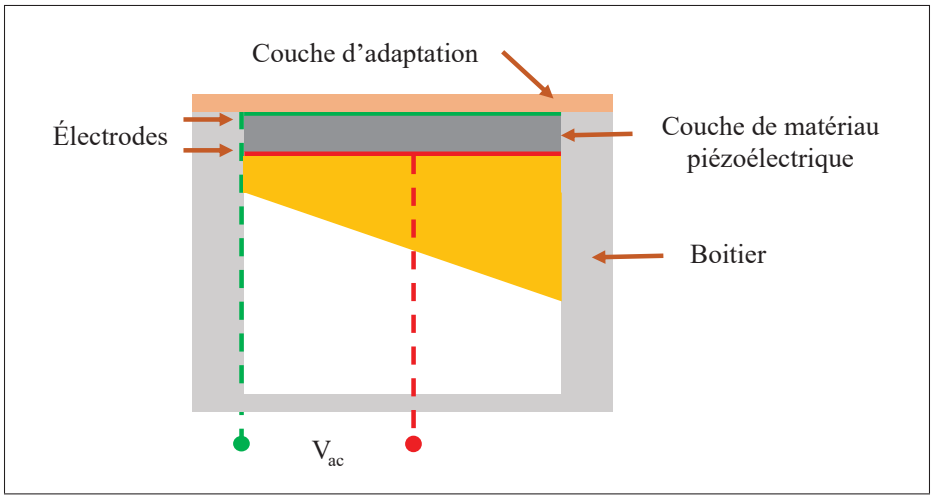

Figure 1.3 Schématique d'un transducteur conventionnel
Adaptée de Qiu (2015)

Le transducteur subit une vibration extensionnelle et la fréquence de résonance est donc dépendante de l'épaisseur de la couche piézoélectrique. Ces transducteurs posent plusieurs problèmes majeurs. L'impédance acoustique (rapport de la pression sur la vitesse de propagation) est beaucoup plus élevée que celle de l'air, de l'eau (34 MRayls contre 1.5 MRayls et 340 MRayls). Cela réduit l'énergie ainsi que la largeur de bande du signal transmis. Généralement, une couche d'adaptation est utilisée pour diminuer l'impact de ce problème. Toutefois, cette couche doit avoir une épaisseur et des propriétés bien précises difficiles à obtenir surtout à des fréquences plus élevées (Akasheh, Myers, Fraser, Bose & Bandyopadhyay, 2004a). Ainsi, la

fabrication d'un seul élément est complexe. Puis, la réalisation de matrice avec une haute densité d'éléments, nécessaire pour faire de la formation de faisceaux et augmenter la résolution ajoute un niveau de complexité puisque tous les éléments doivent avoir les mêmes propriétés (Qiu, Gigliotti, Wallace, Griggio, Demore, Cochran & Trolier-McKinstry, 2015a). Finalement, les transducteurs conventionnels sont souvent fabriqués à l'aide de bandes de PZT (une céramique à base de plomb) difficile à miniaturiser et généralement de l'ordre des millimètres. Or pour effectuer de l'imagerie haut résolution, des pixels de plus petite taille de l'ordre des centaines ou des dizaines de micromètres sont nécessaire (Muralt, Ledermann, Paborowski, Barzegar, Gentil, Belgacem, Petitgrand, Bosseboeuf & Setter, 2005). En poussant les limites de cette technologie, il est possible d'effectuer de l'imagerie 4D mais, pour les raisons énumérées plus haut, le cout de ces appareils est très élevé. Ainsi, quoique grandement utilisée, cette technologie est peu adaptée à l'imagerie par ultrason et est très couteuse.

Un nouveau type de transducteurs, les transducteurs ultrasoniques micromachinés (MUT) promettent de résoudre ces problèmes. Ils sont constitués de membranes qui vibrent de haut en bas s'apparentant en quelque sorte à un hautparleur. Il existe deux types de MUT, les transducteurs ultrasoniques capacitifs micromachinés (CMUT) et les transducteurs ultrasoniques piézoélectriques micromachinés (PMUT). Les matrices de transducteurs faites avec cette technologie sont beaucoup plus faciles à fabriquer, peuvent aisément être produites à la chaine, sont compatibles avec le procédé CMOS et peuvent être fabriquées directement sur le circuit intégré, tout en présentant des performances semblables voir meilleures que celles des transducteurs conventionnels (Gurun, Qureshi, Balantekin, Guldiken, Zahorian, Peng, Basu, Karaman, Hasler & Degertekin, 2008).

Les CMUT sont constitués d'une membrane métallisée suspendue au-dessus d'un substrat qui est lui aussi métallisé. Lorsqu'une différence de potentiel DC est appliquée entre la membrane et le substrat, la membrane est attirée vers le substrat par force électrostatique. Puis, lorsque la différence de potentiel est remise à zéro, la membrane retourne à sa position initiale par force mécanique. Ainsi, en appliquant une tension AC, il est possible d'induire une oscillation dans la membrane et de générer des ondes acoustiques (Jin, Ladabaum & Khuri-Yakub, 1998).

Les CMUT présentent de nombreux avantages. En raison de leur mode de vibration, l'impédance acoustique est beaucoup plus basse se rapprochant de celle de l'air, l'eau et des tissus. Ainsi, l'adaptation acoustique vers le milieu est meilleure ce qui permet d'avoir une plus grande largeur de bande et une meilleure résolution d'image (Caronti, Caliano, Carotenuto, Savoia, Pappalardo, Cianci & Foglietti, 2006). De plus, il a été démontré que la pression acoustique générée par les CMUT est plus élevée que celle des transducteurs conventionnels et que le couplage électromécanique lui est comparable (Eccardt & Niederer, 2000). Aussi, il est plus simple et moins couteux de fabriquer des CMUTs de petite taille et ainsi d'en intégrer un grand nombre dans des matrices à haute densité de transducteurs. Pour cette raison, les CMUTs ont gagné en popularité dans le domaine de la recherche sur les transducteurs pour l'imagerie 3D (Oralkan, Ergun, Cheng, Johnson, Karaman, Lee & Khuri-Yakub, 2003). Finalement, la couche d'adaptation devient moins nécessaire, ce qui peut diminuer grandement la complexité du système. Puis, en raison du mode de vibration, la fréquence de résonance dépend surtout du diamètre et non plus de l'épaisseur. Pour ajuster la fréquence, il suffit de modifier le diamètre ce qui facilite le design.

Pour pouvoir fonctionner à la réception, il faut appliquer une tension DC de polarisation entre les électrodes du CMUT en plus du signal AC. Lorsqu'une onde acoustique percute la membrane, la capacité du CMUT subit une variation et un signal est perçu. Généralement, la tension DC appliquée est près de la tension d'affaissement ce qui peut entrainer la destruction du CMUT (Bayram, Hæggstrom, Yaralioglu & Khuri-Yakub, 2003). Aussi, la tension DC appliquée doit généralement être assez élevée ce qui complexifie la conception. La figure 1.4 présente le schématique d'un CMUT.

Les PMUTs sont constitués d'une couche piézoélectrique disposée entre deux électrodes. Le tout est placé sur une membrane qui comme pour les CMUT est suspendue. Lorsqu'une différence de potentiel est appliquée entre les deux électrodes, la couche piézoélectrique subit une déformation. La structure entre en résonance lorsqu'une tension AC de fréquence appropriée est appliquée. Or, puisque la membrane est ancrée sur son périmètre, elle se voit contrainte de se déplacer perpendiculairement au plan (Perçin & Khuri-Yakub, 2002). Il s'agit donc d'un dispositif

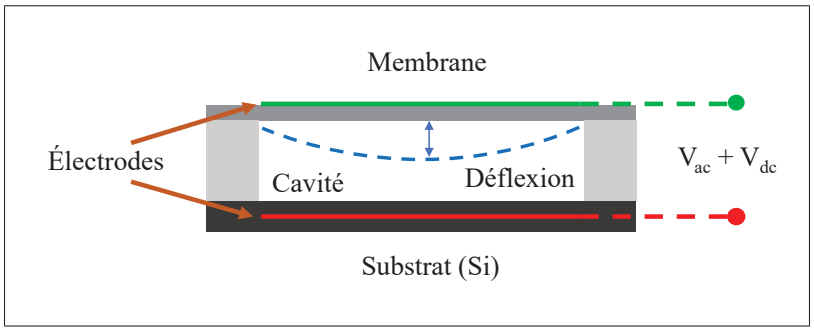

Figure 1.4 Schématique d'un CMUT
Adaptée de Qiu (2015)

piézoélectrique de flexion et non pas extensionnel comme c'est le cas pour les transducteurs conventionnels. Le déplacement de la membrane des CMUT et des PMUT est donc similaire et tout comme pour les CMUT, la fréquence de résonance dépend surtout du diamètre de la membrane et l'impédance acoustique est plus basse que celle des transducteurs conventionnels. La figure 1.5 présente le schématique d'un PMUT.

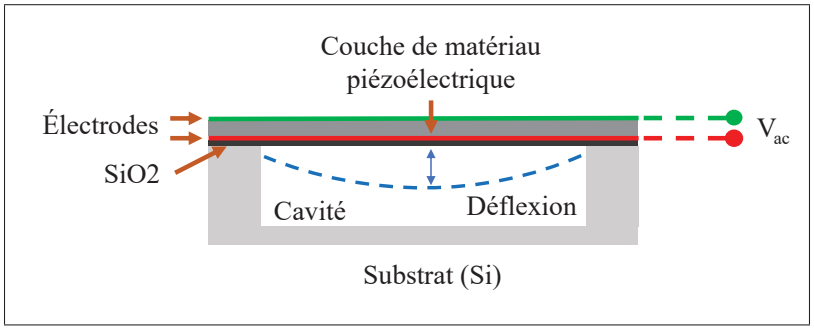

Figure 1.5 Schématique d'un PMUT
Adaptée de Qiu (2015)

Les PMUT présentent plusieurs avantages par rapport aux CMUT. Tout d'abord, une tension DC de polarisation n'est pas nécessaire. Aussi, les PMUT ont une haute sensibilité, un haut ratio entre la pression émise et la tension appliquée. Ainsi, une tension électrique inférieure est suffisante pour obtenir la même pression acoustique émise par un CMUT. Finalement, les électrodes étant généralement plus rapprochées, la capacité des PMUT est plus élevée que celle des CMUT ce qui permet de minimiser les effets négatifs des parasites du système électrique sur

la sensibilité et le couplage du transducteur et d'augmenter la sensibilité et le ratio signal sur bruit (SNR) (Akasheh, Fraser, Bose & Bandyopadhyay, 2005a).

Chaque PMUT peut être utilisé comme émetteur ou récepteur de façon aussi efficace. Ce n'est pas tout à fait le cas pour les CMUT. En effet, à la réception, le CMUT doit être le plus sensible possible. Ainsi, il est souhaitable d'avoir des électrodes le plus près possible. À l'émission, par contre, il est nécessaire d'avoir le signal acoustique le plus élevé possible. Pour ce faire, on doit laisser suffisamment de place à la membrane pour se déplacer et il faut donc avoir une distance entre les électrodes plus grandes qu'à l'émission et ainsi des CMUT d'architecture différente à l'émission et à la réception (Akasheh *et al.*, 2004a).

Ensuite, la distance entre les électrodes des PMUT est fixe ce qui n'est pas le cas pour les CMUT. En effet, dans les CMUT une des électrodes est sur le substrat et l'autre sur la membrane. Lorsque la membrane bouge, la distance entre les électrodes est modifiée. De ce fait, les PMUT présentent une meilleure linéarité que les CMUT.

Ainsi, les PMUT sont quant à leurs caractéristiques électriques et mécaniques très souvent supérieures aux autres technologies considérées. Ils ont une plus haute linéarité et sensibilité, un signal sur bruit plus élevé et une bande passante plus grande et une impédance acoustique se rapprochent du milieu en observation. De plus, ils nécessitent une tension d'activation plus faible, ne nécessitent pas de tension de polarisation DC et la même architecture peut-être utilisée à l'émission et à la réception. Pour toutes ces raisons, les PMUT peuvent être considérés comme un excellent candidat pour devenir les transducteurs ultrasoniques du futur. Dans la prochaine section, les avancements de la recherche sur les PMUT seront présentés.

1.3 Les transducteurs ultrasoniques piézoélectriques micromachinés (PMUT)

1.3.1 Formation de faisceaux

Dans plusieurs travaux, des matrices de PMUT sont utilisées pour permettre de faire de la formation de faisceaux. Toutefois, très peu d'articles (Dausch, Gilchrist, Carlson, Hall,

Castellucci & von Ramm, 2014a) utilisent seulement la formation de faisceaux pour faire l'imagerie. Dans plusieurs articles la surface à imager est trop grande pour être imagée en une seule fois. De ce fait, souvent un balayage mécanique est combiné à la formation de faisceaux afin de pouvoir couvrir toute la surface à caractériser (Lu, Tang, Fung, Wang, Tsai, Daneman, Boser & Horsley, 2015a), (Tang, Lu, Fung, Horsley & Boser, 2015)), ((Przybyla, Tang, Guedes, Shelton, Horsley & Boser, 2015). De plus, la plupart utilisent à la réception seulement un petit nombre de PMUT par exemple la colonne du milieu de la matrice. Plusieurs réussissent certes à obtenir des images d'une certaine qualité. En optimisant les PMUT, en utilisant des matrices de plus grande taille et en utilisant tous les PMUT à la réception, il serait possible de couvrir de plus grandes surfaces et d'éliminer la nécessité d'utiliser le balayage mécanique.

Dans un réseau à commande de phase (phased array), la distance centre à centre entre les éléments doit être plus petite que la moitié de la longueur d'onde pour éviter les lobes latéraux. Cela implique qu'il faut utiliser des PMUT de taille très petite ce qui est problématique, car le couplage acoustique diminue rapidement pour un PMUT donc le diamètre est plus petit qu'une longueur d'onde (Shelton, Rozen, Guedes, Przybyla, Boser & Horsley, 2014). Une technique pour augmenter le couplage acoustique consiste à utiliser un « tube de couplage » qui est en quelque sorte un guide d'onde (Shelton *et al.*, 2014). Cela fonctionne bien pour des fréquences basses et la longueur de tube optimale pour obtenir le gain maximal diminue avec l'augmentation de la fréquence.

Il est possible de modifier le signal appliqué aux bornes des PMUTs pour augmenter la pression acoustique. Par exemple, on peut appliquer une tension à l'émission au-delà du champ coercitif. L'effet piézoélectrique cause une élongation des cellules alors que le « domaine switching » permet d'aligner les cristaux dans la direction du champ électrique (Kungl, Theissmann, Knapp, Baehtz, Fuess, Wagner, Fett & Hoffmann, 2007). En appliquant une tension à l'émission au-delà d'une tension de seuil, la pression augmente rapidement pour finalement saturer (Dausch, Gilchrist, Carlson, Castellucci, Chou & Von Ramm, 2010). Une autre technique consiste à terminer l'émission de la dernière période du sinus prématurément afin de conserver une

polarisation positive du PMUT. En d'autres mots, appliquer une tension DC aux bornes du PMUT avant la réception permet d'augmenter la pression du signal reçu (Dausch *et al.*, 2010).

1.3.2 Matériaux piézoélectriques utilisés dans la fabrication des PMUT

Le PZT est un matériau qui présente d'excellentes propriétés piézoélectriques ce qui lui vaut sa popularité pour la fabrication de transducteurs ultrasoniques. Les PMUT ne font pas l'exception, et l'utilisation du PZT pour leur fabrication est bien documentée (Muralt *et al.*, 2005), (Baborowski, Ledermann & Muralt, 2002). Ce matériau est à base de plomb ce qui n'est pas très écologique et voué à disparaitre de l'industrie de l'électronique (Li, Moon & Wong, 2005). De plus, il n'est pas CMOS compatible et ne permet pas une intégration monolithique.

L'Aln, un matériau alternatif au PZT qui est souvent utilisé pour la fabrication de PMUT (Guedes, Shelton, Przybyla, Izyumin, Boser & Horsley, 2011), (Lu *et al.*, 2015a), (Shelton *et al.*, 2014). L'Aln est CMOS compatible et beaucoup plus écologique que le PZT. Malgré le fait que l'Aln ait un coefficient piézoélectrique beaucoup plus bas que le PZT, il a aussi une basse constante diélectrique ce qui permet d'obtenir une sensibilité comparable. Il a été démontré que ce matériau est un bon choix pour la fabrication de PMUTs (Lu, Heidari & Horsley, 2014).

Un autre matériel incontournable dans le monde de l'imagerie par ultrason est le PVDF (Polyvinylidene fluoride) dont les premières utilisations dans ce domaine remontent à plus de 30 ans (Ohigashi, Nakanishi, Itoh, Suzuki & Omoto, 1979). Le couplage électromécanique du PVDF est inférieur à celui du PZT réduisant sa performance ce qui explique pourquoi le PZT est plus largement utilisé dans les matrices de transducteurs effectuant la formation de faisceaux (Foster, Harasiewicz & Sherar, 2000). Or, ce matériau permet d'obtenir une bande passante plus large ce qui est tout à fait ce dont on a besoin pour l'imagerie par ultrason à haute résolution d'image (Carey, Gregory, Brewin, Birch, Ng & Hatfield, 2004).

Le PVDF est CMOS compatible, peu couteux et facile à polariser (Chao, Lam, Kwok & Chan, 2006). De plus, il a une impédance acoustique plus près de celles des milieux imagés et plus basse que celle de l'Aln et du PZT, ce qui permet d'éliminer la nécessité d'avoir une couche

d'adaptation pour maximiser le transfert d'énergie vers le domaine acoustique (Ramadan, Sameoto & Evoy, 2014).

Certains travaux récents utilisent le PVDF dans la fabrication des PMUT. Par exemple, une matrice de PMUT ciblant les applications de rétroaction haptique à base de PVDF pour l'intégration directe sur de grands écrans a été fabriquée (Halbach, Gijsenbergh, Jeong, Devriese, Gao, Billen, Torri, Chare, Cheyns, Rottenberg et al., 2019). Aussi, des matrices de PMUT à multiples fréquences de résonance à base de PVDF ont été fabriquées (Gao, Gijsenbergh, Halbach, Serrahima, Torri, Jeong, Billen, Cheyns, Haouari, Rottenberg et al., 2019).

1.3.3 Technique de fabrication des membranes suspendues

La fabrication des PMUT est à plusieurs égards plus simple que celle des CMUT et des MUT conventionnels. Toutefois, elle présente plusieurs défis. L'enjeu est de fabriquer des matrices de haute densité et composées de membranes de petit diamètre qui soient suspendues. Une première technique est l'utilisation du procédé DRIE pour faire des trous à travers la gaufre de silicium et ainsi relâcher les membranes. Avec cette technique, la distance entre les membranes et donc la densité sont limitées par l'épaisseur de la gaufre et la précision du procédé. Il est possible d'atteindre une distance entre les membranes de 50 μm (Eovino, Liang & Lin, 2019).

Un autre problème avec cette technique est le fait que la fréquence de résonance de la membrane est influencée par les variations de diamètre des trous. Toutefois, il est possible de minimiser cette influence en utilisant un procédé DRIE en deux étapes (Liao, Liu, Rogers, Usmani, Tang, Wang, Jiang & Xie, 2013). L'utilisation du procédé DRIE

Une autre technique pour fabriquer des membranes suspendues est l'utilisation d'une gaufre de type « cavitySOI ». Des trous d'une certaine profondeur sont gravés dans une gaufre de silicium avant d'ajouter la couche d'oxyde et de silicium. La figure suivante illustre le procédé (http ://www.icemostech.com/).

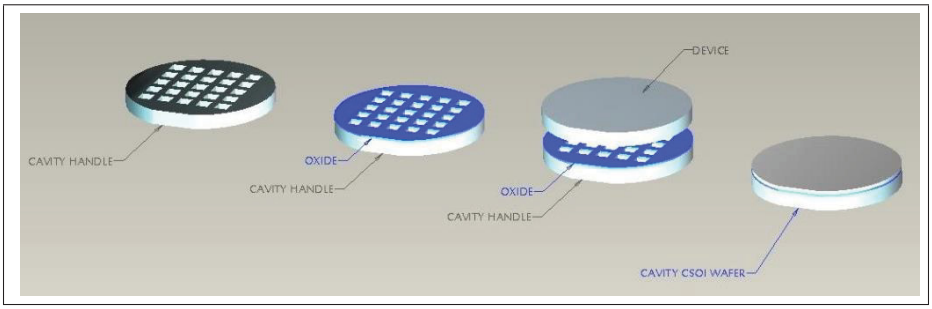

Figure 1.6 Schéma de fabrication d'une gaufre de silicium de type cavity SOI
http ://www.icemostech.com
(Consulté le janvier 2020)

Cette technologie permet d'atteindre une résolution et densité plus élevée qu'avec le procédé DRIE (Liu, He, Wang, Zhou, Xu, Smagin, Toubal, Yu, Gu, Xu et al., 2019), (Lu & Horsley, 2015), (Wang & Lee, 2015), (Lu, Tang, Fung, Boser & Horsley, 2015e). Finalement, une dernière technique consiste à graver la cavité sous la membrane à même le dessus de la gaufre. Pour ce faire, un trou est fait dans la membrane ou à côté de la membrane (Lu, Rozen, Tang, Smith, Fung, Boser, Polcawich & Horsley, 2015d), (Lu *et al.*, 2014).

Finalement, la génération d'ondes acoustiques à l'aide de PMUT miniature présente certains défis. En effet, lorsque le diamètre de ceux-ci est petit la pression acoustique qu'il peut fournir diminue rapidement. Une solution a été proposée qui consiste à connecter plusieurs PMUT de petite taille en parallèle. De cette façon, la pression de tous les PMUT est additionnée tout en conservant la même fréquence (Cheng, Dangi, Ren, Tiwari, Benoit, Qiu, Lay, Agrawal, Pratap, Kothapalli et al., 2019), (Lu *et al.*, 2014).

1.3.4 Circuit intégré pour la formation de faisceaux

Les réseaux à commande de phase permettent d'ajuster la profondeur de champ et d'effectuer un balayage 3D. Comme il a été expliqué à la section 3.1, à l'émission, les signaux sont envoyés aux transducteurs délayés dans le temps afin de concentrer l'énergie acoustique à l'endroit désiré. À la réception, les signaux sont alignés dans le temps et additionnés afin d'obtenir un signal de plus grande amplitude. La communication avec les transducteurs peut être faite à l'aide de

câbles coaxiaux connectés à un microcontrôleur ou un FPGA pour effectuer la génération et le traitement des signaux. Or, un grand nombre de connexions serait nécessaire et le système serait volumineux. Une approche pour limiter le nombre de connexions est de multiplexer les signaux pour n'avoir qu'une connexion.

Une approche plus prometteuse est l'utilisation d'un circuit intégré dédié et directement connecté aux transducteurs. Les connexions peuvent être faites à l'aide de câblage par fil (wire bonding) (Gurun, Zahorian, Sisman, Karaman, Hasler & Degertekin, 2012) ou à l'aide de la technologie puce retournée (flip microplaquette) (Wygant, Zhuang, Yeh, Oralkan, Ergun, Karaman & Khuri-Yakub, 2008), (Wygant, Jamal, Lee, Nikoozadeh, Oralkan, Karaman & Khuri-Yakub, 2009), (Tang *et al.*, 2015), (Bhuyan, Choe, Lee, Wygant, Nikoozadeh, Oralkan & Khuri-Yakub, 2013). Il est aussi possible d'effectuer une intégration monolithique. Un circuit intégré est fabriqué à l'aide d'une technologie commerciale puis les transducteurs sont fabriqués directement sur le dé de silicium (Jiang, Lu, Tang, Tsai, Ng, Daneman, Boser & Horsley, 2017), (Gurun *et al.*, 2014), (Rozen, Block, Mo, Bland, Hurst, Tsai, Daneman, Amirtharajah & Horsley, 2016). Cette technique permet de réduire les capacités parasitiques et la taille du dispositif au maximum. De plus, pour augmenter la résolution d'image, il faut augmenter le nombre de transducteurs et donc le nombre de connexions ce qui rend cette approche d'autant plus intéressante.

Finalement, depuis très peu de temps, il existe une une platforme MEMS-on-CMOS de la compagnie SilTerra qui permet la fabrication de MEMS piezoélectriques directement sur circuit CMOS. Tout récemment, des PMUTS sur circuit CMOS ont été fabriquiés utilisant cette technologie (Ledesma, Zamora, Torres, Uranga, Tzanov, Barniol, Marigo & Soundara-Pandian, 2019), (Chan, Patel, Barniol, Bhowmick, Cases & Wong, 2020), (Zamora, Ledesma, Uranga & Barniol, 2020).

CHAPITRE 2

FREQUENCY TUNING TECHNIQUE OF PIEZOELECTRIC ULTRASONIC TRANSDUCERS FOR RANGING APPLICATIONS

Alexandre Robichaud[1], Dominic Deslandes[1], Frederic Nabki[1], Paul-Vahé Cicek[2]

[1] Département de Génie électrique, École de Technologie Supérieure,
1100 Notre-Dame Ouest, Montréal, Québec, Canada H3C 1K3
[2] Département d'informatique, Université du Québec à Montréal,
201, avenue Président-Kennedy, Montréal, Québec, Canada H2X 3Y7

Article soumis à la revue « IEEE Journal of Microelectromechanical Systems » en mai 2018.

This paper proposed a novel technique for PMUT frequency tuning that is low cost and effective, requiring only a post-processing step in the form of a Parylene-C thin film deposition. Moreover, a simple theoretical model was developed to predict the resonance frequency of partially clamped membranes, allowing for more effective design of this type of PMUT. Results confirm that the post-processing technique can be used to accurately tune the frequency of high Q-factor PMUTs in order to optimize the transmission characteristic between two PMUTs despite fabrication process variations. In this fashion, chip-to-chip communication between two devices initially at different resonance frequencies was achieved, with significantly-improved transmission efficiency and ranging capability.

2.1 Introduction

Conventional ultrasonic transducers pose challenges in terms of efficiency, fabrication complexity and implementation costs. Moreover, they are typically bulky and difficult to integrate. Alternatively, capacitive micromachined ultrasonic transducers (CMUTs) and piezoelectric micromachined ultrasonic transducers (PMUTs) are generating sustained interest as a means to overcome these limitations. These devices are fabricated using microfabrication processes and techniques originating from MEMS and semiconductor technologies, and therefore can be mass produced at very low cost and can also be made amenable to monolithic integration with CMOS electronics (Gurun *et al.*, 2014 ; Lemmerhirt *et al.*, 2012 ; Tang, Lu, Jiang, Ng, Tsai,

Horsley & Boser, 2016a ; Zahorian, Hochman, Xu, Satir, Gurun, Karaman & Degertekin, 2011a). A CMUT consists of a suspended conductive membrane separated from an electrode by an air gap. The CMUT is biased with a DC voltage and excited with an AC signal to make the membrane vibrate, thus producing acoustic waves. In order to maximize performance, the CMUT must usually be biased near its pull-in voltage, increasing the likelihood of device failure (Akasheh *et al.*, 2005a). Also, the optimal gap size is different for transmission and reception, causing the need for a different structure for each case (Akasheh *et al.*, 2004a). PMUTs, on the other hand, are operated by means of the piezoelectric effect. PMUTs do not require a DC bias voltage, and the same structure can be used for both transmission and reception. Moreover, a lower AC voltage is required, and the signal to noise ratio of PMUTs is generally higher than that of CMUTs (Qiu *et al.*, 2015a). PMUTs have successfully been demonstrated in several applications like distance sensing (Przybyla, Flynn, Jain, Shelton, Guedes, Izyumin, Horsley & Boser, 2011b), gesture recognition (Przybyla, Tang, Shelton, Horsley & Boser, 2014a) and medical imaging (Dausch *et al.*, 2010,1). Fabrication of state-of-the-art PMUT arrays presents several challenges, as they require a large number of elements (Lu, Heidari & Horsley, 2015c ; Zahorian *et al.*, 2011a). Moreover, all transducer elements are expected to have almost identical resonant frequencies. The conventional fabrication process uses a silicon on insulator (SOI) substrate and releases the PMUT's membrane by using a deep reactive-ion etch (DRIE) process to etch trenches through the entire thickness of the substrate wafer (Dausch, Castellucci, Chou & Von Ramm, 2008a ; Dausch *et al.*, 2014a ; Guedes *et al.*, 2011 ; Wang, Miao & Zhu, 2008). The main disadvantage thereof lies in the fact that the resonant frequency becomes dependent of the trench diameter and thus process variations. Hence, this approach tends to produce PMUTs having resonant frequencies with large inter-chip variance. Although it is possible to reduce this effect by using a two-step DRIE process (Liao *et al.*, 2013), two masks are then necessary and the required fabrication process becomes more complex and costly. Another reported technique is based on cavitySOI wafers to fabricate suspended membranes (Lu & Horsley, 2015 ; Lu *et al.*, 2015e ; Wang & Lee, 2015). CavitySOI wafers are provided with pre-fabricated cavities between the insulating and silicon layers, with very accurate dimensions that can be selected by the customer. This approach is suitable for producing high quality PMUTs, although it is more expensive. Finally, it is also

possible to release the membrane by etching from above. To do so, an opening must be made in the membrane to allow a selective etchant to remove a sacrificial layer from underneath the membrane (Lu *et al.*, 2015c,1 ; Mehdizadeh & Piazza, 2017). This technique and affects membrane geometry. Furthermore, it has been shown that a trench going through the substrate can be used to improve acoustic power transmission if designed to act as an acoustic waveguide (Lu, Tang, Wang, Fung, Tsai, Daneman, Boser & Horsley, 2015b ; Shelton *et al.*, 2014), which is not possible with the aforementioned top-side release approach. The quality (Q) factor of PMUTs is generally higher than their capacitive counterparts (Smyth & Kim, 2015a). Some reported values of Q-factor range from 20 to 135 (Lu *et al.*, 2015c ; Muralt *et al.*, 2005 ; Przybyla *et al.*, 2011b). Accordingly, without decreasing their Q-factor, PMUTs are not ideal candidates for pulse echo imaging with high axial resolution, for which a wide transducer bandwidth is desirable to reduce the acoustic pulse duration. Some effective techniques to increase the bandwidth of an ultrasonic transducer have been proposed, such as the deposition of a damping layer (Lu *et al.*, 2015c) or signal processing like pulse compression (Jensen, Holm, Jerisen, Bendsen, Nikolov, Tomov, Munk, Hansen, Salomonsen & Hansen, 2005 ; Misaridis & Jensen, 2005a,0,0). On the other hand, PMUTs generally produce high acoustic power which makes them appealing for distance ranging or continuous wave imaging despite their high Q-factor. Generally, the resonance frequency of a high Q-factor device must be precisely adjusted to meet the specifications of the driving electronics so as to maximize efficiency. In this work, a PMUT is proposed for ranging applications. The device is optimized to maximize output acoustic power at the target frequency, resulting in a PMUT with a relatively high Q-factor. Therefore, it is critical for the device to have its resonant frequency match the application frequency to reduce path loss and achieve maximum power transfer. Accordingly, a novel low-cost technique for the frequency tuning of PMUTs fabricated using the PiezoMUMPS SOI commercial fabrication process is presented. With the base technology, membranes are released by DRIE and suffer from the frequency matching issues detailed earlier. The tuning technique presented in this paper requires one additional post-processing step that consists in a conformal deposition of a thin layer of Parylene-C (C16H12Cl2) on top of the PMUT. No additional photolithography or patterning is necessary, and the effect on the resonant frequency can be accurately predicted. The application

cases for the proposed method focus on single transducer devices or small arrays thereof since Parylene deposition simultaneously occurs on all elements of a chip and results in a uniform frequency tuning of all exposed elements. Similarly to integrated circuits, MEMS can be batch produced using micro-fabrication processes, allowing for very low production costs per unit. The additional processing proposed in this work can effortlessly be incorporated in the batch production process, with no extra photolithographic mask required. As such, any cost increase is expected to be marginal with respect to baseline device fabrication. The paper first presents the theory and modeling of the PMUT, then outlines its design and fabrication, and reports on the measurement results. Deposition of Parylene on the entire wafer allows for coarse tuning of the average resonant frequency of all the PMUTs, which may be sufficient for many use cases since intra-wafer process variations are relatively low. However, for more precise tuning, the gradient of the resonant frequency over a wafer could be estimated by sampling the characteristics of a PMUT device in a given region, with the region size depending on the level of tuning precision required, and repeating the process to cover the entire wafer. At the assembly stage, dies from the wafer could be separated and categorized by region, with each subset tuned independently using Parylene deposition. In this scenario, a designer would need to set a trade-off between tuning accuracy and overall calibration costs. For extreme accuracy, each PMUT could be tuned independently, although at the expense of parallelization and costs.

2.2 Theory and Modeling

The PMUT is a multi-layer device that can be modeled as a clamped circular plate, as reported in (Perçin, 2003 ; Perçin & Khuri-Yakub, 2002 ; Sammoura & Kim, 2012). The silicon layer acts as a structural membrane and as the bottom electrode, the aluminium nitride layer acts as the piezoelectric layer and the aluminium layer as the top electrode. Also, a layer of Parylene-C is deposited on top of the device to adjust the resonant frequency. Hence, the PMUT has a total of 4 layers, as depicted in Fig. 2.1.

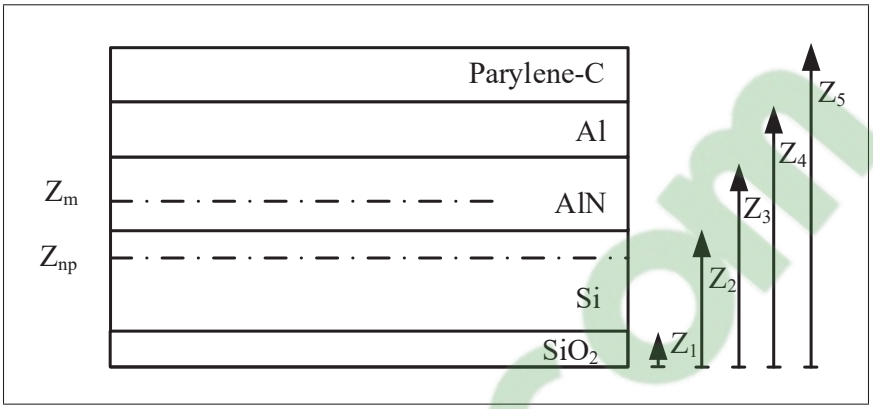

Figure 2.1 Representation of the multi-layer PMUT for the calculation of the neutral plane

The neutral plane Z_{np}, i.e. the plane of the device where internal stress is zero (Muralt *et al.*, 2005), is calculated as a function of the Young's modulus and Poisson ratio of each layer such that (Dubois & Muralt, 1998).

$$Z_{np} = \frac{1}{2}\left[\sum\left(\frac{Y_n\left(z_n^2 - z_{n-1}^2\right)}{1-\nu_n^2}\right)\Big/\sum\left(\frac{Y_n t_n}{1-\nu_n^2}\right)\right], \tag{2.1}$$

where z_n is the z position of the upper part, Y_n the Young's modulus, υ_n the Poisson ratio and t_n the thickness of layer n. Using (11), the flexural rigidity and the mass per area as a function of the neutral plane can be expressed as (Muralt *et al.*, 2005) :

$$D = \frac{1}{3}\sum Y_n \frac{\left(z_n - Z_{np}\right)^3 - \left(z_{n-1} - Z_{np}\right)^3}{3\left(1-\upsilon_n^2\right)} \tag{2.2}$$

$$\mu = \sum \rho_n t_n. \tag{2.3}$$

The resonance frequency can be calculated using the following equation (Reddy, 2006) :

$$f_0 = \frac{\lambda^2}{2\pi r^2}\sqrt{\frac{D}{\mu}}, \tag{2.4}$$

where λ^2 is the root of Bessel functions for a specific resonance mode. Examples of values for different modes of interest are presented in Fig. 2.1.

Tableau 2.1 Value of λ_{ij} for selected modes.

λ_{ij}	**i = 0**	**i = 1**	**i = 2**
i = 0	10.2158	21.26	34.88
i = 1	39.771	60.82	84.58

The PMUT presented in this work is partially anchored using beams. This anchoring topology leads to a reduction of flexural rigidity. Indeed, a smaller anchored perimeter results in lower flexural rigidity. Hence, a correction factor, D_{corr}, representing the portion of the membrane that is anchored, is defined by taking the ratio of the anchored perimeter to the total perimeter of the membrane such that

$$D_{corr} = \frac{P_{anc}}{P_{tot,ex}}, \tag{2.5}$$

$$P_{tot,ex} = 2\pi\left(r + A_l\right), \tag{2.6}$$

$$P_{anc} = N_{anc}A_w, \tag{2.7}$$

where P_{anc} is the anchored perimeter, $P_{(tot,ex)}$ is the total perimeter, A_l is the length of the anchors, N_{anc} is the number of anchors, and A_w is the width of the anchors. From (14)-(17), the corrected resonant frequency can be given by

$$f_{0,corr} = f_0\sqrt{D_{corr}} \ . \tag{2.8}$$

This corrected frequency, as will be shown, provides a reasonable approximation of the impact of the anchors' rigidity.

2.3 Design and Fabrication

The PMUT devices were fabricated using the PiezoMUMPS process (Cowen, Hames, Glukh & Hardy, 2013), a cost-effective 5-mask technology. Fig. 2.2 illustrates the steps to fabricate a PMUT device. All layer thicknesses are dictated by the commercial technology and cannot be customized. The process starts with a SOI wafer, with a 400 nm thick insulator and a 10 μm thick device layer (Fig. 2.2a). The wafer is doped using a phosphosilicate glass (PSG) layer deposited onto the wafer and annealed for 1 hour at around 1000 ºC before being wet etched. After doping, the resistivity of the wafer lies between 1 and 10 $\Omega \cdot cm$. Afterwards, the pad oxide layer (200 nm) is thermally grown onto the wafer (Fig. 2.2b). Then, a photoresist is applied and patterned using standard photolithography, and finally the oxide layer is patterned by wet etching (Fig. 2.2c). This oxide layer prevents short circuits between the doped silicon layer acting as the bottom electrode and the aluminium top electrode later deposited. In the following step, a 500 nm aluminium nitride piezoelectric layer is deposited by sputtering (Fig. 2.2d). Subsequently, the aluminium nitride layer is patterned using standard lithography and wet etching in order to produce a circular membrane of 200 μm diameter (Fig. 2.2e). Then, a resist is deposited on top in preparation for lift-off of the aluminum pads (Fig. 2.2f). The resist is then patterned (Fig. 2.2g) through standard photolithography. Subsequently, a 1 μm thick aluminium layer is deposited by e-beam evaporation (Fig. 2.2h) and lifted off, leaving a circular aluminium layer with a 190 μm diameter and aluminium rectangles allowing electrical connections to the device (Fig. 2.2i). The diameter of the aluminium circle is smaller than that of the aluminum nitride in order to ensure no overlap with the bottom electrode. Later, the silicon device layer is etched by deep reactive-ion etching (DRIE), resulting in a circular silicon membrane and four anchors (Fig.

2.2j). The diameter of the silicon structure is larger than the aluminium nitride to ensure no overhang. Finally, the membrane is released by etching a trench from the back of the handle wafer by DRIE followed by a wet oxide etch (Fig. 2.2k) using a polyimide coating serving as protection material. Note that a front side protection material is used during this step. Finally, the device is post-processed to apply a variable thickness Parylene-C film onto it in order to tune its resonant frequency (Fig. 2.2l), as will be detailed later.

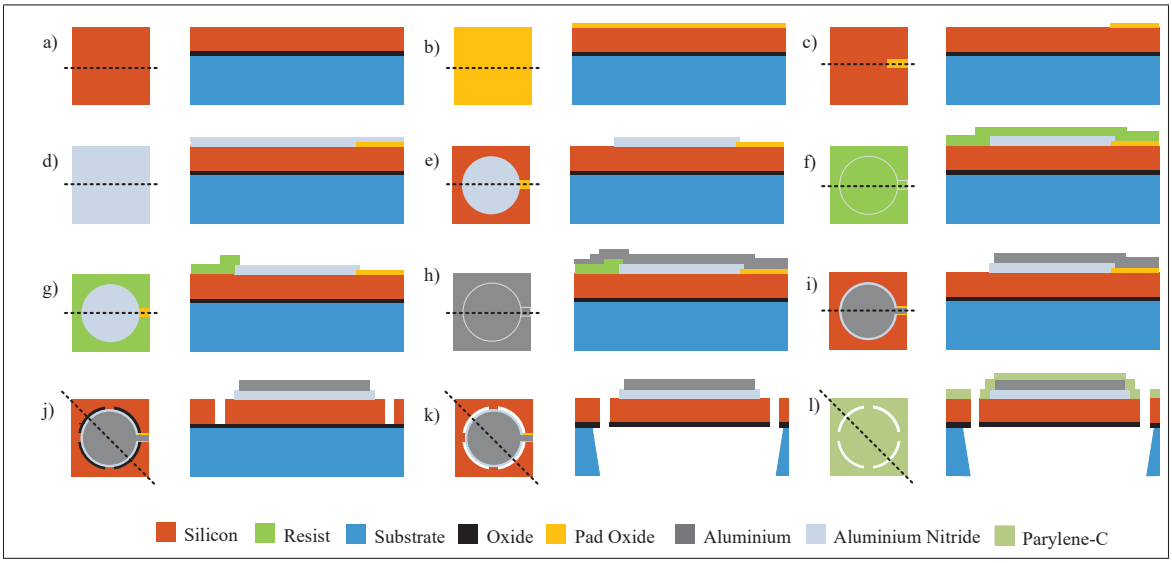

Figure 2.2 PiezoMUMPS process flow for the fabrication of a PMUT and post-processing.
a) SOI wafer, b) growth of thermal oxide, c) patterning of thermal oxide by wet etching,
d) deposition of aluminum nitride by reactive sputtering, e) AlN patterning by wet etching
f) resist deposition, g) resist patterning, h) aluminum pad deposition, i) resist removal,
j) DRIE etching of silicon, k) membrane release, and
l) post processing with Parylene-c coating

Fig. 2.3 shows SEM micrographs of a fabricated PMUT device and a PMUT matrix. The fabricated device is a 200 μm-radius suspended membrane anchored by four orthogonal beams. The anchors have a width of 20 μm and a length of 15 μm. A set of 4 PMUTs are connected in parallel. The doped silicon serves as the bottom electrode and is grounded. The aluminium layer constitutes the top electrode and is fed with the input signal.

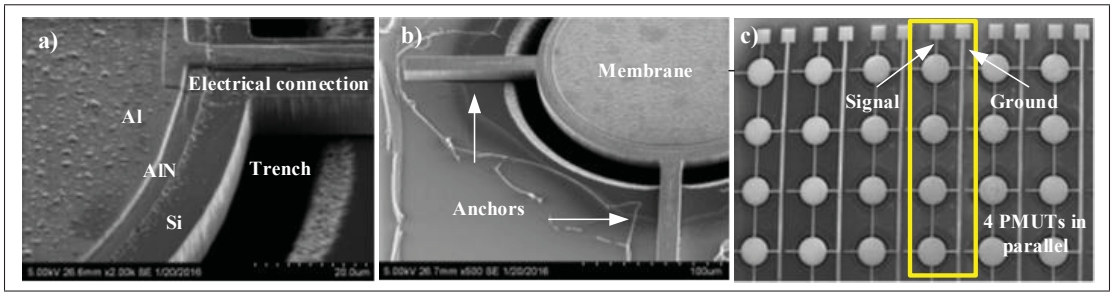

Figure 2.3 SEM micrographs of the fabricated PMUTs. a)-b) close-up of a device, and c) matrix of PMUTs, each column with 4 PMUTs connected in parallel

2.4 Simulations

Finite-element simulations were undertaken with COMSOL Multiphysics using the following physical parameters of the PiezoMUMPS technology : young's modulus (Y_n), Poisson's ratio (υ_n), density (ρ_n), thickness (t_n), piezoelectric constant (d_{31}), dielectric constant (ϵ_{33}) and transverse piezoelectric constant ($e_{(31,f)}$). The parameters are listed in Table 2.

To minimize simulation time while remaining accurate, the substrate was modeled as a tube of 400 μm thickness with an inner radius of 107 μm and an outer radius of 165 μm. A fixed displacement constraint was assigned to the outer perimeter of the tube. A 10 μm thick silicon membrane with 4 anchors of 20 μm width and 15 μm length was positioned above the tube. Finally, a 500 nm thin film of AlN and a 1 μm thin film of aluminum were positioned on top of the membrane. However, because of process variations, the dimensions of the fabricated devices were slightly different than designed. As such, an over etching of the membrane and trench of 2 μm and 6 μm respectively was estimated and taken into account in the simulations. Harmonic simulations of the deflection at the center of the membrane (i.e. r = 0) over a range of frequencies were performed in order to identify the resonance modes with high deflection and consequently high acoustic pressure output. Then, eigenfrequency simulations were carried-out for the determined resonance mode in order to identify the mode shape. Fig. 2.4 shows the results for the first and second modes of resonance.

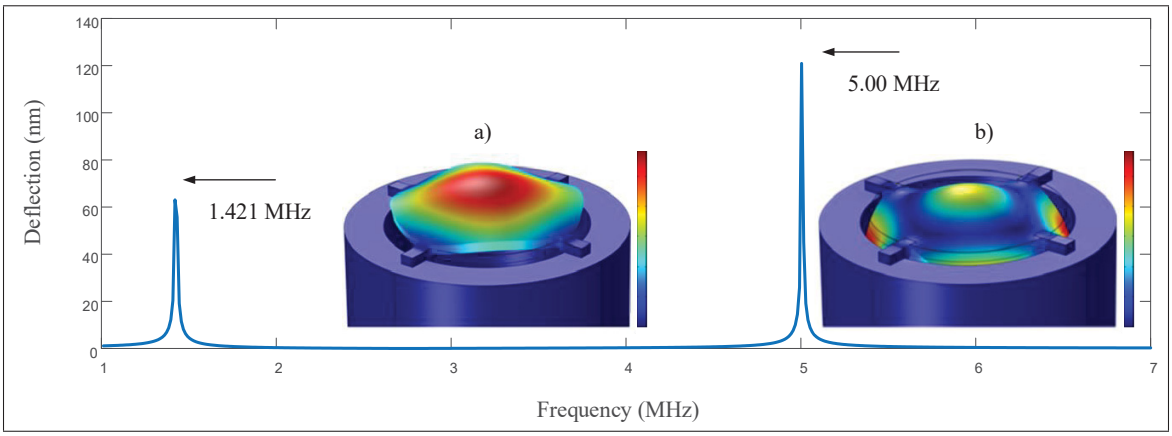

Figure 2.4 Harmonic simulation at the center of the membrane and eigenvalue simulation for the first (a) and second (b) modes of resonance of the PMUT without Parylene-C

In order to evaluate the impact of Parylene-C deposition on the PMUT resonance frequency, a thin film of Parylene-C was modeled on the top and sides of the suspended membrane. Four eigenfrequency simulations were performed with varying Parylene-C thicknesses of up to 1070 nm. Fig. 2.5 shows a comparison between simulated, theoretical and measured values. Measured values will be discussed in section IV-A. Theoretical calculations were performed following the procedure explained in the previous section for modes (0,0) and (0,1). One can see that the simulated and calculated values are in reasonable agreement, with the slopes of the graphs almost identical. However, the calculated values are slightly higher than the simulated ones, which may be related to the simplified frequency correction factor applied and also to the fact that the resonant modes do not correspond exactly to the modes of a perfectly clamped circular plate. Nonetheless, the theoretical approach remains a useful tool for initial approximation. Finally, one can see that, in simulation, by using only 1 μm of Parylene-C, the frequency of the first and second modes can be tuned over a range of 40 KHz and 100 KHz, respectively.

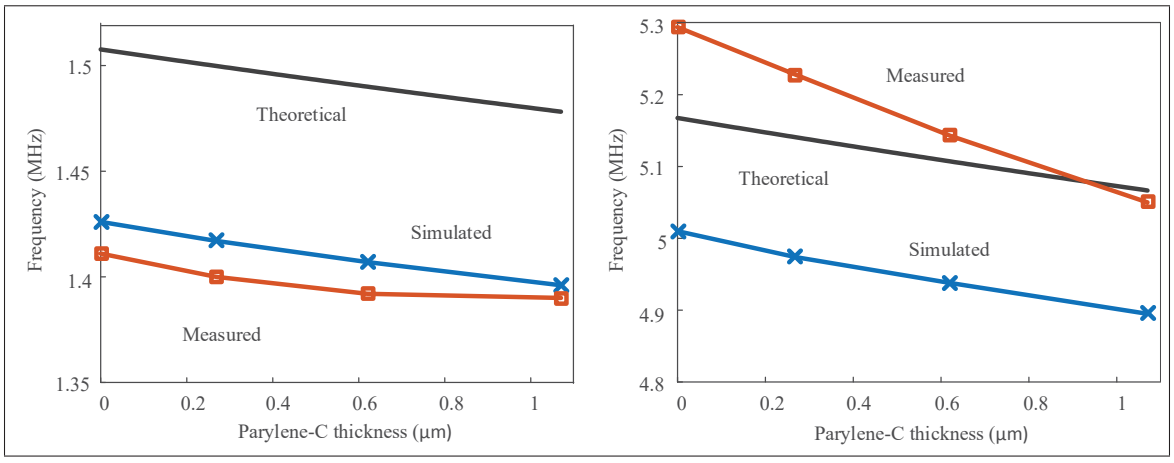

Figure 2.5 Comparison between theoretical, simulated and measured resonant frequencies as a function of Parylene-C thickness for the (a) first mode and (b) second mode of resonance

2.5 Electrical Characterisation Results

2.5.1 Effect of Parylene-C on eigenfrequency

Characterization was undertaken on 16 fabricated dies (totaling 128 sets of 4 PMUTs devices connected in parallel) using an EP6 Cascade Probe Station and an E5061B Keysight PNA Network Analyzer in combination with GSG probes. The power transferred (i.e. measured via the S12 scattering parameter) between both electrodes was measured in order to identify the resonant frequency. Due to process variations, significant inter-chip frequency deviation occurs. Indeed, according to the specificatiosn of the PiezoMUMPS technology, the trench size created by DRIE etching can vary by up to 50 μm. While variations to this extent were not observed during this work, trench dimension size variations of multiple micrometeres were observed across different chips. To quantify the frequency variation between chips, the standard deviation between the average frequency of the 16 dies was calculated. This value is 0.199 MHz for an average frequency of 1.3136 MHz. However, on a single die, trench size variation between different PMUT devices is moderate, resulting in a relatively precise resonant frequency for all of them and a standard deviation of 0.007 MHz. To verify the effect of adding Parylene-C, four

different thicknesses were deposited using the Parylene-C Deposition System Labcoter 2 (PDS 2010) : 180 nm, 280 nm, 620 nm and 1070 nm. Fig. 2.6 presents the results for the first and second modes, confirming that resonant frequency can effectively be tuned using Parylene-C. The deposition of 1 μm of Parylene-C allows for a reduction of resonant frequency of the first and second modes by 25 KHz and 250 KHz, respectively.

Tableau 2.2 List of the different physical parameters used to perform eigenfrequency simulation

Parameter	**Si**	**AlN**	**Al**
Y_n $[GPa]$	180	348	69
ν_n $[-]$	0.22	0.24	0.346
ρ_n $[g/cm^3]$	2.329	3.6	2.7
t_n $[m]$	10	0,5	1
d_{31} $[nC/N]$	-	-1.9e-12	-
ϵ_{33} $[-]$	-	9	-
$e_{31,f}$ $[C/m2]$	-	-0.58	-

The quality factor has been calculated based on the results presented in Fig. 2.6.

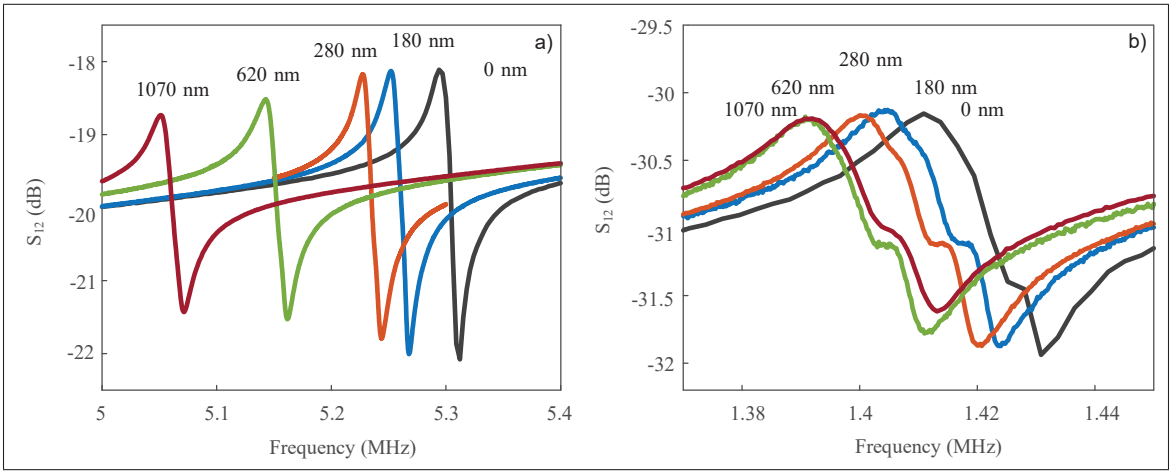

Figure 2.6 Measurement of the resonance frequency for different Parylene thicknesses for the (a) first mode and (b) the second mode of resonance

Because the resonance curve does not reach a peak of 3 dB, the calculation was performed using the phase derivative of the impedance as described in (Bi & Barber, 2008). First, the data of

Fig. 2.6 was fitted to a Butterworth van dyke equivalent circuit to determine its impedance. The quality factor was then calculated using the following equation :

$$Q_{s,p} = \frac{f}{2}\left|\frac{d\phi}{df}\right|_{f=f_s \text{ or } f_p} \tag{2.9}$$

where $Q_{(s,p)}$ is the quality factor at the resonance and anti-resonance frequencies. After depositing 1 μm of Parylene, for the first and second modes, the quality factor decreases from 10.6 to 8.7, and from 79.44 to 31.995, respectively.

As seen in Fig. 2.5, the measured values for the first mode of resonance are in excellent agreement with simulations. For the second mode, simulation underestimated the values compared to the measurements while exhibiting a similar slope. The discrepancies between simulation and measurement are due to the fact that an exactly symmetrical model with estimated values of over-etching was used for simulations, while the fabricated device is in fact slightly asymmetrical. Indeed, the fabricated membrane is not exactly centered over the trench. Also, an etching gradient may exist over the device which is not considered in simulation.

2.5.2 1.4.2 Chip-to-chip transmission

To verify that the deposition of Parylene-C can effectively increase transmission efficiency, chip-to-chip ultrasonic transmission was performed. Two sets of 4 PMUTs (shown in Fig. 2.3c) connected in parallel and of slightly different resonant frequencies were mounted in a 28-pin surface mount LCC02834 package and electrically connected through ball wirebonding. The packages were incorporated onto a test PCB and placed in front of each other at a distance of 2 mm.

Using a VNA, the transmission characteristics were measured for the first and second modes of resonance for all deposited Parylene-C thicknesses. Fig. 2.7 and Fig. 2.8 present the results for transmission in the first and second modes, respectively.

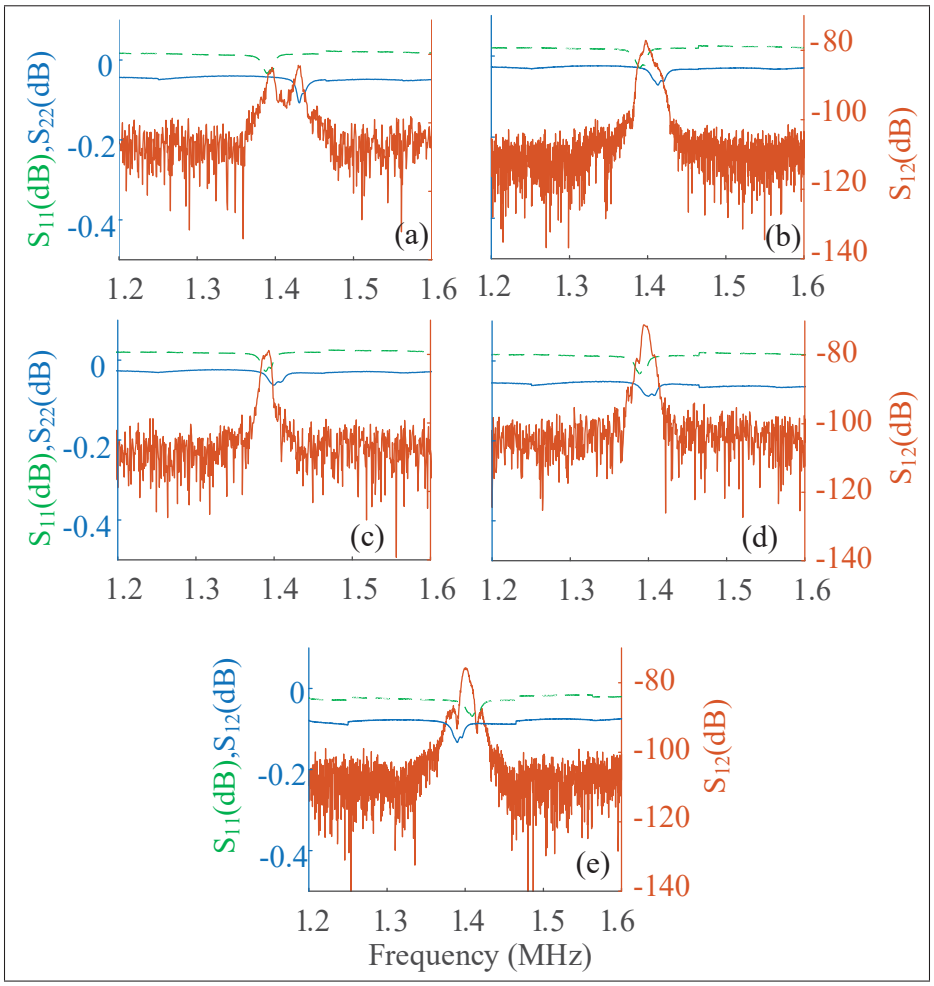

Figure 2.7 Scattering parameter measurements for chip to chip transmission with a Parylene-c thickness of (a) 0 nm, (b) 180 nm, (c) 280 nm, (d) 620 nm and (e) 1079 nm for the 1st mode of resonance

For the first mode, without any Parylene-C, the frequency mismatch between the PMUT transmitter and receiver results in a large overall signal transmission loss of around -84 dB. A deposition of 180 nm and 280 of Parylene-C reduces the resonant frequency of the second PMUT and increases acoustic power transfer. The deposition of 620 nm of Parylene-C further reduces the resonant frequency of the second PMUT in such a way that both resonant frequencies are matched. In this case, the transmission loss is optimal with a value of -71 dB. Finally, when 1070 nm of Parylene-C is deposited, the resonant frequency of the second PMUT moves lower than that of the first PMUT, thus re-increasing the transmission loss. Similarly, for the

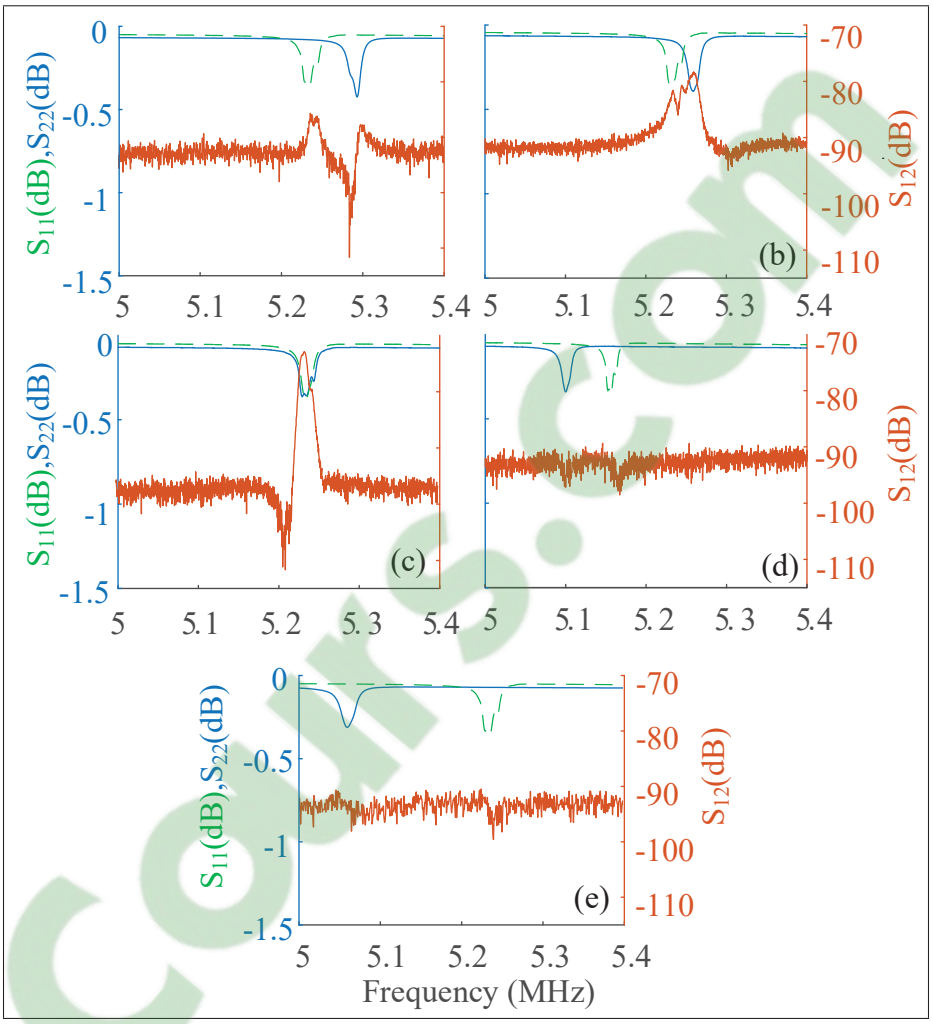

Figure 2.8 Scattering parameter measurements for chip to chip transmission with a Parylene-c thickness of (a) 0nm, (b) 180 nm, (c) 280 nm, (d) 620 nm and (e) 1079 nm for the 2nd mode of resonance

second mode, without any Parylene-C, signal transmission loss is around -86 dB. A deposition of 180 nm of Parylene-C reduces the resonant frequency of the second PMUT and increases acoustic power transfer. For a deposition of 280 nm of Parylene-C, both resonant frequencies are matched. In this case, the transmission loss is optimal with a value of -72 dB. Finally, when 620 nm and 1070 nm of Parylene-C are deposited, the resonant frequency of the second PMUT moves lower than that of the first PMUT, thus re-increasing the transmission loss. Using this

Parylene-C tuning technique, it is thus possible to maximize acoustic power transfer efficiency in chip-to-chip PMUT communications.

In order to test chip-to-chip communication in the time domain for different thicknesses of Parylene-C, the same two sets of PMUTs were placed at the same distance as for the transmission measurements. A Keysight 33220A signal generator was used to excite the first set of PMUTs with a sinusoidal signal of 4 periods at their resonant frequency. It was observed that misalignment between emitter and receiver results in a reduction of the amplitude of the transmitted signal. Hence, it is important to be able to perform alignment in a repeatable fashion to ensure the accuracy of measurements for different Parylene thicknesses. To do so, the test PCBs were mounted onto a THORLABS translation stage using screws (Fig. 2.11a). The stage makes it possible to precisely control the alignment of the PCBs. For the measurement of the first thickness, the stage was carefully translated in X and Y until achieving the strongest transmission, corresponding to the best alignment of transmitter and receiver. After each Parylene deposition, the stage adjustment was maintained in order to preserve the same alignment conditions for all measurements. The acoustic signal received by the second set of PMUTs was amplified using a transimpedance amplifier (TIA) and measured using a Keysight DSO-X 3034A oscilloscope. Fig. 2.9 and Fig. 2.10 show the time domain measurement results. One can see that for a thickness of 280 nm, the amplitude of the received signal is maximal, which agrees with the results obtained from the transmission measurements.

2.5.3 Ranging

With the optimal Parylene-C coating, ranging measurements were performed using a THORLABS translation stage. Figure 11 shows the measurement setup. The test PCB was screwed onto the stage vertically. A copper sheet was positioned facing the PCB to act as an acoustic reflector. An excitation signal composed of an 8 period-long sine wave with a frequency of 1.4 MHz and an amplitude of 10 Vpp was applied to the transmitting PMUTs in order to generate an acoustic wave. The receiving PMUTs, on the same chip as the transmitting ones and at a distance of 200

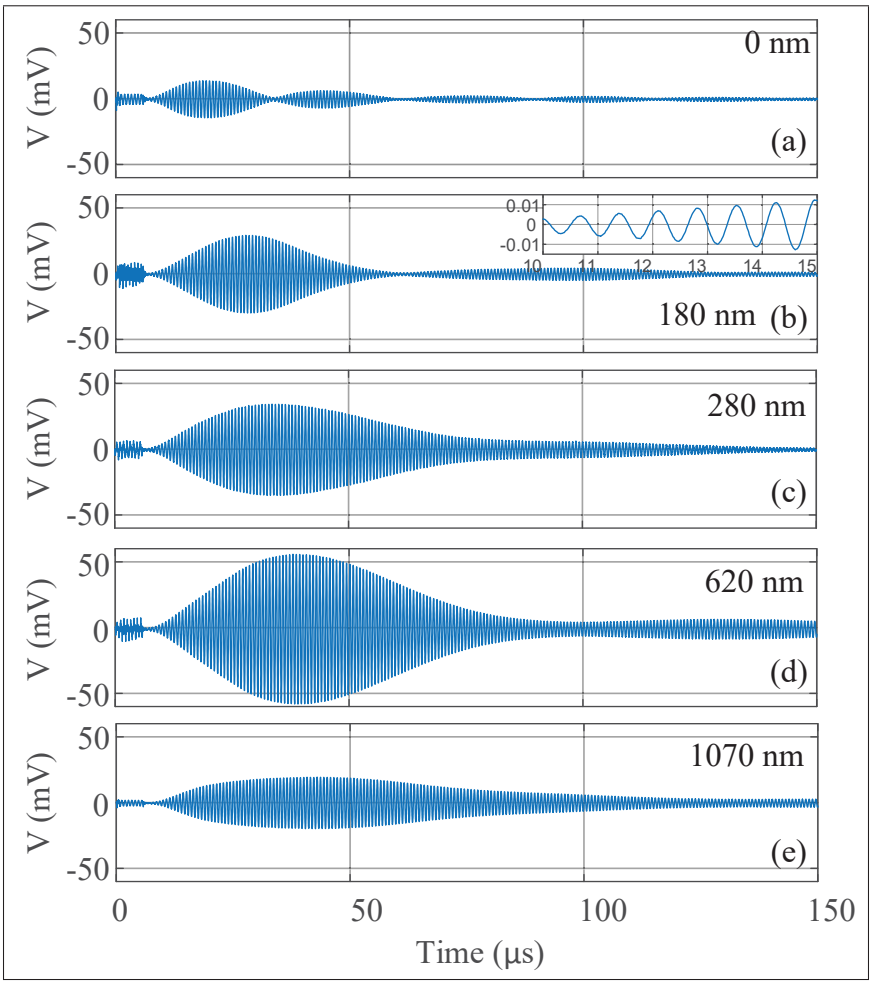

Figure 2.9 Chip to chip transmission measurements in time domain with a Parylene-c thickness of (a) 0nm, (b) 180 nm, (c) 280 nm, (d) 620 nm and (e) 1079 nm for the 1st mode of resonance

μm, was used to detect the reflected signal. The stage was gradually displaced transversely to vary the separation distance between the chip and the reflector.

Before acquiring the ranging measurements, cross-talk between the emitting and receiving PMUT was measured and characterized. Afterwards, cross-talk was subtracted from the received signal to best represent the acoustic transmission. Fig. 2.12 shows the measurements obtained for separation distances ranging from 2 mm to 20 mm. Separation distance can be calculated from measurements as

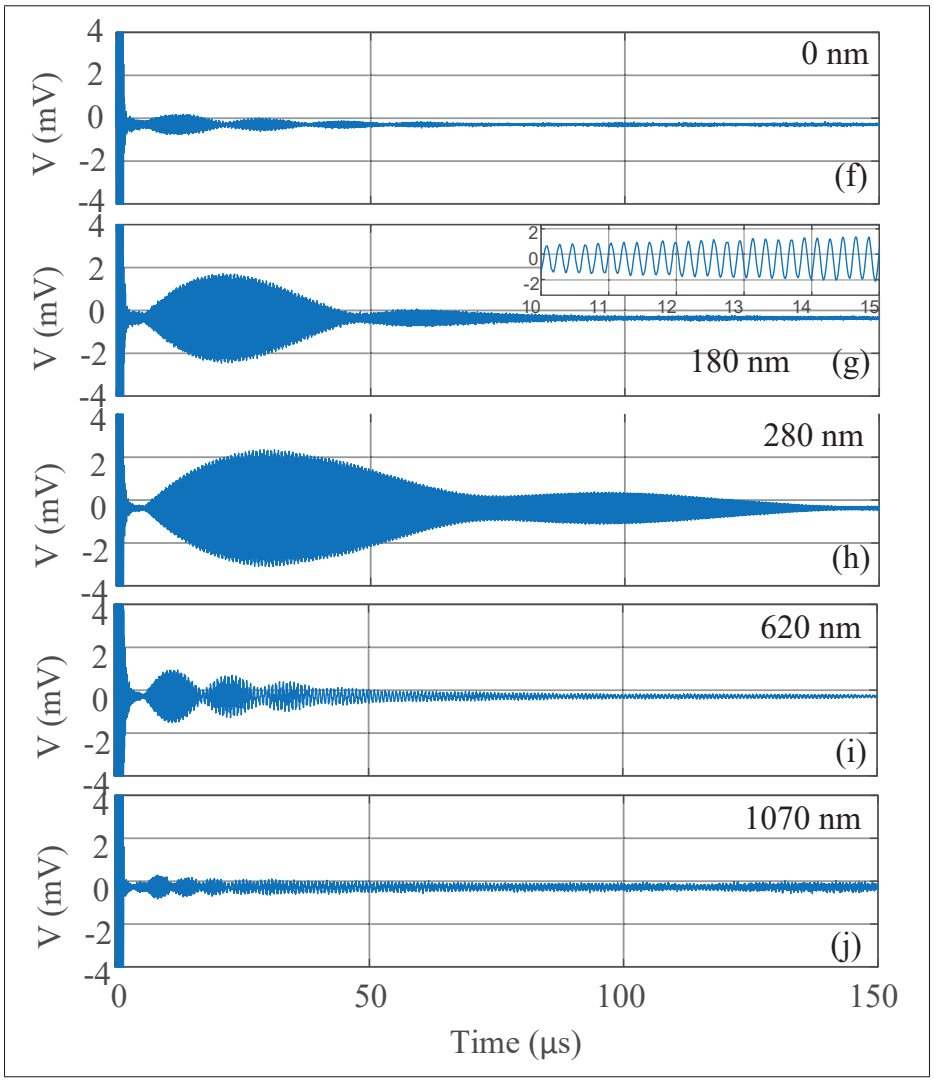

Figure 2.10 Chip to chip transmission measurements in time domain with a Parylene-c thickness of (a) 0nm, (b) 180 nm, (c) 280 nm, (d) 620 nm and (e) 1079 nm for the 2nd mode of resonance

$$d = \frac{tc}{2}, \tag{2.10}$$

where c is the speed of sound and t is the travel time. The distance is divided by two to take into account the fact that the sound has to travel to the reflector and back again. Results show that

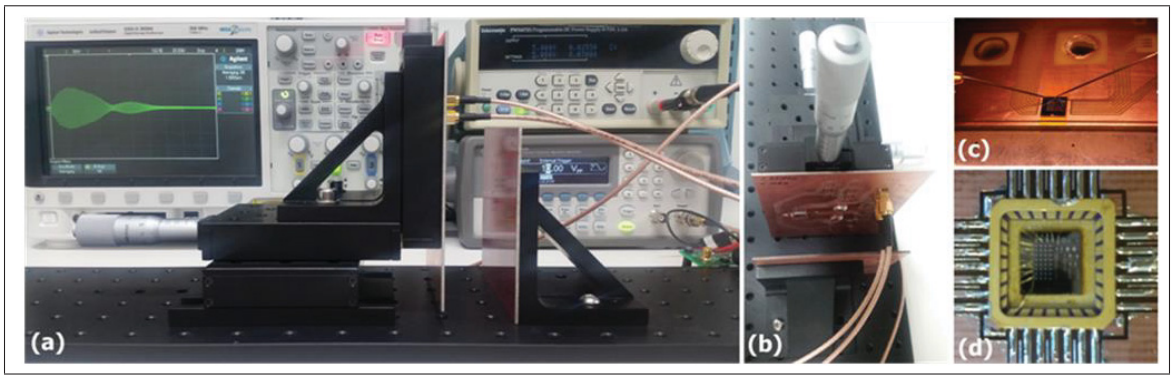

Figure 2.11 Measurement setup : a) time domain ranging measurements, b) close-up of the PCB for time domain measurements, c) close-up of the chip under frequency domain measurements, and d) close-up of the chip and package for time domain measurements

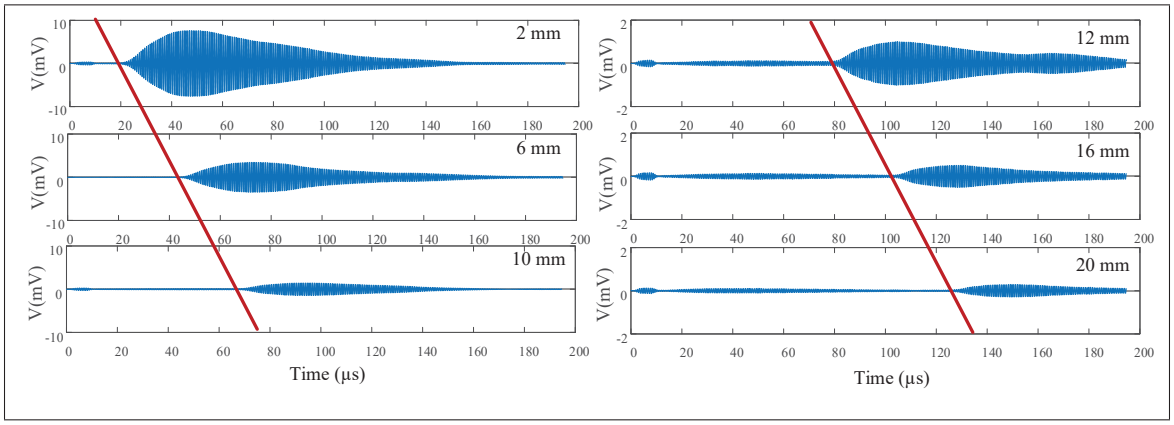

Figure 2.12 Measurements of the received pulse for six different reflection distances : 2 mm, 6 mm, 8 mm, 12 mm, 16 mm and 20 mm

the PMUT can be used to accurately measure distances with millimeter accuracy even with an excitation signal of relatively low amplitude.

2.6 Conclusion

This paper proposed a novel technique for PMUT frequency tuning that is low cost and effective, requiring only a post-processing step in the form of a Parylene-C thin film deposition. Moreover, a simple theoretical model was developed to predict the resonance frequency of partially clamped

membranes, allowing for more effective design of this type of PMUT. Results confirm that the post-processing technique can be used to accurately tune the frequency of high Q-factor PMUTs in order to optimize the transmission characteristic between two PMUTs despite fabrication process variations. In this fashion, chip-to-chip communication between two devices initially at different resonance frequencies was achieved, with significantly-improved transmission efficiency and ranging capability.

CHAPITRE 3

A NOVEL TOPOLOGY FOR PROCESS VARIATION-TOLERANT PIEZOELECTRIC MICROMACHINED ULTRASONIC TRANSDUCERS

Alexandre Robichaud[1], Dominic Deslandes[1], Frederic Nabki[1], Paul-Vahé Cicek[2]

[1] Département de Génie électrique, École de Technologie Supérieure,
1100 Notre-Dame Ouest, Montréal, Québec, Canada H3C 1K3
[2] Département d'informatique, Université du Québec à Montréal,
201, avenue Président-Kennedy, Montréal, Québec, Canada H2X 3Y7

Article soumis à la revue « IEEE Journal of Microelectromechanical Systems » en mai 2018.

3.1 Introduction

In recent years, there has been growing interest in micromachined ultrasonic transducers (MUT) as a low-cost and efficient alternative to conventional devices. Indeed, these have the potential to be integrated monolithically with integrated circuits (IC) since they are typically fabricated using similar processes, which also makes it possible to mass produce them at very low cost (Tang *et al.*, 2016a ; Zahorian *et al.*, 2011a). MUT can be implemented to use either capactive (CMUT) or piezoelectric (PMUT) transduction.

A CMUT is constituted of a suspended conductive membrane separated from an electrode by an air gap. The device is biased using a DC voltage and driven by an AC signal to make the membrane vibrate, thus producing acoustic waves. In order to maximize ultrasound generation, the CMUT must usually be biased close to its electrostatic pull-in voltage, increasing the likelihood of device failure (Akasheh *et al.*, 2005a). Furthermore, optimal air gap size is different for transmission and reception modes. Indeed, to achieve strong transmission, the air gap must be large to allow for driving the device with a high-amplitude signal without electrostatic collapse, whereas, for sensitive reception, the air gap should be narrow in order to maximize capacitive coupling. As such, optimal ultrasonic performance relying on CMUT may impose the use of two distinct sets of device parameters for transmitter and receiver (Akasheh *et al.*, 2004a). PMUT operation, on the other hand, relies on the piezoelectric effect. As such, no DC bias voltage

is required, and the same structure can thus be used for optimal ultrasonic transmission and reception. Moreover, the signal to noise ratio is generally superior for PMUT (Qiu *et al.*, 2015a). PMUT have successfully been demonstrated in several applications such as distance sensing (Przybyla *et al.*, 2011b), gesture recognition (Przybyla *et al.*, 2014a) and medical imaging (Dausch *et al.*, 2010,1).

Many of the fabrication technologies used to implement PMUT start with a silicon on insulator (SOI) wafer of which the bottom silicon layer serves as the handle substrate and the top silicon layer is patterned as needed to form the device structural membranes, with a deep reactive-ion etch (DRIE) process used to etch through the substrate from the back and release the membranes (Dausch, Castellucci, Chou & von Ramm, 2008b ; Guedes *et al.*, 2011 ; Wang *et al.*, 2008). Because of significant process variations during the long DRIE step required to release the membrane, it becomes challenging to accurately fabricate transducer elements at a set resonant frequency as device dimensions are in fact affected by the final DRIE trench size. As a result high inter-chip variance is often observed when using this fabrication approach.

Fabricating PMUT using cavity bonded SOI wafers can provide a more accurate and robust alternative. These specialized wafers feature pre-etched cavities readily embedded under the top silicon layer. Compared to etching a deep trench completely through the bottom silicon layer, this technique allows for lower process variation impact on device dimensions, but at a higher cost (Lu & Horsley, 2015 ; Lu *et al.*, 2015e ; Wang & Lee, 2015).

Instead, it is also possible to fabricate PMUT by surface micromachining, in which case the vibrating membrane is deposited and released by means of etching an underlying sacrificial layer (Lu *et al.*, 2015d ; Mehdizadeh & Piazza, 2017 ; Wang & Lee, 2015). However, since the membrane is deposited on top of a sacrificial layer rather than crystalline silicon, it is highly challenging to realize a high quality piezoelectric film on a surface micromachined PMUT.

In (Boser, Horsley, Przybyla, Rozen & Shelton, 2016), it is shown that the sensitivity of resonant frequency to process variation can be decreased by reducing the internal residual stress in the device membrane. This is achieved by a combination of introducing perforations at the perimeter

of the membrane, using a ring-shaped top electrode, and removing the piezoelectric material at the center of the membrane. Although this indeed reduces the sensitivity of the resonant frequency to process variations, the diameter of the membrane is still subject to variation, resulting only in a partial improvement of resonant frequency accuracy. Similarly, in (Boser *et al.*, 2016), the piezoelectric layer and backside electrode are etched to form rib structures, with the additional benefit of increasing the bandwidth of the PMUT.

Finally, in (Robichaud, Cicek, Deslandes & Nabki, 2018a), a post-processing technique for PMUT resonant frequency tuning is presented, using the deposition of a layer of Parylene to tune the mass and spring constant of the device. While effective, precise and relatively simple, this technique is limited to tuning all transducers on a single wafer in the same manner, failing to mitigate the impact of intra-wafer process variations.

In this work, a PMUT device topology with a novel anchoring pattern is proposed, reducing the influence of process variations on the resonant frequency of the PMUT. The topology is demonstrated using the PiezoMUMPS SOI commercial fabrication process. Using this technology, with a basic anchoring approach, yields membranes released by DRIE that suffer from the frequency matching issues detailed earlier, outlining the advantage of the proposed anchoring topology to significantly reduce the impact of process variation. This paper begins by a presentation of the theory behind the proposed method, followed by the details of device design, and finally presents and discusses measurement results.

3.2 Theoretical Background

In this section, the anchoring method proposed in this work to reduce the influence of fabrication process variations on the resonant frequency of PMUT devices is explained and its theoretical basis is detailed.

In the proposed topology shown in 3.1 , the top silicon layer of a SOI wafer is lithographically patterned to form a membrane within a toroid anchor, both connected together by several supporting arms as illustrated in Fig. 3.1b. Then, a trench is etched in the bottom silicon layer

to release the membrane using DRIE. According to the PiezoMUMPS design rules, trench dimensions can vary by as much as 50 μm due to process variations in the trench release DRIE step. As a consequence, the diameter of the anchored toroid is exposed to significant variations, but these will not influence the support and membrane dimensions. As shown in Fig. 3.1a and Fig. 3.1b, regardless of DRIE trench size variation, the entire circumference of the toroid anchor remains fully anchored to the silicon handle wafer. This is in contrast to the typical anchors shown in Fig. 1c which will have their size depend on the trench achieved dimension. Therefore, in the proposed anchoring scheme, the resonant frequency of the device is dominated by the dimensions of the top silicon layer pattern (PMUT membrane and supports) rather than the size of the DRIE trench, making this topology less sensitive to process variations. Indeed, support and membrane dimensions will mostly depend on the top layer patterning process that is subject to a much lower process variation of 3 μm.

The resonant frequency of a mechanical structure can be expressed as

$$f_0 = \frac{1}{2\pi}\sqrt{\frac{k}{m}}, \tag{3.1}$$

where m represents its mass and k its spring constant. For the device of interest in this work, mass, which is concentrated in the suspended membrane, is not affected significantly by fabrication process variations. As such, the impact of process variations on k is the main cause for resonant frequency variations from device to device. For a device without a toroidal anchor, as illustrated in Fig. 3.1c and 3.1e, the total support spring constant is given by

$$\frac{1}{k_{tot}} = \frac{1}{k_1} \pm \frac{1}{\Delta k_1}, \tag{3.2}$$

where k_1 is the spring constant of the nominal-length support and Δk_1 its variation caused by DRIE process variation. Because

$$\frac{1}{\Delta k_1} \propto \frac{\Delta l_1}{w_1}, \tag{3.3}$$

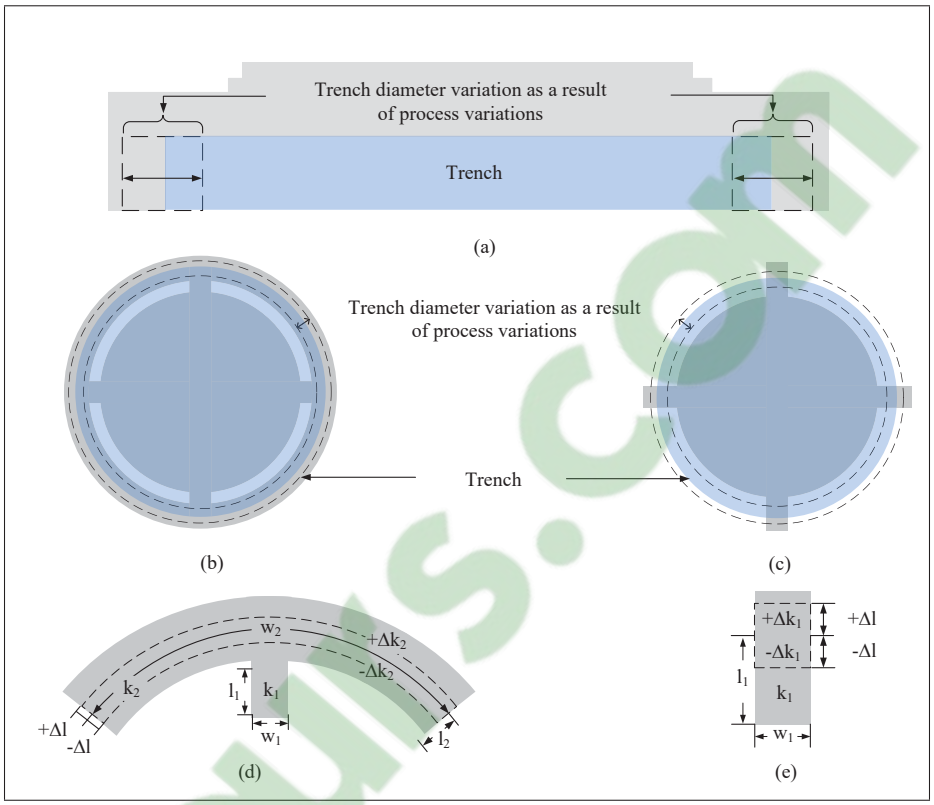

Figure 3.1 Schematic of a PMUT with toroid anchor; (a) Cross view of the PMUT with toroid anchor with the designation of the trench and its variation as a result of process variations. (b) Top view of the PMUT with toroid anchor with the designation of the section illustrated in (d). (c) Top view of the PMUT without toroid anchor with the designation of the section illustrated in (e). (d) Anchor section of the PMUT with toroid and identification of the spring constant, length and width and their variations. (e) Anchor section of the PMUT without toroid and identification of the spring constant, length and width and their variations

where $_1$ is the length and w_1 the width of the support, and because support length is generally in the order of a few micrometers, the effects of DRIE process variation would be expected to cause substantial variations in k_{tot}.

With the PMUT anchoring topology proposed in this work, as shown in Fig. 3.1b and Fig. 3.1d, the total spring constant k_{tot} can be approximated as :

$$\frac{1}{k_{tot}} = \frac{1}{k_1} + \frac{1}{k_2} \pm \frac{1}{\Delta k_2}, \tag{3.4}$$

where k_2 is the spring constant of the nominal suspended portion of the toroid and Δk_2 is the variation of k_2 induced by DRIE process variations. Since

$$\frac{1}{\Delta k_2} \propto \frac{\Delta l_2}{w_2}, \tag{3.5}$$

where Δl_2 is the variation in length of the suspended portion of the toroid and w_2 is the arc length of the toroid, and

$$\frac{1}{k_2} \propto \frac{l_2}{w_2}, \tag{3.6}$$

where $_2$ is the length of the toroid, it follows that, for $l_1 \geq l_2$ and $w_2 >> w_1$,

$$\frac{1}{k_2} \pm \frac{1}{\Delta k_2} << \frac{1}{k_1}. \tag{3.7}$$

Hence, from (3) and (6), the total spring constant can be approximated as

$$k_{tot} \approx k_1, \tag{3.8}$$

showing that the toroidal architecture can greatly reduce the influence of DRIE process variations on the accuracy of the resonant frequency.

3.3 Design

3.3.1 Fabrication Process

The PiezoMUMPS process (Cowen & et al., 2013) was used to fabricate the PMUT of this work, with the necessary sequence of process steps illustrated in Fig. 3.2. The process starts with a SOI wafer, covered with a 400 nm thick insulator layer and a 10 μm thick silicon device layer (Fig. 3.2a). The wafer is doped using a phosphosilicate glass (PSG) layer deposited onto the wafer and annealed for 1 hour at around 1000°C before being wet etched. Afterwards, the pad oxide layer (200 nm) is thermally grown onto the wafer (Fig. 3.2b). Then, a photoresist is applied and patterned using standard photolithography, and the oxide layer is patterned by wet etching (Fig. 3.2c). This oxide layer prevents short circuits between the doped silicon layer acting as the bottom electrode and the aluminium top electrode later deposited. In the following step, a 500 nm aluminium nitride piezoelectric layer is deposited by sputtering (Fig. 3.2d). Subsequently, the aluminium nitride layer is patterned using standard lithography and wet etching in order to produce a circular membrane of 200 μm diameter (Fig. 3.2e). Then, a photoresist is deposited on the top surface in preparation for lift-off of the aluminum pads (Fig. 3.2f), and is then patterned through standard photolithography (Fig. 3.2g). Subsequently, a 1 μm thick aluminium layer is deposited by e-beam evaporation (Fig. 3.2h) and lifted off, leaving a circular aluminium layer with a 190 μm diameter and aluminium rectangles allowing electrical connections to the device (Fig. 3.2i). The diameter of the aluminium circle is smaller than that of the aluminum nitride in order to prevent contact to the bottom electrode. Later, the silicon device layer is etched by DRIE, resulting in a circular silicon membrane and four supports embedded in a toroid (Fig. 3.2j). The diameter of the silicon structure is made larger than the aluminium nitride to ensure no overhang of the piezoelectric material. Finally, the membrane is released by etching a trench from the back of the handle wafer by DRIE, followed by a wet etch to traverse the oxide (Fig. 3.2k). Fig. 3.3 shows a SEM micrograph of a fabricated device. The PMUT device has a membrane diameter of 200 μm, a support width of 20 μm, and a support length of 10 μm. The trench has a diameter of 240 μm and the toroid has a total width of 80 μm, of which 10 μm is anchored.

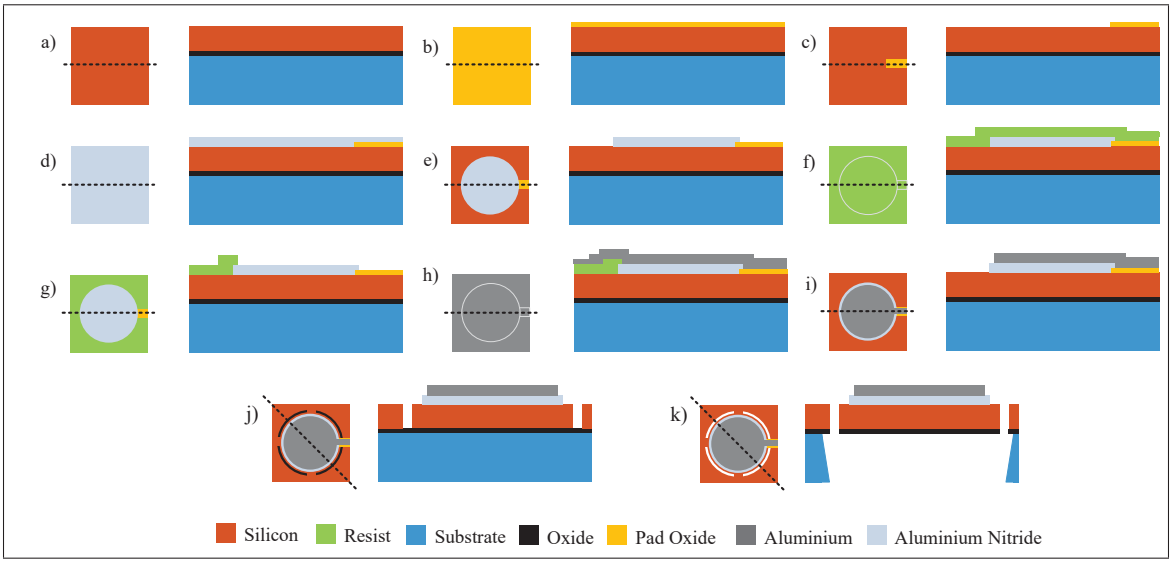

Figure 3.2 PiezoMUMPS process flow for the fabrication of a PMUT and post-processing. a) SOI wafer, b) growth of thermal oxide, c) patterning of thermal oxide by wet etching, d) deposition of aluminum nitride by reactive sputtering, e) AlN patterning by wet etching f) resist deposition, g) resist patterning, h) aluminum pad deposition, i) resist removal, j) DRIE etching of silicon and k) membrane release

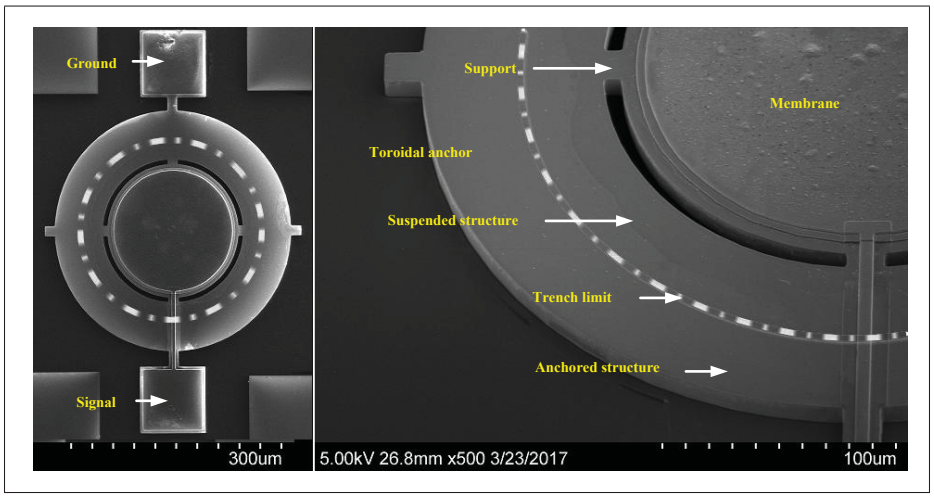

Figure 3.3 SEM micrographs of the fabricated PMUTs. a) Top view of the device and, b) close-up of a device

3.3.2 Finite-element Simulations

The finite-element simulator COMSOL Multiphysics was used for device design, and to predict the impact of process variations on the resonance frequency of the proposed PMUT. Eigenfrequency simulations were performed using the physical parameters listed in table I, which, as for the thicknesses of the different layers, were selected in accordance with the PiezoMUMPs specifications.

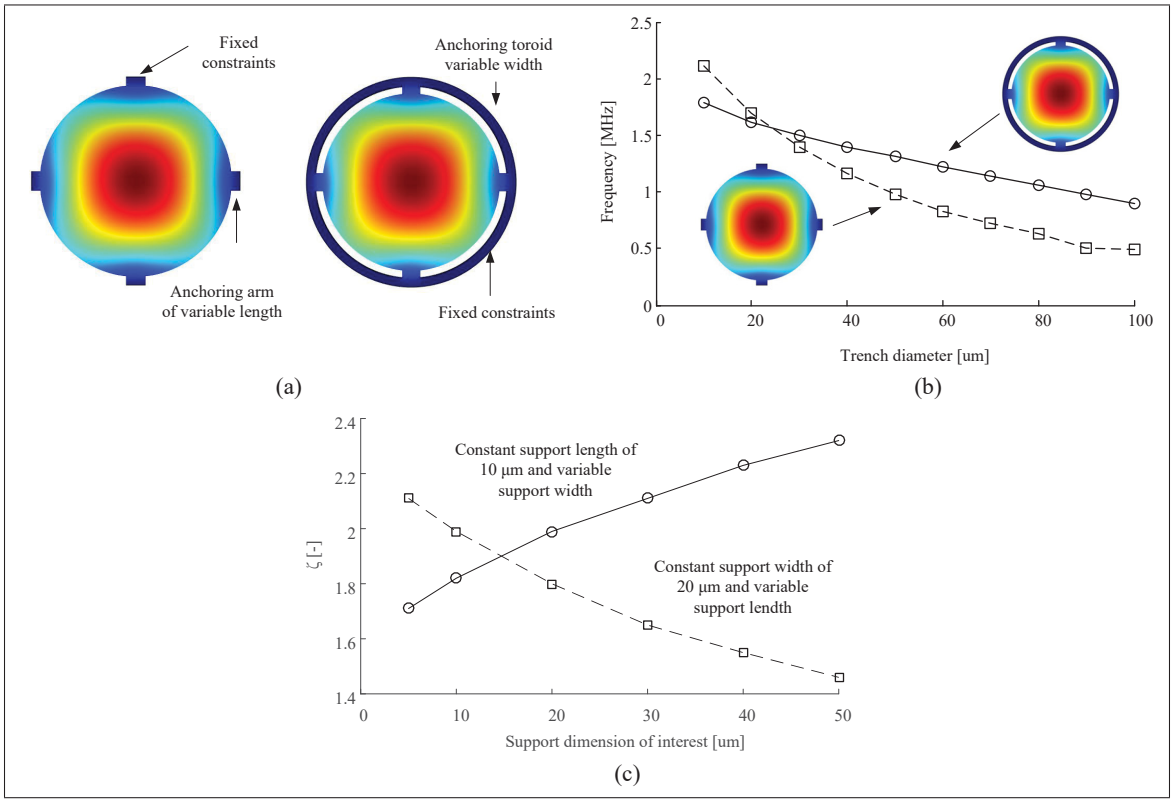

Figure 3.4 Simulation of frequency variation for PMUT devices with and without a toroidal anchor. (a) Schematic of the PMUT devices illustrating the used fixed constraints and variable dimensions, (b) frequency variation as a function of trench diameter, and (c) resonant frequency variation ratio, ζ, as a function of the support dimension of interest (width or length) for a PMUT with toroidal anchor

To assess the effectiveness of the method presented in this work, similar PMUT devices were simulated with and without toroidal anchors. The structures simulated are presented in fig. 3.4(a). For both topologies, the membrane has a diameter of 400 μm and the supports have a width of

Tableau 3.1 List of the different physical parameters used to perform eigenfrequency simulation

Parameter	**Si**	**AlN**	**Al**
Y_n $[GPa]$	180	348	69
ν_n $[-]$	0.22	0.24	0.346
ρ_n $[g/cm^3]$	2.329	3.6	2.7
t_n $[m]$	10	0,5	1
d_{31} $[nC/N]$	-	-1.9e-12	-
ϵ_{33} $[-]$	-	9	-
$e_{31,f}$ $[C/m2]$	-	-0.58	-

20 μm. For the PMUT with simple anchoring, a fixed constraint is set at the extremity of the supports, whereas, for toroidal anchoring, the fixed constraint is set on the outer perimeter of the toroid. Simulations were then performed, sweeping the support length between 10 μm and 100 μm for the simple anchor, and, for the toroidal anchor, sweeping the supported toroidal width from 10 μm to 100 μm, while maintaining a support length of 10 μm. These sweep parameters make it possible to compare the impact of similar trench size variations for both device topologies.

As shown in Fig. 3.4(b), one observes that trench size variation has a much more severe impact on the PMUT with simple anchoring, where a trench size variation of 90 μm lowers the resonant frequency from 2.1 MHz to 0.49 MHz, a factor of 4.3. In contrast, for the toroidal anchoring topology, the same trench size variation only lowers the resonant frequency from 1.8 MHz to 0.9 MHz, a factor of 2.

In the previous simulations, the support dimensions of the PMUT with toroidal anchor were kept constant. Varying these parameters allows one to fine tune the toroidal anchoring topology and further optimize it to make it even more robust against process variations. Throughout simulations, for a constant support width of 20 μm, support length was varied between 5 μm and 50 μm. The parameter ζ, defined as the ratio of the resonance frequency of a PMUT with a trench of 10 μm to the resonance frequency of a PMUT with a trench of 100 μm, was then plotted as a function of the support dimension of interest (in this case support length). The parameter ζ

serves as a measure of robustness : a frequency invariant structure would have a ratio of 1 and a robust structure would have a ratio near that. The results are presented in Fig. 3.4(c). One can see that an increase of the length leads to an increase of the robustness. Recalling (3.8), k_{tot} is equal to k_1 and independent of trench diameter when $k_1 \ll k_2$. Increasing the support length reduces k_1 compared to k_2 and therefore increases the resonant frequency robustness.

Similarly, for a constant support length of 10 μm, the support width was varied between 5 μm and 50 μm. Then the same ratio ζ as previously was plotted as a function of support dimension of interest, in this case the support width. The results are presented in Fig. 3.4(c). One can see that an increase of the support width leads to a decrease of the resonant frequency robustness. The value of k_1 increases compared to k_2 leading to the opposite effect of the case above.

Hence, to increase the robustness of the PMUT resonant frequency against trench variations, the spring constant of the supports compared to the spring constant of the toroid must be decreased, which is consistent with the theory. Indeed, as stated in (7) and (8), for k_2 significantly greater than k_1, k_{tot} becomes approximately equal to k_1 and relatively unaffected by variations in k_2. However, it must be noted that modifying the dimensions of the supports may also have an influence on PMUT output acoustic power, which must also be taken into consideration during device design.

3.4 Measurement Results

The resonant frequency of the devices was acquired by measuring the s_{12} scattering parameter between both device electrodes. Measurements were made using an EP6 Cascade Probe Station and an E5061B Keysight PNA Network Analyzer in combination with GSG probes. PiezoMUMPs is a commercial technology offered by MEMSCAP. For this fabrication run, the 16 sourced dies from the foundry were tested, which is believed by the authors to be a sufficient amount to showcase the benefits of the proposed device in terms of mitigating inter-die performance variations. Each 5 x 5 mm die holds 12 PMUT devices with toroidal anchoring and 12 PMUT devices with regular supports.

In order to assess inter-die variations, a PMUT device with and without toroidal anchoring was characterized on each die. The PMUT device has a membrane diameter of 200 μm, a support width of 20 μm, and a support length of 10 μm. The trench has a diameter of 240 μm and the toroid has a total width of 80 μm, of which 10 μm is anchored. As shown in Fig. 3.5a and Fig. 3.5b, the average resonant frequency and standard deviations were respectively 1.401 MHz / 23.07 kHz for the PMUT with toroidal anchoring and 1.353 MHz / 101.2 kHz for the PMUT with simple anchoring. This represents an improvement of more than 4X in resonant frequency variation reduction using the toriodal anchoring scheme, which matches the theoretical expectations. Indeed, trench variation has a reduced impact on the toroidal architecture because k_2 is much larger than k_1 and, according to (8), k_{tot} therefore becomes approximately equal to k_1.

As was discussed, using the toroidal anchoring scheme provides an improvement of more than 4X in the resonant frequency variation. In order to compare this trend with simulation, the standard trench diameter variation was estimated to be about 20 μm, which would make the anchored portion of the toroid vary between 10 μm to 30 μm. From Fig. 3.4b, a simulated variation from 10 μm to 30 μm of the anchored portion of the toroid leads to a frequency variation of 0.7 MHz (from 2.1 MHz to 1.4 MHz) for the PMUT without toroid and of 0.3 MHz (from 1.8 MHz to 1.5 MHz) for the PMUT with toroid. This represents an improvement of 2.33X in resonant frequency variation reduction. These simulated results confirm the measured improvements through the toroidal anchoring scheme, and indicate that the actual trench diameter variation was greater than 20 μm in this process run.

In order to assess intra-die variations, 12 PMUT devices with and without toroidal anchoring were characterized on the same die. As shown in Fig. 3.5c and Fig. 3.5d, the average resonant frequency and standard deviations were respectively 1.39 MHz / 5.89 kHz with toroidal anchoring and 1.31 MHz / 20.1 kHz with simple anchoring. This represents a near 3.7X improvement in resonant frequency variation, again consistent with theory. Intra-die variations are observed to be in general smaller than inter-die variations. This can be explained by the fact that, in terms of

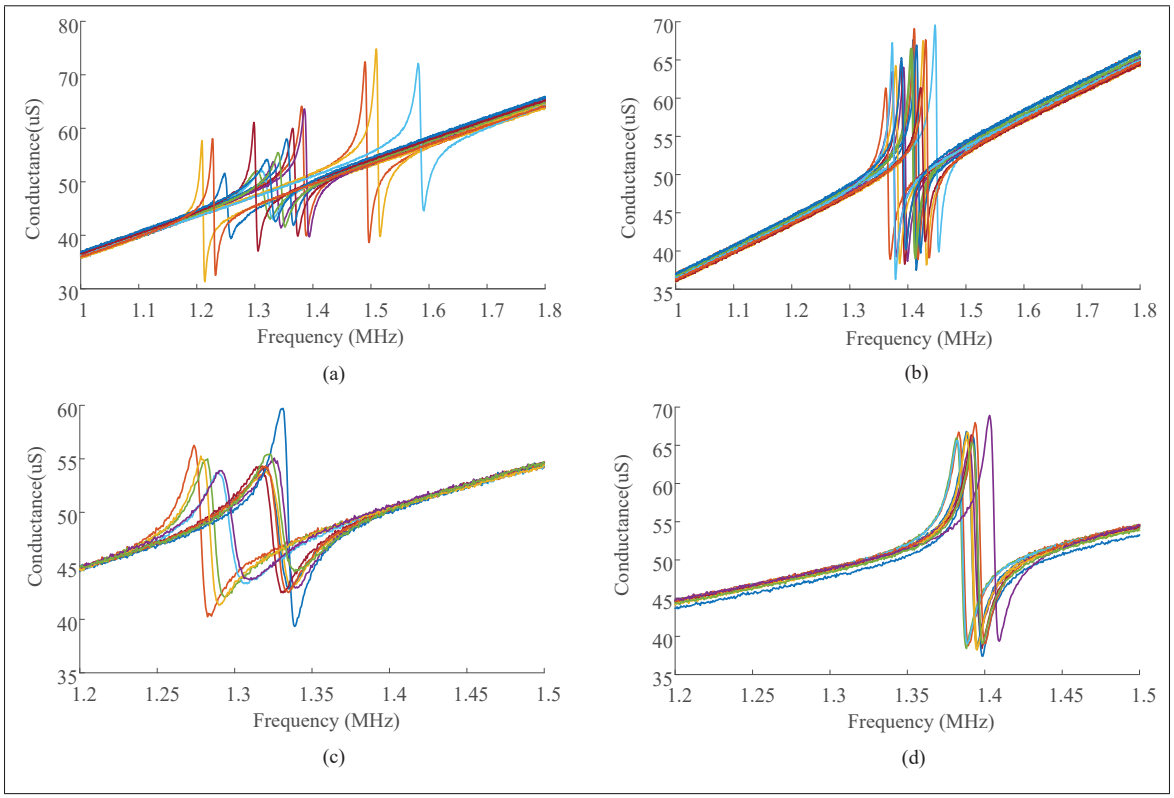

Figure 3.5 Impedance of PMUT devices from 16 different dies (a) for PMUT devices without toroid and (b) for PMUT devices with toroid anchor. Impedance of 12 PMUT devices on same die (c) for PMUT devices without toroid anchor and (d) for PMUT devices with toroid anchor

fabrication process, trench variations on a single die are expected to be smaller and thus have less influence on the resonant frequency.

The improvement of intra-die resonant frequency accuracy provided by the toroidal topology makes it more feasible to use an array with multiple PMUT elements for applications such as nondestructive testing (NDT), imaging and certain types of distance ranging. In this context, fabricated PMUT devices from this work were used to perform ranging measurements, using the test setup shown in Fig. 3.6a. A THORLABS translation stage was used to mount a supporting PCB in vertical position. A 4 period-long sine wave with a frequency of 1.4 MHz and an amplitude of 60 V_{pp} was used to drive a first PMUT device in order to generate acoustic waves. A

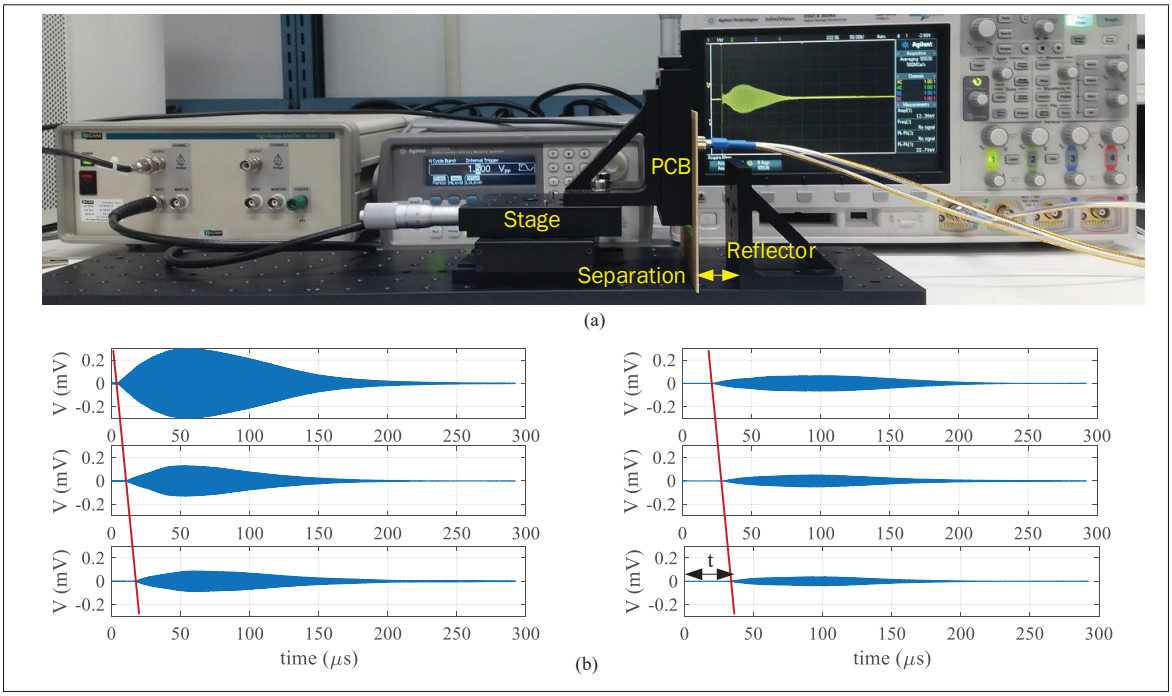

Figure 3.6 Photograph of the measurement setup and (b) ranging measurement results in air for distances from 1 mm to 6 mm

second PMUT device on the same die, adjacent to the transmitting PMUT device, was then used to detect the reflected acoustic signal. The received signal was measured using an oscilloscope.

The distance between transducers and reflector was varied and measurements were performed for separation distances ranging from 1 mm to 6 mm. The results are presented in Fig. 3.6b. Travel distance can be calculated as $d = \frac{tc}{2}$ where c is the speed of sound in air and t corresponds to the round trip travel time. This ranging measurement using different PMUT devices showcases the anchoring technique effectiveness and allowing sufficiently matched resonant frequencies to enable ranging applications.

3.5 Conclusion

This paper presented a novel PMUT device anchoring topology using a toroidal anchoring technique to reduce the resonant frequency dependency induced by DRIE process variations. Results show that inter- and intra-die resonant frequency standard variations can be reduced from

101 kHz to 23 kHz and 20 kHz to 5.9 kHz respectively, by using the proposed anchoring topology. This confirms that the method is indeed effective to reduce the impact of process variations on the resonant frequency of PMUT. Finally, the PMUT were demonstrated for distance ranging measurements.

Acknowledgement

The authors would like to thank CMC Microsystems for providing the layout design tools and enabling chip fabrication. The authors also wish to thank the Natural Science and Engineering Research Council (NSERC) of Canada for its financial support of this work.

CHAPITRE 4

ELECTROMECHANICAL DAMPING FOR LONG-RANGE AND HIGH-PRECISION PIEZOELECTRIC ULTRASONIC TRANSDUCERS

Alexandre Robichaud[1], Dominic Deslandes[1], Frederic Nabki[1], Paul-Vahé Cicek[2]

[1] Département de Génie électrique, École de Technologie Supérieure,
1100 Notre-Dame Ouest, Montréal, Québec, Canada H3C 1K3
[2] Département d'informatique, Université du Québec à Montréal,
201, avenue Président-Kennedy, Montréal, Québec, Canada H2X 3Y7

Article soumis à la revue « IEEE Journal of Microelectromechanical Systems »
en novembre 2019.

4.1 Introduction

In recent years, there has been growing interest in micromachined ultrasonic transducers (MUT) as a low-cost and efficient alternative to conventional devices. Indeed, these have the potential to be integrated monolithically with integrated circuits (IC) since they are typically fabricated using similar processes, which also makes it possible to mass produce them at very low cost (Tang *et al.*, 2016a ; Zahorian *et al.*, 2011a). MUT can be implemented to rely either on capacitive (CMUT) or piezoelectric (PMUT) transduction.

A CMUT is constituted of a suspended conductive membrane separated from an electrode by an air gap. The device is biased using a DC voltage and driven by an AC signal to make the membrane vibrate, thus producing acoustic waves. In order to maximize ultrasound generation, the CMUT must usually be biased close to its electrostatic pull-in voltage, increasing the likelihood of device failure (Akasheh *et al.*, 2005a). Furthermore, optimal air gap size is different for transmission and reception modes. Indeed, to achieve strong transmission, the air gap must be large to allow for driving the device with a high-amplitude signal without electrostatic collapse, whereas, for sensitive reception, the air gap should be narrow in order to maximize capacitive coupling. As such, optimal ultrasonic performance relying on CMUT may impose the use of two distinct sets of device parameters for transmitter and receiver (Akasheh *et al.*, 2004a). PMUT

operation, on the other hand, relies on the piezoelectric effect. As such, no DC bias voltage is required, and the same structure can thus be used for optimal ultrasonic transmission and reception. Moreover, the signal to noise ratio is generally superior for PMUT (Qiu *et al.*, 2015a). PMUT have successfully been demonstrated in several applications such as distance sensing (Przybyla *et al.*, 2011b), gesture recognition (Przybyla *et al.*, 2014a) and medical imaging (Dausch *et al.*, 2010,1).

For imaging in air using an array of transducer elements, an important application of MUT transducers, two of the critical system performance parameters are :

1) *pixel depth resolution*, determined by the duration of the acoustic signal emitted by a transducer element. Shorter signal duration allows for higher transverse resolution due to the smaller spread of the emitted pulse.

2) *imaging range*, depending on the power of the acoustic signal emitted by a transducer element. Higher output power makes it possible to perform imaging at a longer imaging range.

In order to achieve reasonable pixel depth resolution, typical ultrasonic imaging systems have no choice but to resort to low quality factor (Q) transducers, so as to minimize the ringing that would otherwise significantly increase the duration of the produced acoustic pulse. However, because of their distribution of power over a large bandwidth, low-Q transducers exhibit a modest imaging range, thus placing a limit on possible applications. Alternatively, a high-Q transducer, driven by a continuous-wave signal at its resonance frequency, would provide significantly higher acoustic power output, but could not be used in time-of-flight measurements, which typically require pulsed operation.

Accordingly, the objective of this work is to combine the best of both worlds, by demonstrating a method for using high-Q transducers to allow for long-range, high-resolution imaging. This is accomplished by introducing an electromechanical damper, making it possible to selectively control Q of the transducer over time.

Several works have already presented filters and electromagnetic resonators that are tunable using MEMS techniques. In (Yan & Mansour, 2007), a thermal actuator, and in (Reines, Park & Rebeiz, 2010), RF-MEMS switches are used to tune band-stop filters. In (Lin, Hsieh, Huang & Chang, 2012), a MEMS comb-drive serves to implement a frequency-tunable slot antenna, and, in (Liu, Katehi, Chappell & Peroulis, 2010), the frequency of electromagnetic cavity resonators is tuned using electrostatically-actuated thin diaphragms. Similarly, in (Lee & Wu, 2006), the coupling regime of a silicon micro disk optical resonator is tuned using MEMS actuation.

Actuators have similarly been used to tune the frequency of energy harvesters. In (Leland & Wright, 2006), the resonant frequency of a piezoelectric energy harvester is lowered by axially compressing the structure, yielding a frequency shift of 24 %. In (Eichhorn, Tchagsim, Wilhelm & Woias, 2011) a system consisting of an energy harvester, an actuator and a control unit is presented. Based on the ambient vibration, the control unit adjusts the frequency of the harvester by enabling the actuator. Also, in (Eichhorn, Goldschmidtboeing & Woias, 2009 ; Peters, Maurath, Schock, Mezger & Manoli, 2009 ; Wischke, Masur, Goldschmidtboeing & Woias, 2010), the frequency is tuned by applying mechanical stress by means of piezoelectric actuation. Finally, in (Wu, Lin, Kato, Zhang, Ren & Liu, 2008), the frequency of an energy harvester is tuned using a movable mass. However, the aforementioned tunable energy harvester does not make use of MEMS technology.

In this work, an electrostatically-controlled actuator is used to quickly dampen the oscillation of a PMUT device in order to decrease the pulse duration in the time domain, which can be harnessed to improve axial resolution for imaging or ranging applications, without sacrificing acoustic power transmission.

The paper first describes the theoretical background in section II, presents the design in section III, and reports on the measurement results in section IV.

4.2 Theoretical Background

This section presents the topology of the proposed device, as illustrated in Fig. 4.1a. The structure of the PMUT membrane held by four support arms is similar to that presented in (Robichaud *et al.*, 2018a ; Robichaud, Deslandes, Cicek & Nabki, 2018b). However, it is surrounded by two spring-mounted masses that can be displaced by two electrostatic actuators in order to exert mechanical force onto the PMUT membrane, as shown in Fig. 4.1b.

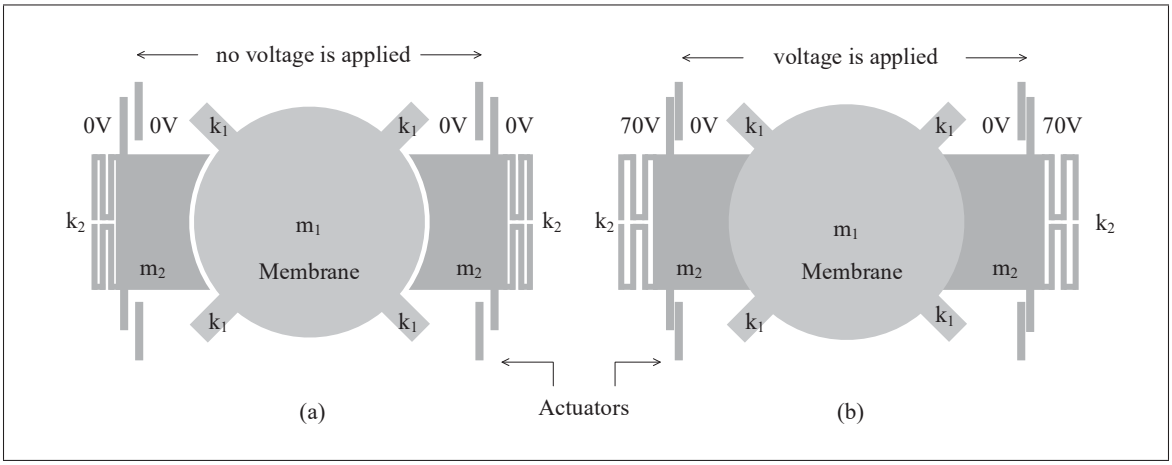

Figure 4.1 Schematic of the PMUT and its actuator (a) when no voltage is applied and (b) when voltage is applied

4.2.1 Operating principle

Although high-Q transducers are more efficient energy-wise, they also produce acoustic pulses with a longer ring-out time than lower-Q transducers. This in turn has a negative impact on the axial resolution which can be defined as the minimum distance between two reflectors on the travelling axis of an acoustic pulse that allows for the two pulse reflections to be properly discriminated (Swanevelder & Ng, 2011). It is given by the following equation :

$$Res_{ax} = \frac{\Delta t \cdot c}{2}, \tag{4.1}$$

where Δt is the pulse duration and c is the speed of sound.

Conventional transducers use a damping layer to reduce their quality factor and therefore increase axial resolution, at the expense, however, of transmission power efficiency. The technique proposed in this work aims to reduce the duration of the acoustic pulse by dynamically using an electromechanical damper to maximize axial resolution while still preserving the superior power transmission efficiency of a higher Q. This electromechanical damper can be activated at any point in time to quickly stop the ringing of the PMUT membrane. Fig. 4.2(a) illustrates the potential effect of the actuator in the time domain. When no actuator is used, the acoustic pulse is long. When using the actuator, the same pulse can be shortened as depicted on the bottom of the same figure. This method could therefore be used to perform high efficiency, high precision acoustic imaging. In a practical application, one would need to synchronize activation of the PMUT and of the actuator in order to modulate a pulse of the desired length to achieve the target resolution.

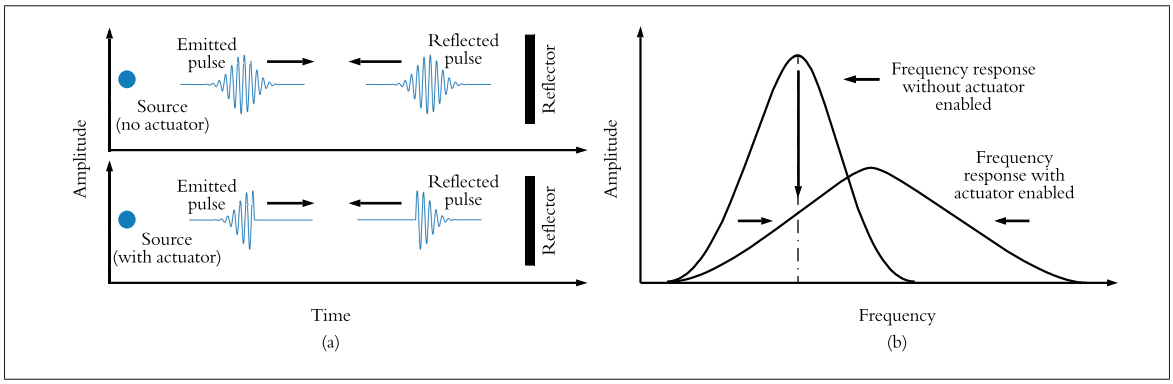

Figure 4.2 Schematic representation of the influence of the actuator on the acoustic pulse (a), and (b) conceptual impact of the actuator on the PMUT resonant frequency

4.2.2 Influence of the mechanical damper on the resonant frequency

The structure is modeled in a lumped fashion in order to establish a baseline understanding of the influence of the actuated dampers on the structure. Note that tribological properties are not considered here.

First, the influence of the dampers on the resonant frequency is considered. When no voltage is applied at the driving terminals of the two electrostatic actuators, the PMUT can resonate freely and is not influenced by the dampers. In this case, its resonant frequency in the first transverse mode can be expressed as

$$f_{0,1} = \frac{1}{2\pi}\sqrt{\frac{k_1}{m_1}}, \tag{4.2}$$

where k_1 is the total spring constant of the four supports and m_1 the mass of the PMUT. Note that (5.1) assumes minimal impact of the membrane's flexion on the resonant frequency.

As soon as the actuators are activated, masses m_2 move towards the PMUT membrane until they come into full contact with it. The electrostatic gap width between the driving electrodes of the actuators is carefully chosen to be slightly larger than the displacement required to collapse the masses into the membrane, in order to prevent short-circuits after the motion is complete.

When both masses come into contact with the membrane (see Fig. 4.1b), it is assumed that the electrostatic force keeps them in contact in such a way that they all resonate together as a single structure. In this case, the influence of the spring constant and the mass of the actuator on the overall resonant frequency can be estimated as

$$f_{0,2} = \frac{1}{2\pi}\sqrt{\frac{k_1 + k_2}{m_1 + m_2}}. \tag{4.3}$$

where k_2 is the spring constant of the actuator's spring. Provided that

$$\frac{k_1}{m_1} > \frac{k_2}{m_2}, \tag{4.4}$$

it follows from (5.1) and (4.3) that

$$f_{0,1} > f_{0,2}. \tag{4.5}$$

Alternatively, when

$$\frac{k_1}{m_1} < \frac{k_2}{m_2}, \tag{4.6}$$

we have

$$f_{0,1} < f_{0,2}. \tag{4.7}$$

Hence, the resonant frequency will either increase or decrease depending on the ratio of the spring constant and masses between the PMUT and actuator. In theory, by carefully designing the spring constant and mass of the actuator, the PMUT's resonant frequency can be tuned away from the working frequency (i.e. the base resonant frequency of the PMUT membrane) when the actuator is pulled in. This decreases the effective membrane displacement amplitude at the working frequency, an effect that is further amplified by the damping action of the actuator, as depicted in Fig. 4.2(b). The damper is used to shorten the pulse length in the time domain. When the damper is not enabled, the PMUT benefits from a higher Q and a higher efficiency. Then, the damper is activated to shut down the PMUT. As one can see after activation, the acoustic power is drastically reduced resulting in a shorter pulse in the time domain which is the goal.

4.2.3 Key parameters for stiffnesses k_1 & k_2 and masses m_1 & m_2

The thickness of the membrane is set by the technology and therefore cannot be modified. To increase k_1, the length of the anchor has to be reduced or its width increased. To decrease k_1, the opposite holds. To increase k_2, one can either increase the width of the beam forming the spring or decrease its number of folded sections. For decreasing k_2, the opposite holds. Furthermore, to

increase m_2, the surface area of m_2 has to be increased, while to decrease it, its surface area must be decreased. Finally, k_1 has a direct influence on the quality factor of the device. In fact, k_1 is damping the movement of the membrane and therefore, a higher value of k_1 results in a lower quality factor and vice versa.

4.2.4 Influence of the mechanical damper on the displacement amplitude at resonance

Placing the dampers in contact with the PMUT membrane adds stiffness and mass to the compound structure, while also increasing the effective anchored perimeter of the membrane, which are all expected to introduce mechanical damping and reduce the displacement amplitude.

Furthermore, even though the electrostatic force attracts both structures and keeps them in contact, the interface is likely to experience some degree of slippage, introducing friction and other tribological phenomena (Williams & Le, 2006). Although out of the scope of this work, these effects are expected to further increase damping. Finally, when the actuator is active, a mechanical force is applied on the membrane which in turn may have an impact on the membrane stress and consequently on the resonant frequency of the PMUT. To mitigate this effect, the stiffness of the damper springs was intentionally designed to be much lower than the in-plane stiffness of the ultrasonic membrane.

4.3 Design

4.3.1 Fabrication process

The commercial PiezoMUMPS process (Cowen & et al., 2013) was used to fabricate the devices presented in this work, with the required sequence of process steps illustrated in Fig. 4.3. The process starts with a SOI wafer, covered with a 400 nm thick insulator layer and a 10 μm thick silicon device layer (Fig. 4.3a). The wafer is doped using a phosphosilicate glass (PSG) layer deposited onto the wafer and annealed for 1 hour at around 1000°C before being wet etched. Afterwards, the pad oxide layer (200 nm) is thermally grown onto the wafer (Fig. 4.3b). Then,

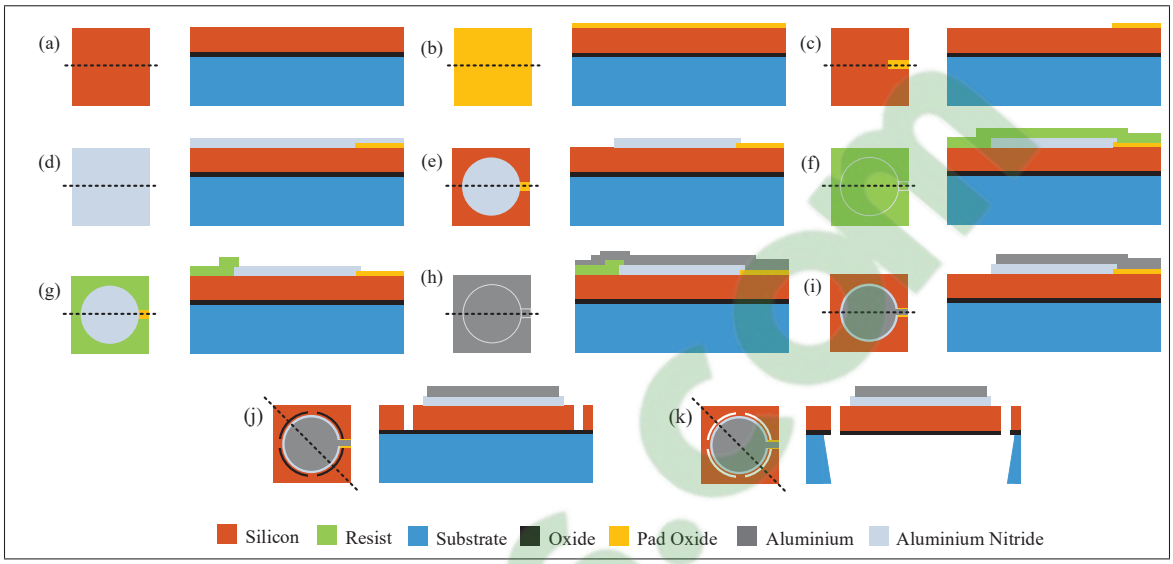

Figure 4.3 PiezoMUMPS process flow for the fabrication of a PMUT. a) SOI wafer, b) growth of thermal oxide, c) patterning of thermal oxide by wet etching, d) deposition of aluminum nitride by reactive sputtering, e) AlN patterning by wet etching f) resist deposition, g) resist patterning, h) aluminum pad deposition, i) resist removal, j) DRIE etching of silicon and k) membrane release

a photoresist is applied and patterned using standard photolithography, and the oxide layer is patterned by wet etching (Fig. 4.3c). This oxide layer prevents short circuits between the doped silicon layer acting as the bottom electrode and the aluminium top electrode later deposited. In the following step, a 500 nm aluminium nitride piezoelectric layer is deposited by sputtering (Fig. 4.3d). Subsequently, the aluminium nitride layer is patterned using standard lithography and wet etching in order to produce a circular membrane of 200 μm diameter as well as the dampers and actuators (Fig. 4.3e).

The diameter corresponds to the minimum achievable size that conforms to the fabrication process design rules. It was chosen to ensure the most compact device. This choice also dictates the resonant frequency. Moreover, the design rules require that the aluminium must enclose the AlN by at least 5 μm, which corresponds to the 95% coverage. Then, a photoresist is deposited on the top surface in preparation for lift-off of the aluminum pads (Fig. 4.3f), and is then patterned through standard photolithography (Fig. 4.3g). Subsequently, a 1 μm thick aluminium layer is deposited by e-beam evaporation (Fig. 4.3h) and lifted off, leaving a circular aluminium

layer with a 190 μm diameter and aluminium rectangles allowing electrical connections to the PMUT and actuator (Fig. 4.3i). The diameter of the aluminium circle is smaller than that of the aluminum nitride in order to prevent contact to the bottom electrode. Later, the silicon device layer is etched by DRIE, resulting in a circular silicon membrane and four supports embedded with two actuators on the sides (Fig. 4.3j). The diameter of the silicon structure is made larger than the aluminium nitride to ensure no overhang of the piezoelectric material. Finally, the membrane is released by etching a trench from the back of the handle wafer by DRIE, followed by a wet etch to traverse the oxide (Fig. 4.3k). Finally, Fig. 4.4 shows the fabricated device, with the PMUT membrane, actuation electrodes and dampers with spring and masses outlined.

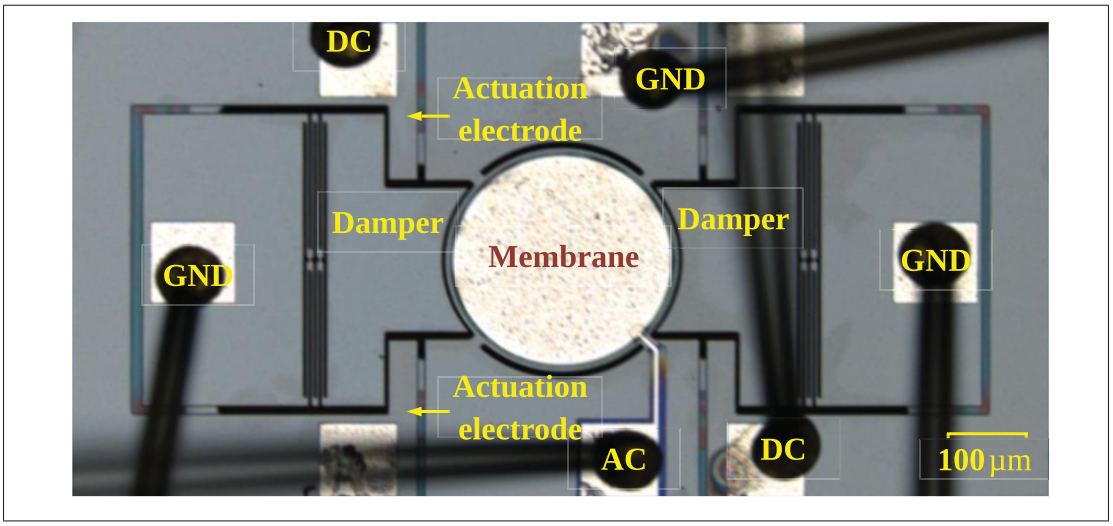

Figure 4.4 Micrograph of the PMUT and its actuators and masses

4.3.2 Finite-element simulations

The finite-element simulator COMSOL Multiphysics was used for device design. Simulations were performed using the specified physical parameters of the PiezoMUMPS technology. The goal of the simulations was to gain more insight into the interaction of the mechanical damper with the PMUT membrane. As discussed in section II, in order to model the effect of the damper on the PMUT, a simplified monolithic structure formed by the combined PMUT and damper was considered, which allows to significantly reduce the complexity of the simulations.

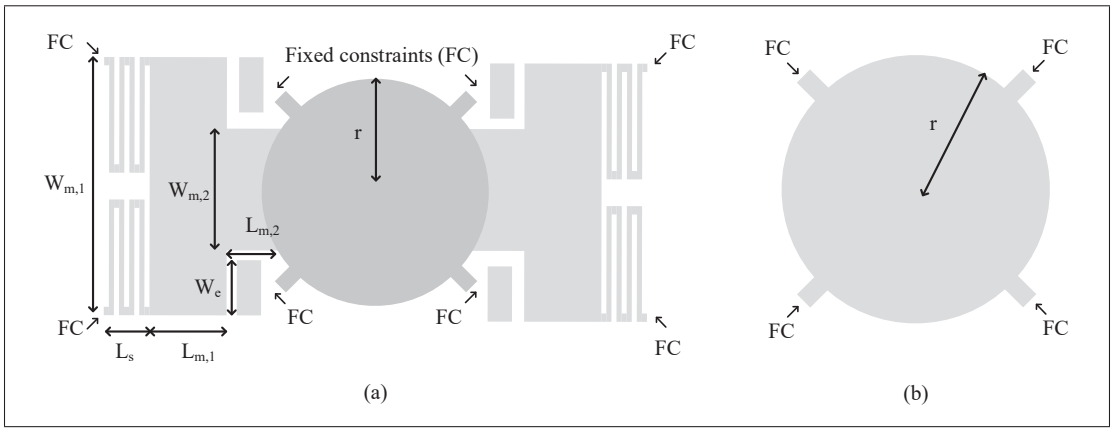

Figure 4.5 Schematic of the simulated structures : (a) PMUT with actuators and masses as a single structure with its design dimensions, and (b) PMUT without actuators or masses

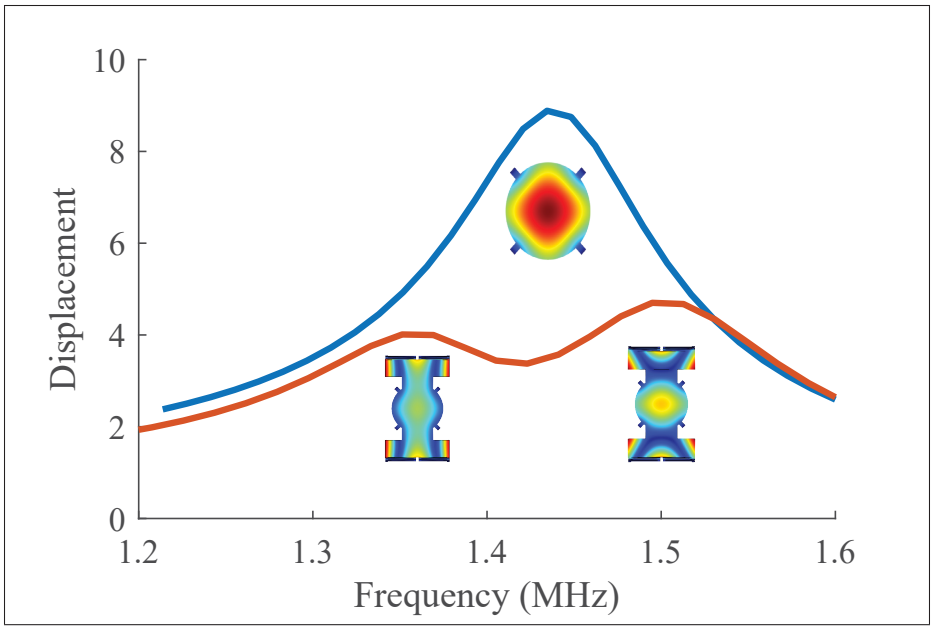

Figure 4.6 Simulation of the displacement of the PMUT device. The displacement is plotted as a function of the frequency with and without the actuator enabled for $L_{m,1}$ equal to 70 μm. Drawings of the mode shapes are included at the corresponding frequencies

As a first step, a design target for the activation voltage was set to about 100 V, and the spring was designed to reach a full collapse into the membrane at this voltage. Fig. 4.5a) shows the structure with the important dimensions. First, a PMUT radius r of 100 μm was selected. Then,

the width of masses m_2, $W_{m,2}$, was chosen to cover the entire perimeter between two membrane anchors, in order to maximize contact area under collapse. Finally, the width of mass m_1, $W_{m,1}$, and the number of spring sections were varied. A higher value of $W_{m,1}$ increases the overall length of the electrode and therefore increases the electrostatic force and reduces the activation voltage. A higher number of spring sections reduces the total spring constant and the activation voltage. The PMUT device dimensions selected are summarized in Table 1.

Tableau 4.1 PMUT dimensions used for fabrication.

Parameter	**Value**
$W_{m,1}$	365 μm
$W_{m,2}$	180 μm
$L_{m,2}$	50 μm
W_e	92.5 μm
Total length of the spring	18 μm

In addition, simulations were undertaken to predict the behavior of the structure under the effect of the dampers. In the case when the actuator is not activated, the structure was modeled as a PMUT with four anchors depicted in Fig. 4.5b). Further, to quantify the effect of the dampers on the resonant frequency in the case when the actuator is enabled, a perfect contact between the dampers and PMUT membrane was assumed. In that case, both the dampers and the PMUT membrane were modeled as a single solid structure, as depicted in Fig. 4.5a).

Eigenfrequency simulations for both actuator states were undertaken in order to estimate the resonant frequencies and the mode shapes. Subsequently, frequency domain simulations were carried-out for both cases. Fig. 4.6 shows the results of these simulations. With this simplified model, the dampers are shown to indeed effectively decrease displacement amplitude at the original working frequency. In fact, the dampers and PMUT membrane act as coupled resonators, exhibiting a frequency response that is composed of two close resonant peaks, leaving a notch at the original working frequency.

Furthermore, as stated in section II, the spring constant and mass, and therefore the dimensions of the dampers, play an important role in the influence of the dampers on the resonant frequency.

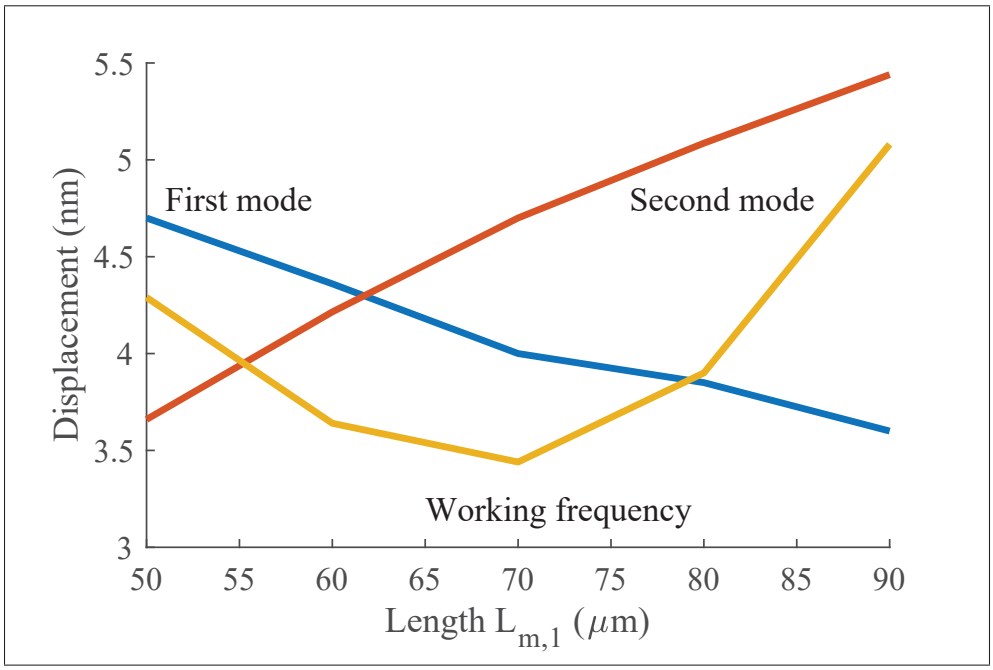

Figure 4.7 For the enabled actuator, the maximum displacement is plotted as a function of $L_{m,1}$ varying between 50 μm and 90 μm. Three frequencies are considered : the working frequency, the frequency of the first mode and the frequency of the second mode

To investigate their influence, a series of simulations was undertaken. First, for the structure depicted in Fig. 4.5*a*), the mass length $L_{m,1}$ was swept from 50 μm to 90 μm. Fig. 4.7 shows the influence of $L_{m,1}$ on the displacement amplitude of the vibration at the working frequency and at the frequency of the first and second modes. The displacement amplitude at the frequency of the first mode decreases with an increase of $L_{m,1}$, and the opposite effect occurs at the frequency of the second mode. Also, the intersection of the two coincides with the minimum of the amplitude at the working frequency. This is consistent with Fig 4.6, where the same phenomenon can be observed. This minimum, the design optimum at which dampers are most effective at damping displacement at the working frequency, is obtained for a value of $L_{m,1}$ of about 70 μm.

Then, to vary k_1 the length of the anchors was varied from 10 μm to 30 μm. Fig. 4.8 shows the results. It can be seen that by varying k_1, the first and second mode resonant frequencies vary, causing a working frequency variation. From the trend shown in Fig. 4.8, it is expected that the displacement will be lower for any variation of k_1 from the optimum. Indeed, for any

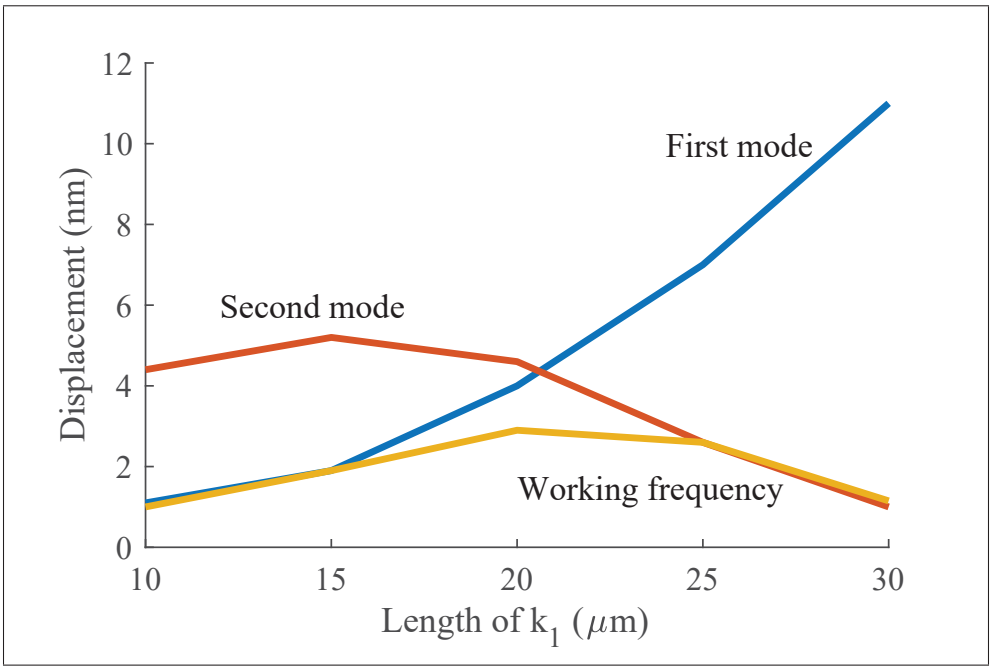

Figure 4.8 For the enabled actuator, the maximum displacement is plotted as a function of the length of k_1 varying between 10 μm and 30 μm. Three frequencies are considered : the working frequency, the frequency of the first mode and the frequency of the second mode

value lower or higher than 20 μm (i.e., the value for which the resonant frequency is 1.4 MHz), the deflection at 1.4 MHz (i.e., the working frequency) is reduced.

Finally, the width of the beam implementing k_2 was varied from 2 μm to 4 μm and the results are shown in Fig. 4.9. The lower limit of 2 μm correspond to the minimum width allowed by the technology and was chosen for this reason. The upper limit was chosen to be reasonably large in order to keep the activation voltage low enough. As can be seen, over the considered rang of value, the influence of k_2 is minimal.

4.4 Measurement Results

The dimensions for the fabricated device of Figure 4.4 were selected based on the simulation results, as presented in Table 1. The actuator was driven using a high voltage Stanford Research PS325 Power Supply. The required activation voltage was found experimentally to be about 80

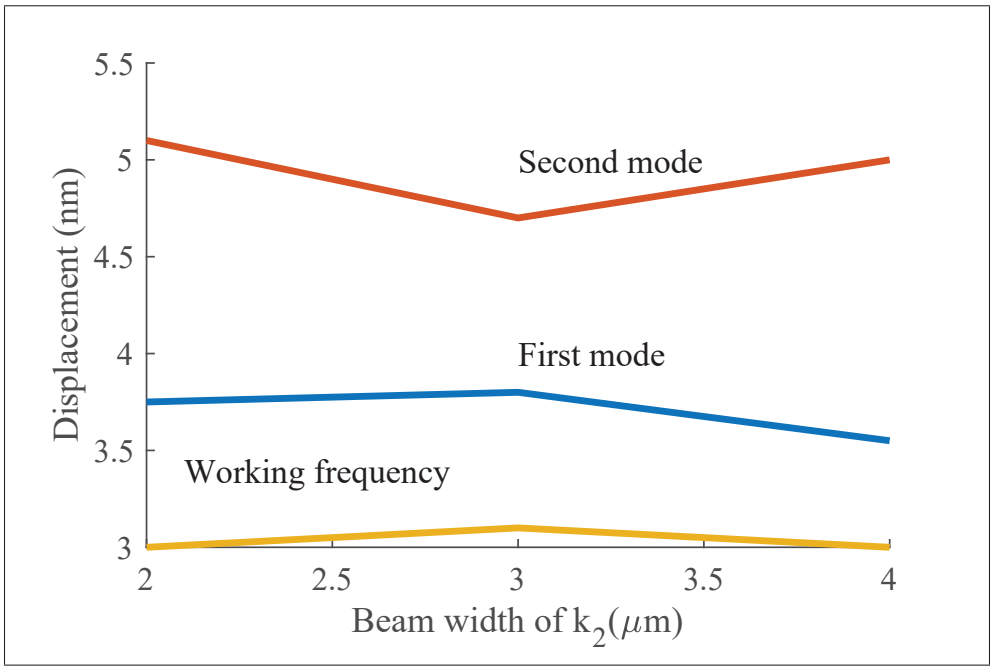

Figure 4.9 For the enabled actuator, the maximum displacement is plotted as a function of the beamwidth of k_2 varying between 2 μm and 4 μm. Three frequencies are considered : the working frequency, the frequency of the first mode and the frequency of the second mode

V. The actuator was switched on and off more than 20 times. The PMUT baseline performance was measured with the VNA, and it remained unchanged after this actuator cycling.

4.4.1 Time domain

In order to perform time domain measurements, a Polytec OFV-5000 vibrometer was used. The laser of the vibrometer was targetted at the center of the PMUT membrane to measure the time-varying transverse velocity at that point. As a first step, the time required for the membrane to stop ringing was measured. To make the PMUT vibrate, a 18 V_{p-p} signal at a frequency of 730 kHz was applied at its terminals while the vibrometer was performing continuous recording of the velocity. The signal driving the PMUT was then deactivated, with the resulting PMUT transition shown in Fig. 4.10a). It took 57 μs for the membrane to reach half of its original velocity amplitude, also corresponding to a halving of the output acoustic power.

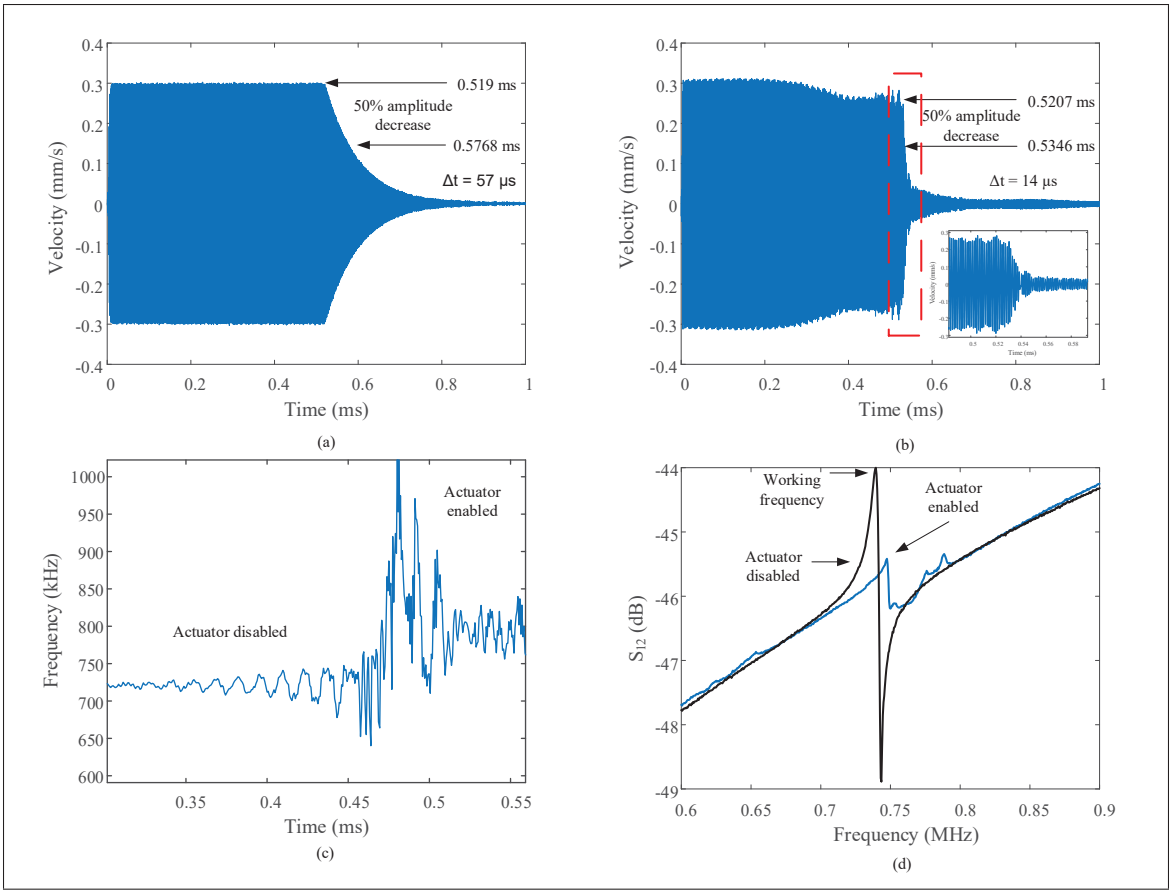

Figure 4.10 Measurement of the PMUT velocity (a) when the actuator is disabled but the excitation signal is turned off, (b) when the actuator is enabled, (c) measurement of the resonant frequency of the PMUT as a function of time during the damper activation, and (d) measurement of the transmission characteristic (S_{12} scattering parameter) with and without the actuator enabled

This baseline was then compared with the use of the actuator to stop the membrane. In this case, the vibrometer was used to perform continuous recording in exactly the same way as previously, but followed by activating the actuator instead of shutting down the driving signal. The actuator was kept enabled after activation. Fig. 4.10b) shows the transient velocity of the membrane during this process. Further, when the PMUT is not damped by the dampers, the deflection is of about 200 nm and, when damped by using the dampers, it is of about 8 nm. One can observe that the time needed to decrease the velocity amplitude by a factor of 2 is 14 μs. Hence, the use of the damper increases shutdown speed by a factor of approximately 4. In principle, the proposed method could therefore provide a fourfold improvement in range or precision, with respect to a

PMUT without the proposed electromechanical damping. Note that no other transient effects than the prompter extinguishing of the membrane vibration were observed after the actuation of the dampers.

Furthermore, Fig. 4.10c) shows the variation of vibration frequency as a function of time. One observes that when the actuator is enabled, the frequency shifts to a higher value. Also, frequency undergoes relatively large variations during this transition which again emphasizes the non-linearity of the phenomenon.

Finally, the mode shape of the PMUTs was mapped using the vibrometer. Fig. 4.11a) shows the results for 8 different phases of the resonance cycle, outlining the symmetry of the mode and the displacement amplitude of about 220 nm. Fig. 4.11b) shows the results for 8 different phases of the resonance cycle when the actuator is enabled. One can see that one side of the PMUT is fully anchored while the other side is solely partially anchored. The anchor not fitting perfectly alongside the PMUT and process variation induced asymmetry could explain this. Nonetheless, this corroborates that the membrane and damper are coupled together after actuation. It is also important to note that the structure behaved in a binary fashion such that when pull-in of the damper was seen, no performance variation was observed at different actuation voltage levels, potentially indicating that once pull-in is acheived the structures are indeed mechanically connected.

4.4.2 Frequency domain

The resonant frequency of the devices was acquired by measuring the S_{12} scattering parameter between the PMUT membrane electrodes. Measurements were performed using an EP6 Cascade Probe Station and an E5061B Keysight PNA Network Analyzer in combination with GSG probes.

The S_{12} scattering parameter measurements were made for the baseline and actuated cases, as shown in Fig. 4.10d). Again, these results confirm that the damper is able to effectively dampen the PMUT at its original working frequency. Also, the damped resonant frequency is shown to

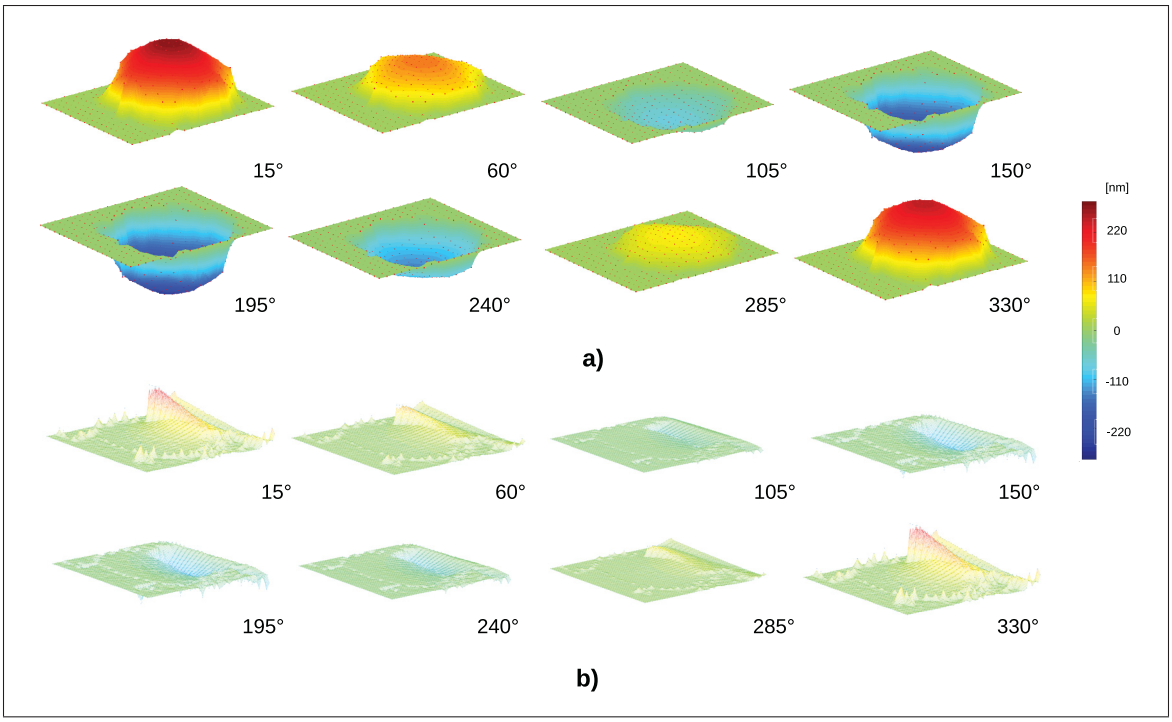

Figure 4.11 Mode shape at 8 different phases of the vibration cycle
a) without actuator enabled and b) with actuator enabled

be translated by more than 100 kHz, which contributes to a further reduction in the amplitude at the working frequency. Overall, this electrical response is reduced by more than 2 dB through electromechanical damping.

Some discrepancies between simulation and measurements were observed. First, measured resonant frequency was found to be about 740 kHz. This value is lower than that expected from simulation. This is most likely caused by a larger trench size than expected, due to process variations. Hence, the PMUT anchors are effectively longer, which in turn causes a decrease of the resonant frequency. Indeed, as can be seen in Fig. 4.4, the trench of the actuator occupies an area underneath the anchors that is larger than expected, since process variations of the PiezoMUMPs technology for the DRIE steps are relatively large. As stated in the technology design guide (Cowen & et al., 2013), variations can be as high as 100 μm. To verify this hypothesis, simulation of a structure with longer anchors has been carried out. It was found that an increase in trench size of 35 μm would result in a structure with a resonant frequency

of 750 kHz. Although the presented structure represents a proof of concept of a new actuation method, a custom fabrication process could be used instead to better control critical process variations and improve fabrication accuracy.

Furthermore, in simulation, the structure presents two resonant frequencies spaced by a few hundred kHz (see Fig. 4.6, which is not observed in measurements. In fact, only one resonant frequency is detectable. In simulation, the lower resonant mode shape could only be produced if both structures were effectively combined as one single solid structure. Only in this fashion can the axial bending outlined in this mode be achieved. As the actuated mass structure is not rigidly connected to the membrane, this mode is not likely to be favoured in practice because it would cause significant strain at the contact interface and both structures are likely to slide on one another. The damper is thus not believed to bend with the PMUT but rather exert friction at the interface, favoring the higher frequency simulated mode.

Finally, the transmission characteristics for the PMUT after actuation is atypical. The resonant peak is sharp and the overall shape is degenerated. This can be explained by the fact that the contact, as explained in section II, is exposed to non-linear effects between the structures. However, a detailed explanation of these phenomena is beyond the scope of this work. The devices of this work were designed for in-air applications. However, they were also validated to be functional in water.

The damper is used to shorten the pulse length in the time domain. When the damper is not enabled, the PMUT is completely unaffected and benefits from a higher Q-factor and a higher resonance efficiency. The damper is activated to quickly reduce the PMUT vibration. As seen in Fig. 4.2b and Fig. 4.10d, after activation, the acoustic power is significantly lower. Thus, the dynamic use of the damper results in a shorter pulse width in the time domain while keeping the same peak pressure.

A comparison of resolutions of state-of-the-art PMUTs is shown in Table 4.2. To be meaningfully comparable, the axial resolutions have been normalized according to the period of the signal. The resolution of the PMUT of this work was estimated based on the measured ring down time.

As can be seen, using the technique presented in this paper, the axial resolution of a high-Q PMUT can be increased to reach a value comparable to that of state-of-the-art PMUTs while maintaining the advantages of a high-Q device, notably in terms of peak pressure.

Tableau 4.2 Comparison of state-of-the-art PMUTs resolutions

	Lu et al. (2015)	**Dausch et al. (2014)**	**Jung et al. (2013)**	**Przybyla et al. (2010)**	**This work**
Frequency (MHz)	8	5	3.5	0.4	0.72
Axial resolution (mm)	0.2	0.5	0.9	9	4.6
Normalized axial resolution (mm)	1.6	2.5	3.15	3.6	3.3

4.5 Conclusion

This paper presented a novel technique for stopping the resonance of PMUTs using mechanical damper controlled by electrostatic actuators. A simplified model was used to understand the principles of the structure in theory and in simulation. This was intended to provide an approximate idea of the influence of the different design parameters. It was found that the dimensions of the damper structures play a crucial role in the way they influence device dynamics. Through vibrometry, it was shown that using the proposed electromechanical damping method is able to reduce the ringing time of a PMUT by a factor of 4. In the time domain, this results in a narrower pulse, which can be potentially leveraged for either higher axial resolution or longer imaging range. Electrical measurement results also show that displacement amplitude at the working frequency can effectively be reduced by more than 2 dB using the proposed technique.

This work embodies the first investigation of this type of PMUT structure, and more investigation will be undertaken at the system level as a result of this work. Notably, synchronisation of the damper actuation signal with the driving acoustic signal will be required to apply the concept

introduced in this work to imaging applications. Ultimately, this work can potentially yield atypical imaging performance metrics that will widen the application scope of PMUT devices.

Acknowledgement

The authors would like to thank CMC Microsystems for providing the layout design tools and enabling chip fabrication. The authors also wish to thank the Natural Sciences and Engineering Research Council (NSERC) of Canada and the Microsystems Strategic Alliance of Quebec (ReSMiQ) for their financial support of this work.

CHAPITRE 5

PIEZOELECTRIC MICROMACHINED ULTRASOUND TRANSDUCER BASED SYSTEM IN PACKAGE FOR ULTRASOUND APPLICATIONS

Alexandre Robichaud[1], Dominic Deslandes[1], Frederic Nabki[1], Paul-Vahé Cicek[2]

[1] Département de Génie électrique, École de Technologie Supérieure,
1100 Notre-Dame Ouest, Montréal, Québec, Canada H3C 1K3
[2] Département d'informatique, Université du Québec à Montréal,
201, avenue Président-Kennedy, Montréal, Québec, Canada H2X 3Y7

Article soumis à la revue « IEEE Journal of Microelectromechanical Systems » en mai 2018.

5.1 Introduction

Because conventional ultrasonic transducers are subject to several drawbacks in terms of cost and efficiency (Jung, Lee, Kang, Shin, Ryu & Choi, 2017), micromachined ultrasonic transducers (MUT) have garnered considerable interest in the research community, due to their potential for integration with integrated circuits (IC) and their ability to be mass-produced at very low cost (Tang, Lu, Jiang, Ng, Tsai, Horsley & Boser, 2016b), (Zahorian, Hochman, Xu, Satir, Gurun, Karaman & Degertekin, 2011b), (Xu, Zhao, Jiang, Guo, Li, Yang, Sun, Luo & Zhang, 2019). MUTs can be implemented to rely either on capacitive (CMUT) or piezoelectric (PMUT) transduction.

For actuation purposes, CMUTs require DC electrostatic biasing, often at a level near membrane pull-in (Akasheh, Fraser, Bose & Bandyopadhyay, 2005b). Furthermore, to achieve full acoustic sensing, multiple devices with different transduction air gap sizes must be realized concurrently in order to achieve strong acoustic signal transmission (large air gap) and sensitive reception (small air gap) (Akasheh, Myers, Fraser, Bose & Bandyopadhyay, 2004b). Contrary to CMUTs, no DC biasing is required to operate PMUTs, while they generally also exhibit superior signal-to-noise ratio (Qiu, Gigliotti, Wallace, Griggio, Demore, Cochran & Trolier-McKinstry, 2015b). PMUTs have successfully been demonstrated in several applications such as distance sensing (Przybyla, Flynn, Jain, Shelton, Guedes, Izyumin, Horsley & Boser, 2011a), (Feng & Liu, 2019), gesture

recognition (Przybyla, Tang, Shelton, Horsley & Boser, 2014b), (Yin, Zhu & Hu, 2019) and medical imaging (Dausch, Gilchrist, Carlson, Hall, Castellucci & von Ramm, 2014b), (**?**), (Dangi, Cheng, Agrawal, Tiwari, Datta, Benoit, Pratap, Trolier-McKinstry & Kothapalli, 2019).

This work presents the design of a complete ultrasonic imaging system in package (SiP) relying on a PMUT matrix. A 4×8 PMUT matrix and its interface CMOS IC are combined in a single package resulting in high performance, compact size, low cost, and reduced power consumption. The transducer matrix is designed with finite element analysis software, followed by model extraction of equivalent lumped electrical elements, which are used as loads in the electronic design of the interface IC. In section II, an overview of the overall system is presented, followed by the PMUT design, fabrication and characterization in section III. Finally, section IV covers the design of the CMOS interface chip.

5.2 System Overview

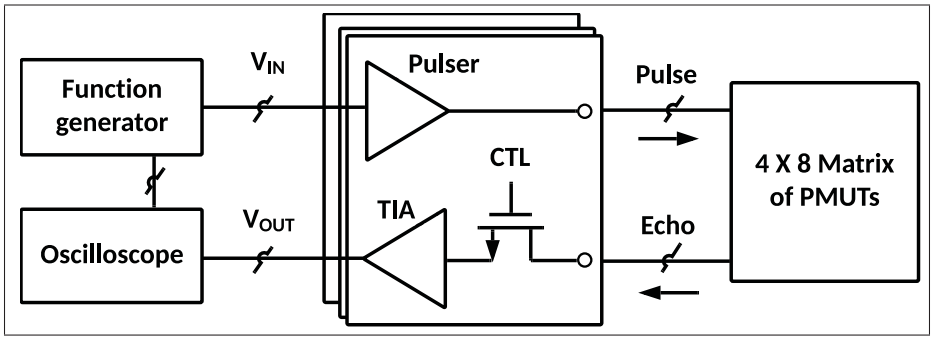

Figure 5.1 Block diagram of the proposed PMUT SiP

The proposed SiP is composed of a PMUT matrix, fabricated using the PiezoMUMPS micro-fabrication technology, along with its interface CMOS IC for signal driving and sensing, as presented in Fig. 5.1. The PMUT matrix, with its 8 columns of 4 PMUTs, is able to perform beamforming by driving each element with properly time-delayed electrical pulses. For this proof-of-concept design, the PMUT of a column are electrically connected together, an approach that was selected in order to reduce the number of channels on the CMOS die to 8, hence minimizing chip size and cost. Therefore, the matrix here is only addressable column-wise and

beamforming is only possible in one dimension. The reader should note that this constitutes a prototyping design choice rather than a technical limitation. Finally, in this work the functionality of the SiP is verified based on a single channel.

The CMOS circuit, designed in high voltage 0.35 μm technology from AMS, is composed of pulsers and transimpedance amplifiers (TIA). Each column of the PMUT matrix requires a pulser and a TIA, for a total of 8 cells.

The role of a pulser is to drive a PMUT with an electrical excitation of sufficient amplitude to generate a strong acoustic pulse. This system provides an amplitude up to 50 V_{pp}, the maximum allowed by the CMOS technology. As for the TIA, its purpose is to sense and amplify the returning acoustic echo to allow for accurate sampling. For each matrix column, a distinct pulser-TIA interface cell is connected to all of the PMUTs of that set. To avoid that the high-voltage output of the pulser causes any damage to the TIA, the latter is decoupled from the circuit by a switch during acoustic transmission.

For this prototype, an external signal generator is used to activate the pulsers, modulate the desired beamforming, and sample the echo back. In future work, this functionality is to be accomplished by the CMOS circuit.

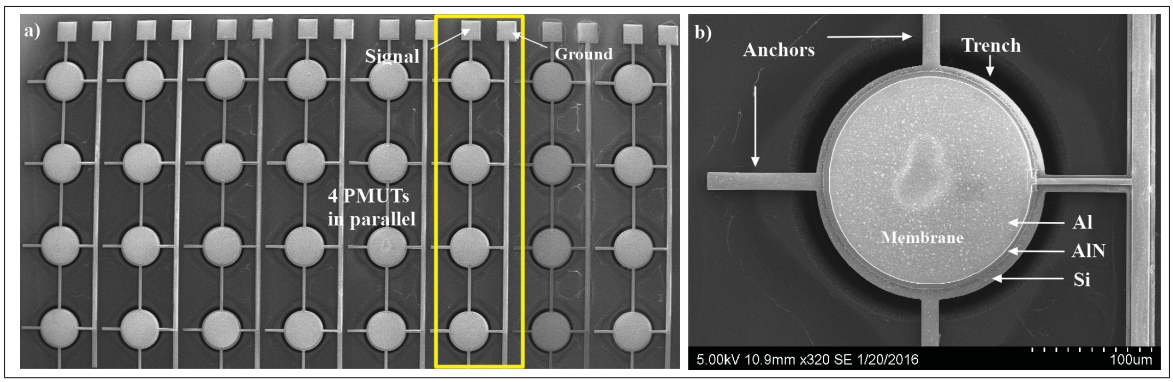

Figure 5.3 Micrograph of the fabricated PMUT matrix

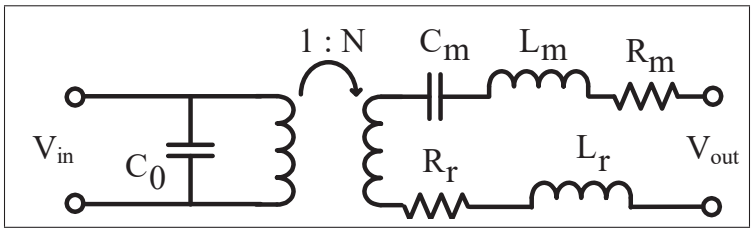

Figure 5.2 Equivalent circuit of a PMUT

5.3 Design, Fabrication and Characterization of the PMUT Matrix

5.3.1 PMUT Equivalent Circuit

A PMUT can be represented by the Butterworth-Van Dyke equivalent circuit presented in Fig. 5.2. The capacitance C_0 is the electrical capacitance of the PMUT and can be estimated using this equation :

$$C_0 = \epsilon_0 \frac{A}{d}. \tag{5.1}$$

The parameters L_m, C_m and R_m represent the mechanical properties of the structure. They correspond to the mass, stiffness and damping, respectively, and are expressed in terms of electrical units (H, F and Ω).

Finally, parameters L_r and R_r correspond to the real and imaginary parts of the acoustic impedance, respectively. Techniques to calculate the values of the lumped parameters can be found in (Bhugra & Piazza, 2017 ; Butler & Sherman, 2016 ; Smyth & Kim, 2015b).

5.3.2 Fabrication Process

The commercial PiezoMUMPS process (Cowen & et al., 2013) was used to fabricate the PMUT matrix presented in this work. The process starts with a SOI wafer, covered with a 400 nm thick insulator layer and a 10 μm thick silicon device layer. On top of the wafer, a 500 nm aluminum nitride (AlN) piezoelectric layer is deposited by sputtering, and patterned using standard lithography and wet etching in order to produce a circular membrane of 200 μm

diameter. Subsequently, a 1 μm thick aluminum layer is deposited by e-beam evaporation and lifted off, leaving a circular aluminum layer with a 190 μm diameter and aluminum pads allowing electrical connections to the PMUT and actuator. The diameter of the aluminum circle is smaller than that of the AlN in order to prevent contact with the bottom electrode. Later, the silicon layer is etched by DRIE, resulting in a circular silicon membrane and four supports. Finally, the membrane is released by etching a trench from the back of the handle wafer by DRIE, followed by a wet etch to traverse the oxide. A matrix of 4×8 PMUTs was fabricated. Fig. 5.3 a) shows the fabricated PMUT matrix and 5.3 b) shows a detailed view of a single PMUT.

5.3.3 Finite-element Simulations

The finite-element simulator COMSOL Multiphysics was used to design the PMUT. Simulations were performed using the specified physical parameters of the PiezoMUMPS process. The modeled PMUT is composed of a silicon membrane of 100 μm radius and 10 μm thickness on top of which a 500 nm AlN layer and a 1 μm aluminum layer are deposited. These layers act as the piezoelectric layer and the top electrode, respectively. The membrane is suspended by four supporting arms in order to increase the acoustic power as compared to a fully anchored membrane. Finally, the membrane is incorporated in a sphere of air to take into consideration air damping and obtain more accurate results. Fig. 5.4 a) shows the COMSOL model configuration and 5.4 b) shows acoustic pressure simulation results.

To identify the device resonant frequency, eigenmode simulations were undertaken. The frequency of the first mode was found to be at around 1.5 MHz.

5.3.4 Characterization

A PMUT were characterized using an E5061B Keysight PNA Network Analyzer, and an EP6 Cascade Probe Station, in combination with GSG probes. Conductance was measured by sweeping the frequency from 1.3 to 1.7 MHz, as presented in Fig. 5.5.

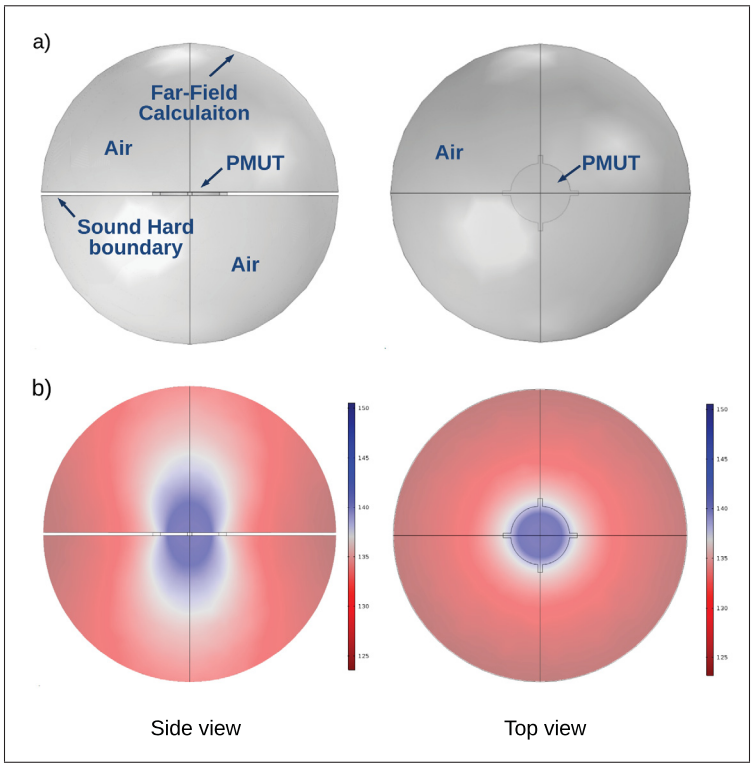

Figure 5.4 COMSOL simulation. a) model used for simulation and b) simulation results of acoustic pressure level in dBV

As a first step, to estimate the values of the lumped parameters of the equivalent circuit described in section III.A, the equations in (Bhugra & Piazza, 2017; Butler & Sherman, 2016; Smyth & Kim, 2015b) were used. Based on the obtained circuit the conductance as a function of frequency was calculate. Finally, curve fitting was made by adjusting the parameters to obtain a match between calculation and measurement. This allows to extract an accurate load model to perform the design of the CMOS chip.

The values of the lumped elements obtained for L_m, C_m, R_m, R_r, L_r and C_0 are 902 pH, 12.6 μF , 25.6 $\mu\Omega$, 14.3 $\mu\Omega$, 0.36 pH and 5.72 pF respectively.

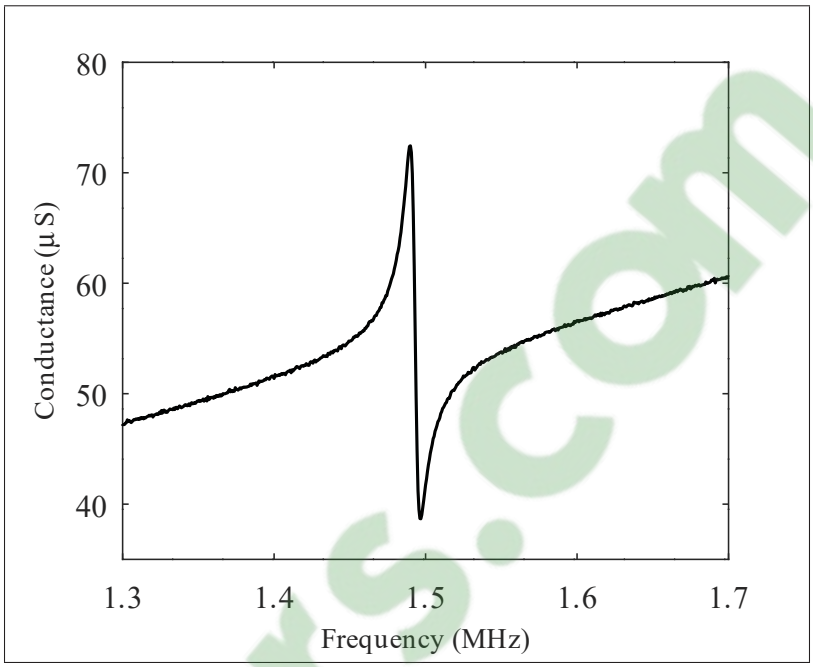

Figure 5.5 Measurement of the conductance of a PMUT as a function of frequency

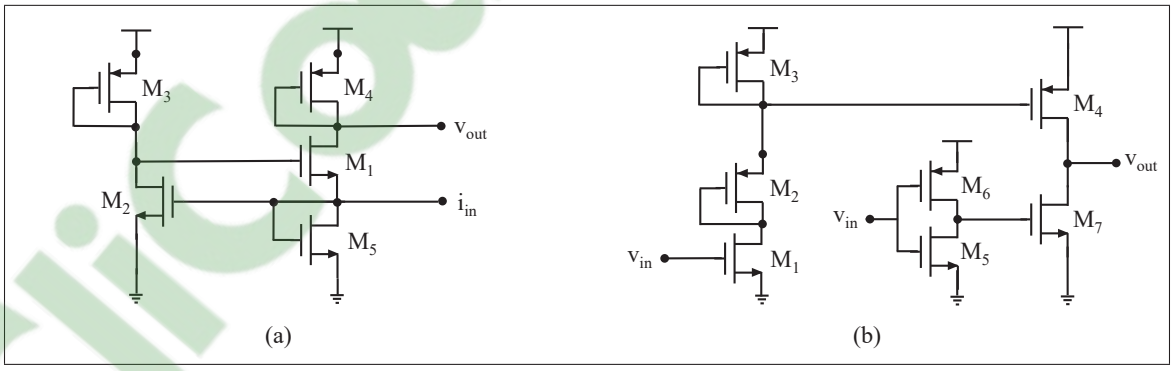

Figure 5.6 Schematic of (a) the RGC TIA and (b) the high-voltage pulser

5.4 Design of the CMOS Chip

The CMOS interface chip is composed of several identical high-voltage pulsers and TIAs, realized in high-voltage AMS 0.35 μm CMOS technology. The high-voltage pulser is driven by a 3.3 V_{PP} square wave at its input, providing at its output a square wave of up to 50 V_{PP}, with the same frequency and duty cycle. The TIA amplifies the electrical signal produced by a PMUT in response to an acoustic echo, with a gain of 87 dBΩ and a 3 dB bandwidth of 12 MHz.

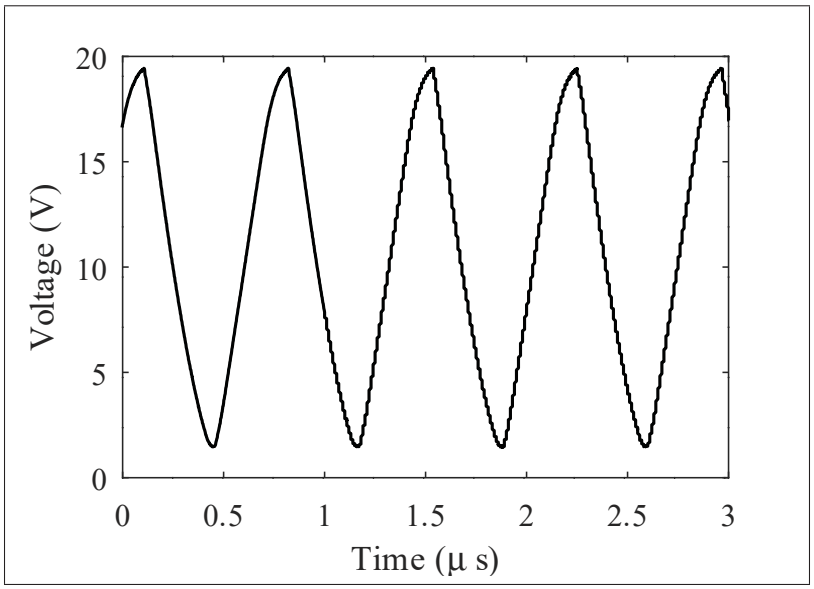

Figure 5.7 Time domain measurements of the high-voltage pulser

5.4.1 Design of the High-voltage Pulser

The pulser is composed of a level shifter followed by a high-voltage driver. Fig. 5.6b) shows the circuit. The 3.3 V input signal is applied at the gate of M1. When V_{in} is 0, the voltage at the drain of M4 (source of M3) is equal to V_{DD}. When V_{in} is equal to 3.3 V, M1 becomes a short-circuit. In this case, diode-connected transistors M2 and M3 behave as a voltage divider with its output taken at the drain of M3 and applied at the gate of M4, thus turning it on. Sizing of the transistors M2-M3 was selected so that the voltage at the drain of M3 vary between approximately 50 V and 45 V allowing to fully turn the high-voltage transistor M4 on and off respectively. V_{in} is also applied to the input of the inverter implemented using M5 and M6, applying the inverse of V_{in} to the gate of M7. Hence, when V_{in} is high, M7 is turned off and M4 is turned on such that V_{out} becomes a high-voltage replica of V_{in}.

5.4.2 Design of the Transimpedance Amplifier

To amplify the echo signal, a regulated cascode (RGC) TIA was chosen. It provides a small input impedance and a high bandwidth. Fig. 5.6a) shows a schematic of the circuit. The input signal

is connected to the source of a common gate (CG) amplifier. The input is also connected to a common source (CS) amplifier. The output of the CS is connected back to the CG forming a feedback which decreases the input impedance by a factor proportional to the gain of the CS. The input impedance is given by :

$$Z_{in} \approx \frac{1}{g_{m,1} \cdot (1 + g_{m,2} \cdot 1/g_{m,3})}. \tag{5.2}$$

and the gain is given by :

$$Z_T \approx 1/g_{m,4}. \tag{5.3}$$

The pad to the input of the RGC is to be placed as close as possible to its corresponding PMUT to minimize noise, and the electrical connection is made using a gold wirebond.

5.5 Measurement Results

The high-voltage pulser was tested using an oscilloscope, as shown in Fig. 5.7. One can see that the minimum output voltage correspond to the V_{tn} of M5. Although the specified working frequency of 1.5 MHz is achieved, the signal suffers slight distortion, which can be attributed to the slew rate of the TIA output.

The RGC TIA sensing amplifier was tested using an oscilloscope, with the resulting transfer function presented in Fig. 5.8. The measured gain is of about 64 dBΩ and the measured bandwidth is of about 1.5 MHz.

The fully-realized system was used to perform ranging measurements. A THORLABS translation stage was used to mount a supporting PCB in vertical position. A 4 period-long square wave with a frequency of 1.5 MHz and an amplitude of 3.3 V_{pp} was used to drive a high-voltage pulser. A supply voltage of 20 V was used for the pulser. The pulser was wire bonded to a first

column of PMUTs in order to generate acoustic waves. The reflected signal was then received by an adjacent column of PMUT which was bonded to the RGC TIA. The stage was gradually displaced transversely to vary the separation distance between the chip and the reflector. Before acquiring the ranging measurements, cross-talk between the emitting and receiving PMUT was measured and characterized. Afterwards, cross-talk was subtracted from the received signal to best represent the acoustic transmission. Fig. 5.9 shows the measurement setup. The output of the RGC was measured using an oscilloscope. Fig. 5.10 shows the measurements obtained for separation distances ranging from 2 mm to 12 mm. This shows that the system can effectively be used to undertake ranging measurement with excellent accuracy. The echo is a very weak signal. Therefore, the TIA was shown to have sufficient gain to amplify the signal in order for it to be perceptible at the output.

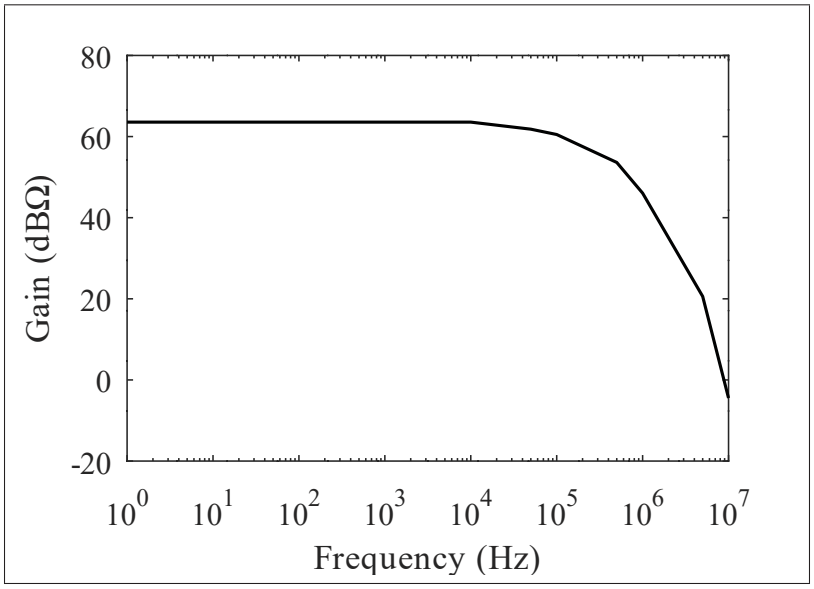

Figure 5.8 Frequency domain measurements of the RGC TIA

5.6 Conclusion

This paper presented a SiP composed of a matrix of PMUTs and their interface CMOS circuit. An equivalent circuit for a PMUT was established and then used as the load for the simulation of the CMOS circuit. The high-voltage pulser was designed to drive the PMUT and simulations showed

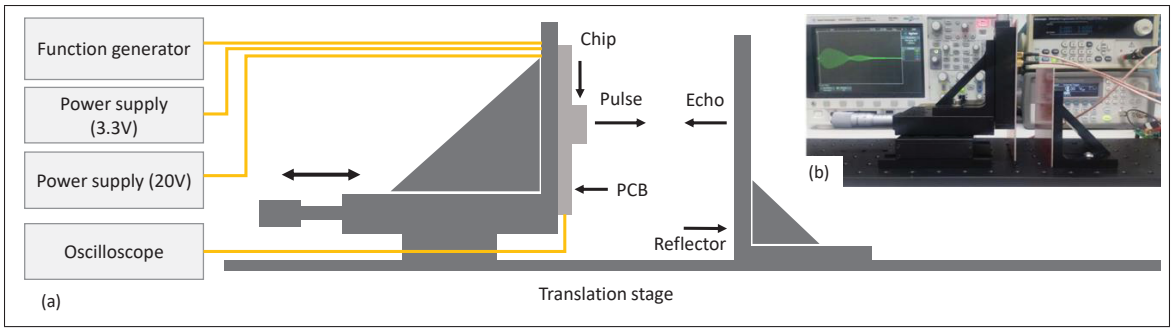

Figure 5.9 (a) Schematic and (b) photograph of the measurement setup

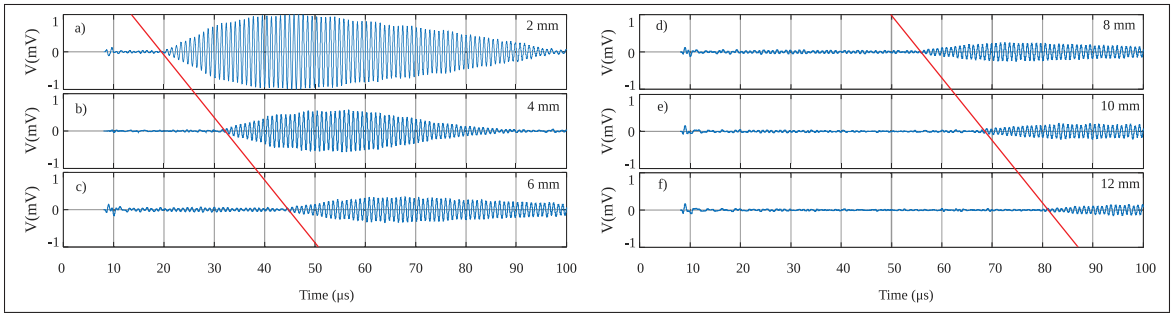

Figure 5.10 Ranging measurement results in air for distances of a) 2 mm, b) 4 mm, c) 6 mm, d) 8 mm, e) 10 mm, and f) 12 mm

that it was capable of doing so with a 20 V_{pp} square wave at 1.5 MHz. A TIA was designed, fabricated and used to amplify the echo received. The fully-realized SiP was successfully used to undertake ranging measurements at up to 12 mm. The results have shown that the SiP can be used to undertake this task and represents a compact implementation that can be the basis for an imaging system in ulterior prototypes building on this work.

Acknowledgement

The authors would like to thank CMC Microsystems for providing the layout design tools and enabling chip fabrication. The authors also wish to thank the Natural Sciences and Engineering Research Council (NSERC) of Canada and the Microsystems Strategic Alliance of Quebec (ReSMiQ) for their financial support of this work.

CONCLUSION ET RECOMMANDATIONS

Cette thèse avait pour objectifs d'investiguer la possibilité de développer une micropuce pour les applications ultrasoniques comme la mesure de distances et l'imagerie qui soit faible coût et facile à intégrer. Les transducteurs ultrasoniques piézoélectriques micromachinés (PMUTs) constituent la technologie clef de cette investigation. Des architectures et des techniques de fabrication des PMUT, des circuits de contrôle et leur intégration ont été investigués.

Tout d'abord, une nouvelle technique de réglage de fréquence PMUT qui est peu coûteuse et efficace ne nécessitant qu'une étape de post-traitement sous la forme d'un dépôt de film mince de Parylene-C est proposée. Les résultats confirment que la technique de post-traitement peut être utilisée pour régler avec précision la fréquence des PMUT à facteur Q élevé afin d'optimiser la caractéristique de transmission entre deux PMUT malgré les variations des procédés de fabrication. De cette façon, une communication puce à puce entre deux dispositifs initialement à des fréquences de résonance différentes a été obtenue, avec une efficacité de transmission considérablement améliorée.

Puis, une nouvelle topologie d'ancrage des PMUT permettant de réduire la dépendance de la fréquence de résonance aux variations. Cette technique s'est montrée particulièrement efficace pour les PMUT fabriqués à l'aide du procédé DRIE comme c'est le cas pour la technologie PiezoMUMPs. Les résultats montrent que les variations de fréquence de résonance entre deux puces peuvent être réduites d'un facteur d'environ 4. Finalement, les PMUT ainsi fabriqués ont été utilisés pour effectuer des mesures de distance.

Ensuite, un amortisseur mécanique contrôlé par des actionneurs électrostatiques a été développé et utilisé pour arrêter la résonance des PMUT. La raison d'être de cette technique novatrice est de réduire la longueur des pulses émis dans le domaine temporel afin d'augmenter la résolution axiale tout en conservant les avantages d'un PMUT à haut facteur de qualité en termes d'efficacité énergétique. Afin de quantifié la diminution de la longueur des pulses des mesures à l'aide d'un

vibromètre ont étés faits. À l'aide de cette technique de mesure, il a été démontré que l'utilisation de la méthode d'amortissement électromécanique proposée est capable de réduire le temps de sonnerie d'un PMUT d'un facteur d'environ 4.

Finalement, un SiP (system in package) composé d'une matrice de PMUT et d'un circuit CMOS pour l'interfaçage a été développé. Le circuit intégré est constitué de pulseurs haute tension pour attaquer les PMUT ainsi que d'amplificateurs transimpédances (TIA) pour amplifié l'écho de retour. Cet écho peut être un signal très faible. L'amplificateur a donc été conçu pour avoir un gain élevé d'environ 80 dB. Finalement, le SiP a été utilisé pour effectuer des mesures de distance avec succès.

Recommandations

Plusieurs recommandations peuvent être élaborées en ce qui concerne la poursuite du travail présenté dans cette thèse. Les recommandations qui seront présentées ont trait tant à l'architecture et à la fabrication des PMUT qu'à l'intégration monolithique du circuit de contrôle.

Le premier ensemble de recommandations porte sur la fabrication des PMUT et les techniques de fabrication nécessaires à cet effet. La fabrication maison des PMUT permettrait de contourner certaines limitations imposées par la technologie PiezoMUMPS telles que la taille minimale de la tranchée et l'épaisseur des couches. En développant des recettes maison, il serait possible de fabriquer des PMUT plus petits ayant une fréquence de résonance plus élevée. Ceci permettrait entre autres d'obtenir une résolution plus importante. Ainsi, cela ouvrirait la porte à l'exploration de nouvelles applications nécessitant une telle résolution. Puis, en diminuant la taille des éléments, il serait aussi possible de fabriquer des matrices avec plus d'éléments offrant de nouvelles possibilités pour étudier la formation de faisceau. Finalement, l'épaisseur des couches pourrait être variée afin de trouver un optimum en termes de performances.

Ensuite, la technique d'actuation présentée dans cette thèse pourrait être étudiée davantage à des fins d'optimisation. Par exemple, il serait intéressant d'étudier la possibilité de réduire la

taille des actuateurs pour permettre leur intégration à une matrice plus compacte. Aussi, dans l'ensemble, le concept de l'amortissement dynamique qui a été décrit dans cette thèse pourrait être davantage étudié et d'autres techniques s'inspirant de ce concept pourraient être mises à l'essai. Par exemple, la possibilité d'utiliser un signal d'excitation pour effectuer l'amortissement dynamique pourrait être étudiée. Finalement, le mécanisme d'actuation utilisé dans ce travail était soumis aux limitations imposées par la technologie utilisée. En développant un procédé de fabrication maison, de nombreuses possibilités additionnelles pour être explorées. Par exemple, l'actuation pourrait être effectuée à la verticale plutôt que dans le plan.

Puis, le travail sur le circuit intégré de contrôle pourrait être poursuivi. Entre autres, la possibilité d'intégrer un grand nombre de canaux sur une même microplaquette qui permettrait de contrôler une matrice de PMUT de plus grande dimension pourrait être explorée. Aussi, il serait intéressant d'investiguer la possibilité d'intégrer plus de fonctionnalité au circuit comme une partie du traitement de signaux par exemple. De plus, un module pourrait être développé permettant d'ajouter le pilotage des actuateurs aux fonctionnalités de contrôle de la matrice. Finalement, diverses techniques de formation de faisceaux et la possibilité de les utiliser en concert avec la matrice de PMUT pourraient être investiguées et finalement intégrées au circuit de contrôle.

Finalement, la possibilité d'effectuer la fabrication de la matrice de PMUT directement sur le circuit contrôlé pourrait être étudiée. Cette possibilité d'obtenir une intégration monolithique est intéressante, car elle présente de nombreux avantages en termes de performance, consommation de puissance, taille du dispositif et coût.

Ainsi, cette thèse a présenté un dispositif ultrasonique compact, incluant une matrice de PMUT et un circuit de contrôle. Cette thèse a permis d'effectuer plusieurs contributions notamment au niveau de l'architecture, du post-traitement et de l'actuation ainsi qu'au niveau du circuit de contrôle des PMUT. Toutes ces contributions faciliteront l'avancement de cette technologie de l'avenir que constituent les transducteurs micromachinés. Finalement, cette technologie permettra sans doute le développement d'une multitude de nouvelles applications qui sauront contribuer à l'avancement de la science.

LISTE DE RÉFÉRENCES

Akasheh, F., Myers, T., Fraser, J. D., Bose, S. & Bandyopadhyay, A. (2004a). Development of piezoelectric micromachined ultrasonic transducers. *Sensors and Actuators A : Physical*, 111(2), 275-287.

Akasheh, F., Myers, T., Fraser, J. D., Bose, S. & Bandyopadhyay, A. (2004b). Development of piezoelectric micromachined ultrasonic transducers. *Sensors and Actuators A : Physical*, 111(2-3), 275–287.

Akasheh, F., Fraser, J. D., Bose, S. & Bandyopadhyay, A. (2005a). Piezoelectric micromachined ultrasonic transducers : Modeling the influence of structural parameters on device performance. *Ultrasonics, Ferroelectrics, and Frequency Control, IEEE Transactions on*, 52(3), 455-468.

Akasheh, F., Fraser, J. D., Bose, S. & Bandyopadhyay, A. (2005b). Piezoelectric micromachined ultrasonic transducers : Modeling the influence of structural parameters on device performance. *IEEE transactions on ultrasonics, ferroelectrics, and frequency control*, 52(3), 455–468.

Baborowski, J., Ledermann, N. & Muralt, P. (2002). *Piezoelectric micromachined transducers (PMUT's) based on PZT thin films*. Conference Proceedings présentée à Ultrasonics Symposium, 2002. Proceedings. 2002 IEEE (pp. 1051-1054).

Bayram, B., Hæggstrom, E., Yaralioglu, G. G. & Khuri-Yakub, B. T. (2003). A new regime for operating capacitive micromachined ultrasonic transducers. *Ultrasonics, Ferroelectrics, and Frequency Control, IEEE Transactions on*, 50(9), 1184-1190.

Bhugra, H. & Piazza, G. (2017). *Piezoelectric MEMS resonators*. Springer.

Bhuyan, A., Choe, J. W., Lee, B. C., Wygant, I., Nikoozadeh, A., Oralkan, O. & Khuri-Yakub, B. T. (2013). *3D volumetric ultrasound imaging with a 32× 32 CMUT array integrated with front-end ICs using flip-chip bonding technology*. Conference Proceedings présentée à Solid-State Circuits Conference Digest of Technical Papers (ISSCC), 2013 IEEE International (pp. 396-397).

Bi, F. Z. & Barber, B. P. (2008). Bulk acoustic wave RF technology. *IEEE microwave magazine*, 9(5).

Boser, B., Horsley, D., Przybyla, R., Rozen, O. & Shelton, S. *(2016)*.

Burrascano, P., Callegari, S., Montisci, A., Ricci, M. & Versaci, M. (2014). *Ultrasonic Nondestructive Evaluation Systems : Industrial Application Issues*. Springer.

Butler, J. L. & Sherman, C. H. (2016). *Transducers and arrays for underwater sound*. Springer.

Carey, S., Gregory, C., Brewin, M., Birch, M., Ng, S. & Hatfield, J. (2004). *PVdF array characterisation for high frequency ultrasonic imaging*. Conference Proceedings présentée à Ultrasonics Symposium, 2004 IEEE (pp. 1930-1933).

Caronti, A., Caliano, G., Carotenuto, R., Savoia, A., Pappalardo, M., Cianci, E. & Foglietti, V. (2006). Capacitive micromachined ultrasonic transducer (CMUT) arrays for medical imaging. *Microelectronics Journal*, 37(8), 770-777.

Chan, K., Patel, M., Barniol, N., Bhowmick, S., Cases, S. & Wong, A. (2020). Three Dimensional Modeling of Piezoelectric Micromachined Transducers Built on Top of Integrated Circuits. *2020 4th IEEE Electron Devices Technology & Manufacturing Conference (EDTM)*, pp. 1–3.

Chao, C., Lam, T.-Y., Kwok, K.-W. & Chan, H. L. (2006). *Piezoelectric micromachined ultrasonic transducers based on P (VDF-TrFE) copolymer thin films*. Conference Proceedings présentée à Applications of ferroelectrics, 2006. isaf'06. 15th ieee international symposium on the (pp. 120-123).

Chen, J. (2010). Capacitive micromachined ultrasonic transducer arrays for minimally invasive medical ultrasound. *Journal of Micromechanics and Microengineering*, 20(2), 023001.

Cheng, C. Y., Dangi, A., Ren, L., Tiwari, S., Benoit, R. R., Qiu, Y., Lay, H. S., Agrawal, S., Pratap, R., Kothapalli, S.-R. et al. (2019). Thin Film PZT-Based PMUT Arrays for Deterministic Particle Manipulation. *IEEE transactions on ultrasonics, ferroelectrics, and frequency control*, 66(10), 1606–1615.

Cowen, A. & et al. (2013). PiezoMUMPsTM Design Handbook.

Cowen, A., Hames, G., Glukh, K. & Hardy, B. (2013). PiezoMUMPs™ Design Handbook. *MEMSCAP Inc.*

Dangi, A., Cheng, C., Agrawal, S., Tiwari, S., Datta, G. R., Benoit, R., Pratap, R., Trolier-McKinstry, S. & Kothapalli, S.-R. (2019). A Photoacoustic Imaging Device using Piezoelectric Micromachined Ultrasound Transducers (PMUTs). *IEEE Transactions on Ultrasonics, Ferroelectrics, and Frequency Control*.

Dausch, D. E., Castellucci, J. B., Chou, D. R. & Von Ramm, O. T. (2008a). Theory and operation of 2-D array piezoelectric micromachined ultrasound transducers. *Ultrasonics, Ferroelectrics, and Frequency Control, IEEE Transactions on*, 55(11), 2484-2492.

Dausch, D. E., Castellucci, J. B., Chou, D. R. & von Ramm, O. T. (2008b). Theory and operation of 2-D array piezoelectric micromachined ultrasound transducers. *ieee transactions on ultrasonics, ferroelectrics, and frequency control*, 55(11).

Dausch, D. E., Gilchrist, K. H., Carlson, J. R., Castellucci, J. B., Chou, D. R. & Von Ramm, O. T. (2010). *Improved pulse-echo imaging performance for flexure-mode pMUT arrays*. Conference Proceedings présentée à Ultrasonics Symposium (IUS), 2010 IEEE (pp. 451-454).

Dausch, D. E., Gilchrist, K. H., Carlson, J. B., Hall, S. D., Castellucci, J. B. & von Ramm, O. T. (2014a). In vivo real-time 3-D intracardiac echo using PMUT arrays. *Ultrasonics, Ferroelectrics, and Frequency Control, IEEE Transactions on*, 61(10), 1754-1764.

Dausch, D. E., Gilchrist, K. H., Carlson, J. B., Hall, S. D., Castellucci, J. B. & von Ramm, O. T. (2014b). In vivo real-time 3-D intracardiac echo using PMUT arrays. *IEEE transactions on ultrasonics, ferroelectrics, and frequency control*, 61(10), 1754–1764.

Dubois, M.-A. & Muralt, P. (1998). PZT thin film actuated elastic fin micromotor. *IEEE transactions on ultrasonics, ferroelectrics, and frequency control*, 45(5), 1169-1177.

Eccardt, P. C. & Niederer, K. (2000). Micromachined ultrasound transducers with improved coupling factors from a CMOS compatible process. *Ultrasonics*, 38(1), 774-780.

Eichhorn, C., Goldschmidtboeing, F. & Woias, P. (2009). Bidirectional frequency tuning of a piezoelectric energy converter based on a cantilever beam. *Journal of Micromechanics and Microengineering*, 19(9), 094006.

Eichhorn, C., Tchagsim, R., Wilhelm, N. & Woias, P. (2011). A smart and self-sufficient frequency tunable vibration energy harvester. *Journal of Micromechanics and Microengineering*, 21(10), 104003.

Eovino, B. E., Liang, Y. & Lin, L. (2019). Concentric PMUT Arrays for Focused Ultrasound and High Intensity Applications. *2019 IEEE 32nd International Conference on Micro Electro Mechanical Systems (MEMS)*, pp. 771–774.

Feng, G.-H. & Liu, H.-J. (2019). Piezoelectric Micromachined Ultrasonic Transducers with a Cost-Effective Bottom-Up Fabrication Scheme for Millimeter-Scale Range Finding. *Sensors*, 19(21), 4696.

Foster, F. S., Harasiewicz, K. A. & Sherar, M. D. (2000). A history of medical and biological imaging with polyvinylidene fluoride (PVDF) transducers. *Ultrasonics, Ferroelectrics, and Frequency Control, IEEE Transactions on*, 47(6), 1363-1371.

Gao, H., Gijsenbergh, P., Halbach, A., Serrahima, C. P., Torri, G. B., Jeong, Y., Billen, M., Cheyns, D., Haouari, R., Rottenberg, X. et al. (2019). Design of polymer-based PMUT array for multi-frequency ultrasound imaging. *2019 IEEE International Ultrasonics Symposium (IUS)*, pp. 1092–1095.

Guedes, A., Shelton, S., Przybyla, R., Izyumin, I., Boser, B. & Horsley, D. (2011). *Aluminum nitride pMUT based on a flexurally-suspended membrane*. Conference Proceedings présentée à Solid-State Sensors, Actuators and Microsystems Conference (TRANSDUCERS), 2011 16th International (pp. 2062-2065).

Gurun, G., Qureshi, M. S., Balantekin, M., Guldiken, R., Zahorian, J., Peng, S.-Y., Basu, A., Karaman, M., Hasler, P. & Degertekin, L. (2008). *Front-end CMOS electronics for monolithic integration with CMUT arrays : circuit design and initial experimental results*. Conference Proceedings présentée à Ultrasonics Symposium, 2008. IUS 2008. IEEE (pp. 390-393).

Gurun, G., Zahorian, J. S., Sisman, A., Karaman, M., Hasler, P. E. & Degertekin, F. L. (2012). An analog integrated circuit beamformer for high-frequency medical ultrasound imaging. *Biomedical Circuits and Systems, IEEE Transactions on*, 6(5), 454-467.

Gurun, G., Tekes, C., Zahorian, J., Xu, T., Satir, S., Karaman, M., Hasler, J. & Degertekin, F. L. (2014). Single-chip CMUT-on-CMOS front-end system for real-time volumetric IVUS and ICE imaging. *Ultrasonics, Ferroelectrics, and Frequency Control, IEEE Transactions on*, 61(2), 239-250.

Halbach, A., Gijsenbergh, P., Jeong, Y., Devriese, W., Gao, H., Billen, M., Torri, G. B., Chare, C., Cheyns, D., Rottenberg, X. et al. (2019). Display Compatible PMUT Array for Mid-Air Haptic Feedback. *2019 20th International Conference on Solid-State Sensors, Actuators and Microsystems & Eurosensors XXXIII (TRANSDUCERS & EUROSENSORS XXXIII)*, pp. 158–161.

Jensen, J. A., Holm, O., Jerisen, L., Bendsen, H., Nikolov, S. I., Tomov, B. G., Munk, P., Hansen, M., Salomonsen, K. & Hansen, J. (2005). Ultrasound research scanner for real-time synthetic aperture data acquisition. *IEEE transactions on ultrasonics, ferroelectrics, and frequency control*, 52(5), 881-891.

Jiang, X., Lu, Y., Tang, H.-Y., Tsai, J. M., Ng, E. J., Daneman, M. J., Boser, B. E. & Horsley, D. A. (2017). Monolithic ultrasound fingerprint sensor. *Microsystems & nanoengineering*, 3(1), 1–8.

Jin, X., Ladabaum, I. & Khuri-Yakub, B. T. (1998). The microfabrication of capacitive ultrasonic transducers. *Microelectromechanical Systems, Journal of*, 7(3), 295-302.

Jung, J., Lee, W., Kang, W., Shin, E., Ryu, J. & Choi, H. (2017). Review of piezoelectric micromachined ultrasonic transducers and their applications. *Journal of Micromechanics and Microengineering*, 27(11), 113001.

Kungl, H., Theissmann, R., Knapp, M., Baehtz, C., Fuess, H., Wagner, S., Fett, T. & Hoffmann, M. J. (2007). Estimation of strain from piezoelectric effect and domain switching in morphotropic PZT by combined analysis of macroscopic strain measurements and synchrotron X-ray data. *Acta materialia*, 55(6), 1849-1861.

Ledesma, E., Zamora, I., Torres, F., Uranga, A., Tzanov, V., Barniol, N., Marigo, E. & Soundara-Pandian, M. (2019). AlN piezoelectric micromachined ultrasonic transducer array monolithically fabricated on top of pre-processed CMOS substrates. *2019 20th International Conference on Solid-State Sensors, Actuators and Microsystems & Eurosensors XXXIII (TRANSDUCERS & EUROSENSORS XXXIII)*, pp. 655–658.

Lee, M.-C. M. & Wu, M. C. (2006). Tunable coupling regimes of silicon microdisk resonators using MEMS actuators. *Optics Express*, 14(11), 4703–4712.

Leland, E. S. & Wright, P. K. (2006). Resonance tuning of piezoelectric vibration energy scavenging generators using compressive axial preload. *Smart Materials and Structures*, 15(5), 1413.

Lemmerhirt, D. F., Cheng, X., White, R. D., Rich, C. A., Zhang, M., Fowlkes, J. B. & Kripfgans, O. D. (2012). A 32 x 32 capacitive micromachined ultrasonic transducer array manufactured in standard CMOS. *IEEE transactions on ultrasonics, ferroelectrics, and frequency control*, 59(7).

Li, Y., Moon, K.-s. & Wong, C. (2005). Electronics without lead. *Science*, 308(5727), 1419-1420.

Liao, W., Liu, W., Rogers, J., Usmani, F., Tang, Y., Wang, B., Jiang, H. & Xie, H. (2013). *Piezoelectric micromachined ultrasound tranducer array for photoacoustic imaging*. Conference Proceedings présentée à Solid-State Sensors, Actuators and Microsystems (TRANSDUCERS EUROSENSORS XXVII), 2013 Transducers Eurosensors XXVII : The 17th International Conference on (pp. 1831-1834).

Lin, C., Hsieh, S., Huang, C. & Chang, C. (2012, July). Frequency-tunable CMOS-MEMS slot antenna. *Proceedings of the 2012 IEEE International Symposium on Antennas and Propagation*, pp. 1-2. doi : 10.1109/APS.2012.6348538.

Liu, W., He, L., Wang, X., Zhou, J., Xu, W., Smagin, N., Toubal, M., Yu, H., Gu, Y., Xu, J. et al. (2019). 3D FEM Analysis of High-Frequency AlN-Based PMUT Arrays on Cavity SOI. *Sensors*, 19(20), 4450.

Liu, X., Katehi, L. P. B., Chappell, W. J. & Peroulis, D. (2010). High-Q Tunable Microwave Cavity Resonators and Filters Using SOI-Based RF MEMS Tuners. *Journal of Microelectromechanical Systems*, 19(4), 774-784. doi : 10.1109/JMEMS.2010.2055544.

Lu, Y., Tang, H., Fung, S., Wang, Q., Tsai, J., Daneman, M., Boser, B. & Horsley, D. (2015a). Ultrasonic fingerprint sensor using a piezoelectric micromachined ultrasonic transducer array integrated with complementary metal oxide semiconductor electronics. *Applied Physics Letters*, 106(26), 263503.

Lu, Y., Tang, H., Wang, Q., Fung, S., Tsai, J., Daneman, M., Boser, B. & Horsley, D. (2015b). Waveguide piezoelectric micromachined ultrasonic transducer array for short-range pulse-echo imaging. *Applied Physics Letters*, 106(19), 193506.

Lu, Y., Heidari, A. & Horsley, D. (2014). A High Fill-Factor Annular Array of High Frequency Piezoelectric Micromachined Ultrasonic Transducers.

Lu, Y. & Horsley, D. A. (2015). Modeling, fabrication, and characterization of piezoelectric micromachined ultrasonic transducer arrays based on cavity SOI wafers. *Microelectromechanical Systems, Journal of*, 24(4), 1142-1149.

Lu, Y., Heidari, A. & Horsley, D. A. (2015c). A high fill-factor annular array of high frequency piezoelectric micromachined ultrasonic transducers. *Journal of Microelectromechanical Systems*, 24(4), 904-913.

Lu, Y., Rozen, O., Tang, H.-Y., Smith, G. L., Fung, S., Boser, B. E., Polcawich, R. G. & Horsley, D. (2015d). *Broadband piezoelectric micromachined ultrasonic transducers based on dual resonance modes*. Conference Proceedings présentée à Micro Electro Mechanical Systems (MEMS), 2015 28th IEEE International Conference on (pp. 146-149).

Lu, Y., Tang, H.-Y., Fung, S., Boser, B. E. & Horsley, D. A. (2015e). *Short-range and high-resolution ultrasound imaging using an 8 MHz Aluminum Nitride PMUT array*. Conference Proceedings présentée à Micro Electro Mechanical Systems (MEMS), 2015 28th IEEE International Conference on (pp. 140-143).

Mehdizadeh, E. & Piazza, G. (2017). *AlN on SOI pMUTs for ultrasonic power transfer*. Conference Proceedings présentée à Ultrasonics Symposium (IUS), 2017 IEEE International (pp. 1-4).

Misaridis, T. & Jensen, J. A. (2005a). Use of modulated excitation signals in medical ultrasound. Part I : Basic concepts and expected benefits. *IEEE transactions on ultrasonics, ferroelectrics, and frequency control*, 52(2), 177-191.

Misaridis, T. & Jensen, J. A. (2005b). Use of modulated excitation signals in medical ultrasound. Part II : Design and performance for medical imaging applications. *IEEE transactions on ultrasonics, ferroelectrics, and frequency control*, 52(2), 192-207.

Misaridis, T. & Jensen, J. A. (2005c). Use of modulated excitation signals in medical ultrasound. Part III : High frame rate imaging. *IEEE transactions on ultrasonics, ferroelectrics, and frequency control*, 52(2), 208-219.

Muralt, P., Ledermann, N., Paborowski, J., Barzegar, A., Gentil, S., Belgacem, B., Petitgrand, S., Bosseboeuf, A. & Setter, N. (2005). Piezoelectric micromachined ultrasonic transducers based on PZT thin films. *Ultrasonics, Ferroelectrics, and Frequency Control, IEEE Transactions on*, 52(12), 2276-2288.

Ohigashi, H., Nakanishi, T., Itoh, T., Suzuki, M. & Omoto, R. (1979). Study on piezoelectric polymer transducers for high resolution ultrasound imaging. *Proc. World Fed. Ultrasound Med. Biol*, 376.

Oralkan, , Ergun, A. S., Cheng, C.-H., Johnson, J. A., Karaman, M., Lee, T. H. & Khuri-Yakub, B. T. (2003). Volumetric ultrasound imaging using 2-D CMUT arrays. *Ultrasonics, Ferroelectrics, and Frequency Control, IEEE Transactions on*, 50(11), 1581-1594.

Perçin, G. (2003). Plate equations for piezoelectrically actuated flexural mode ultrasound transducers. *IEEE transactions on ultrasonics, ferroelectrics, and frequency control*, 50(1), 81-88.

Perçin, G. & Khuri-Yakub, B. T. (2002). Piezoelectrically actuated flextensional micromachined ultrasound transducers. I. Theory. *Ultrasonics, Ferroelectrics, and Frequency Control, IEEE Transactions on*, 49(5), 573-584.

Peters, C., Maurath, D., Schock, W., Mezger, F. & Manoli, Y. (2009). A closed-loop wide-range tunable mechanical resonator for energy harvesting systems. *Journal of Micromechanics and Microengineering*, 19(9), 094004.

Przybyla, R., Flynn, A., Jain, V., Shelton, S., Guedes, A., Izyumin, I., Horsley, D. & Boser, B. (2011a). A micromechanical ultrasonic distance sensor with> 1 meter range. *Solid-State Sensors, Actuators and Microsystems Conference (TRANSDUCERS), 2011 16th International*, pp. 2070–2073.

Przybyla, R., Flynn, A., Jain, V., Shelton, S., Guedes, A., Izyumin, I., Horsley, D. & Boser, B. (2011b). *A micromechanical ultrasonic distance sensor with> 1 meter range*. Conference Proceedings présentée à Solid-State Sensors, Actuators and Microsystems Conference (TRANSDUCERS), 2011 16th International (pp. 2070-2073).

Przybyla, R. J., Tang, H.-Y., Shelton, S. E., Horsley, D. & Boser, B. E. (2014a). *12.1 3D ultrasonic gesture recognition*. Conference Proceedings présentée à Solid-State Circuits Conference Digest of Technical Papers (ISSCC), 2014 IEEE International (pp. 210-211).

Przybyla, R. J., Tang, H.-Y., Shelton, S. E., Horsley, D. A. & Boser, B. E. (2014b). 12.1 3D ultrasonic gesture recognition. *Solid-State Circuits Conference Digest of Technical Papers (ISSCC), 2014 IEEE International*, pp. 210–211.

Przybyla, R. J., Tang, H.-Y., Guedes, A., Shelton, S. E., Horsley, D. A. & Boser, B. E. (2015). 3D Ultrasonic Rangefinder on a Chip. *Solid-State Circuits, IEEE Journal of*, 50(1), 320-334.

Qiu, Y., Gigliotti, J. V., Wallace, M., Griggio, F., Demore, C. E., Cochran, S. & Trolier-McKinstry, S. (2015a). Piezoelectric micromachined ultrasound transducer (PMUT) arrays for integrated sensing, actuation and imaging. *Sensors*, 15(4), 8020-8041.

Qiu, Y., Gigliotti, J. V., Wallace, M., Griggio, F., Demore, C. E., Cochran, S. & Trolier-McKinstry, S. (2015b). Piezoelectric micromachined ultrasound transducer (PMUT) arrays for integrated sensing, actuation and imaging. *Sensors*, 15(4), 8020–8041.

Ramadan, K. S., Sameoto, D. & Evoy, S. (2014). A review of piezoelectric polymers as functional materials for electromechanical transducers. *Smart Materials and Structures*, 23(3), 033001.

Reddy, J. N. (2006). *Theory and analysis of elastic plates and shells*. CRC press.

Reines, I., Park, S. & Rebeiz, G. M. (2010). Compact Low-Loss Tunable*X*-Band Bandstop Filter With Miniature RF-MEMS Switches. *IEEE Transactions on Microwave Theory and Techniques*, 58(7), 1887-1895. doi : 10.1109/TMTT.2010.2050621.

Robichaud, A., Cicek, P. V., Deslandes, D. & Nabki, F. (2018a). Frequency Tuning Technique of Piezoelectric Ultrasonic Transducers for Ranging Applications. *Journal of Microelectromechanical Systems*, 1-10. doi : 10.1109/JMEMS.2018.2831638.

Robichaud, A., Deslandes, D., Cicek, P. & Nabki, F. (2018b). A Novel Topology for Process Variation-Tolerant Piezoelectric Micromachined Ultrasonic Transducers. *Journal of Microelectromechanical Systems*, 27(6), 1204-1212. doi : 10.1109/JMEMS.2018.2876384.

Rozen, O., Block, S. T., Mo, X., Bland, W., Hurst, P., Tsai, J. M., Daneman, M., Amirtharajah, R. & Horsley, D. A. (2016). *Monolithic MEMS-CMOS ultrasonic rangefinder based on dual-electrode PMUTs*. Conference Proceedings présentée à 2016 IEEE 29th International Conference on Micro Electro Mechanical Systems (MEMS) (pp. 115-118).

Sammoura, F. & Kim, S.-G. (2012). Theoretical modeling and equivalent electric circuit of a bimorph piezoelectric micromachined ultrasonic transducer. *IEEE transactions on ultrasonics, ferroelectrics, and frequency control*, 59(5).

Schmerr, L. & Song, J.-S. (2007). *Ultrasonic nondestructive evaluation systems*. Springer.

Schmmer Jr, L. W. (2008). Fundamentals of ultrasonic phased arrays. *Modern Physics Letters B*, 22(11), 917-921.

Shelton, S., Rozen, O., Guedes, A., Przybyla, R., Boser, B. & Horsley, D. (2014). *Improved acoustic coupling of air-coupled micromachined ultrasonic transducers*. Conference Proceedings présentée à Micro Electro Mechanical Systems (MEMS), 2014 IEEE 27th International Conference on (pp. 753-756).

Smyth, K. & Kim, S.-G. (2015a). Experiment and simulation validated analytical equivalent circuit model for piezoelectric micromachined ultrasonic transducers. *IEEE transactions on ultrasonics, ferroelectrics, and frequency control*, 62(4), 744-765.

Smyth, K. & Kim, S.-G. (2015b). Experiment and simulation validated analytical equivalent circuit model for piezoelectric micromachined ultrasonic transducers. *IEEE transactions on ultrasonics, ferroelectrics, and frequency control*, 62(4), 744–765.

Swanevelder, J. & Ng, A. (2011). Resolution in ultrasound imaging. *Continuing Education in Anaesthesia Critical Care Pain*, 11(5), 186-192. doi : 10.1093/bjaceaccp/mkr030.

Tang, H.-Y., Lu, Y., Fung, S., Horsley, D. & Boser, B. E. (2015). *11.8 Integrated ultrasonic system for measuring body-fat composition*. Conference Proceedings présentée à Solid-State Circuits Conference-(ISSCC), 2015 IEEE International (pp. 1-3).

Tang, H.-Y., Lu, Y., Jiang, X., Ng, E. J., Tsai, J. M., Horsley, D. A. & Boser, B. E. (2016a). 3-D Ultrasonic Fingerprint Sensor-on-a-Chip. *IEEE Journal of Solid-State Circuits*, 51(11), 2522-2533.

Tang, H.-Y., Lu, Y., Jiang, X., Ng, E. J., Tsai, J. M., Horsley, D. A. & Boser, B. E. (2016b). 3-D ultrasonic fingerprint sensor-on-a-chip. *IEEE Journal of Solid-State Circuits*, 51(11), 2522–2533.

Wang, T. & Lee, C. (2015). Zero-Bending Piezoelectric Micromachined Ultrasonic Transducer (pMUT) With Enhanced Transmitting Performance. *Microelectromechanical Systems, Journal of*, 24(6), 2083-2091.

Wang, Z., Miao, J. & Zhu, W. (2008). Micromachined ultrasonic transducers and arrays based on piezoelectric thick film. *Applied Physics A*, 91(1), 107-117.

Williams, J. & Le, H. (2006). Tribology and MEMS. *Journal of Physics D : Applied Physics*, 39(12), R201.

Wischke, M., Masur, M., Goldschmidtboeing, F. & Woias, P. (2010). Electromagnetic vibration harvester with piezoelectrically tunable resonance frequency. *Journal of Micromechanics and Microengineering*, 20(3), 035025.

Wu, X., Lin, J., Kato, S., Zhang, K., Ren, T. & Liu, L. (2008). A frequency adjustable vibration energy harvester. *Proceedings of PowerMEMS*, 245–248.

Wygant, I. O., Zhuang, X., Yeh, D. T., Oralkan, , Ergun, A. S., Karaman, M. & Khuri-Yakub, B. T. (2008). Integration of 2D CMUT arrays with front-end electronics for volumetric ultrasound imaging. *Ultrasonics, Ferroelectrics, and Frequency Control, IEEE Transactions on*, 55(2), 327-342.

Wygant, I. O., Jamal, N. S., Lee, H. J., Nikoozadeh, A., Oralkan, , Karaman, M. & Khuri-Yakub, B. T. (2009). An integrated circuit with transmit beamforming flip-chip bonded to a 2-D CMUT array for 3-D ultrasound imaging. *Ultrasonics, Ferroelectrics, and Frequency Control, IEEE Transactions on*, 56(10), 2145-2156.

Xu, T., Zhao, L., Jiang, Z., Guo, S., Li, Z., Yang, P., Sun, L., Luo, G. & Zhang, L. (2019). Array design of piezoelectric micromachined ultrasonic transducers with low crosstalk and high emission performance. *IEEE Transactions on Ultrasonics, Ferroelectrics, and Frequency Control*.

Yan, W. D. & Mansour, R. R. (2007, June). Compact Tunable Bandstop Filter Integrated with Large Deflected Actuators. *2007 IEEE/MTT-S International Microwave Symposium*, pp. 1611-1614. doi : 10.1109/MWSYM.2007.379994.

Yin, X., Zhu, Y. & Hu, J. (2019). 3D Fingerprint Recognition based on Ridge-valley-guided 3D Reconstruction and 3D Topology Polymer Feature Extraction. *IEEE transactions on pattern analysis and machine intelligence*.

Yole Développement. Ultrasound sensing - Product Technology roadmap. Accessed : 2020-01-02.

Zahorian, J., Hochman, M., Xu, T., Satir, S., Gurun, G., Karaman, M. & Degertekin, F. L. (2011a). Monolithic CMUT-on-CMOS integration for intravascular ultrasound applications. *Ultrasonics, Ferroelectrics, and Frequency Control, IEEE Transactions on*, 58(12), 2659-2667.

Zahorian, J., Hochman, M., Xu, T., Satir, S., Gurun, G., Karaman, M. & Degertekin, F. L. (2011b). Monolithic CMUT-on-CMOS integration for intravascular ultrasound applications. *IEEE transactions on ultrasonics, ferroelectrics, and frequency control*, 58(12), 2659–2667.

Zamora, I., Ledesma, E., Uranga, A. & Barniol, N. (2020). Miniaturized 0.13-μm CMOS Front-End Analog for AlN PMUT Arrays. *Sensors*, 20(4), 1205.